DIGITAL ACCESS TO SCHOLARSHIP AT HARVARD
DASH.HARVARD.EDU

HARVARD LIBRARY
Office for Scholarly Communication

Extrusion 3D-Printing of Integrated Soft Materials for Ionotronic Applications

Citation

Tian, Kevin. 2019. Extrusion 3D-Printing of Integrated Soft Materials for Ionotronic Applications. Doctoral dissertation, Harvard University, Graduate School of Arts & Sciences.

Permanent link

http://nrs.harvard.edu/urn-3:HUL.InstRepos:42029812

Terms of Use

This article was downloaded from Harvard University's DASH repository, and is made available under the terms and conditions applicable to Other Posted Material, as set forth at http://nrs.harvard.edu/urn-3:HUL.InstRepos:dash.current.terms-of-use#LAA

Share Your Story

The Harvard community has made this article openly available.
Please share how this access benefits you. Submit a story .

Accessibility

Extrusion 3D-Printing of Integrated Soft Materials for Ionotronic Applications

A DISSERTATION PRESENTED
BY
KEVIN TIAN
TO
THE DEPARTMENT OF ENGINEERING AND APPLIED SCIENCES

IN PARTIAL FULFILLMENT OF THE REQUIREMENTS
FOR THE DEGREE OF
DOCTOR OF PHILOSOPHY
IN THE SUBJECT OF
APPLIED PHYSICS

HARVARD UNIVERSITY
CAMBRIDGE, MASSACHUSETTS
MAY 2019

©2019 – Kevin Tian
all rights reserved.

Dissertation advisor: Professor Joost J. Vlassak Kevin Tian

Extrusion 3D-Printing of Integrated Soft Materials for Ionotronic Applications

Abstract

Stretchable electronics is an emerging field responding to the demands of soft robotics and biological applications. Whereas the materials of traditional electronics are hard and rigid – like silicon and metals – stretchable materials are soft and compliant like rubber. Conventional stretchable electronics integrate the hard within the soft. Hydrogel-based ionic devices represent an alternative approach to stretchable electronics. Metallic conductors can be replaced with soft ionic conductors that are both highly stretchable and transparent. However, these devices require the integration of dissimilar materials, hydrophobic elastomers and hydrogels, into a single system—a process thus far achieved primarily via the combination of several different manufacturing techniques. The concurrent rise of additive manufacturing presents an opportunity to develop a new fabrication platform for hydrogel-based devices. This dissertation will delve into recent progress made in the 3D extrusion printing of these dissimilar soft materials for a range of engineering applications, the challenges that one encounters, and those that remain on the horizon.

Chapter 1 reports a study of high ionic strength hydrogel materials for their unusual thermal, mechanical, and electrical properties. Chapter 2 presents an extrusion 3D-printing platform for the simultaneous fabrication of hydrogel and hydrophobic elastomer. Chapter 3 further characterizes the initial platform developed in a study of the adhesion characteristics of the hydrogel-elastomer interface over time. Chapter 4 adapts a new silane-based chemistry in order to fully integrate hydrogel and elastomer for extrusion 3D-printing.

Contents

Listing of figures

To my parents and my brother, George, without whom I'd have had no foundation to build myself on.

Acknowledgments

The longest of journeys requires an even longer pause, especially as the end draws near. This chapter of my life has been surprisingly long, but has done so much for enriching my life in so many ways. It would not have been remotely the same if not for my great fortune in meeting so many awesome people, all so brilliant in their own special way. I'd like to take the time to acknowledge as many folks as I can remember (it's not personal if I missed you, really T_T):

First and foremost, my advisor Joost Vlassak has taught me much about being a rigorous and proficient experimental researcher. I cannot thank him enough for his eternal patience through experimental difficulty (and my accident-prone nature) and for giving me both opportunity and careful guidance along the way. My co-advisor Zhigang Suo has also been tremendously helpful in providing a bigger picture perspective to my scientific endeavors. His constant reminders to step back have helped me to see the impact of my own work and appreciate its intellectual value. Of course all the other faculty at SEAS I've had to pleasure of interacting with deserve mention: David Clarke (for kindly receiving me as I took my first steps into my PhD), Frans Spaepen (for AP282), Katia Bertoldi (for your guidance in computational mechanics and beyond), and Shmuel Rubinstein (for serving on my qualifying and dissertation committees).

To all ye kind folks that resided in the dorms (Perkins!) and at Beckwith Circle: Anna Wang, Aileen Li, George Somi, George Xu, Tony Z. Jia, Chris Miller, Paul Loschak, Neil Tennenholtz, Yue Zhang, Ignacio Galiana, Ruth Peña Velasco, James Tam, Amy Koenig, Helen Wu, Oliver and Emily Hauser, Sicong Shan, Morgan McDaniel, Vayu Maini Rekdal, Anne-Sophie Pratte, Naomi Woods.

Fellow researchers from the Suo and Vlassak labs made every lab day interesting, especially: Jinhye Bae, Juanjuan Zheng, Gayatri Cuddalorepatta, Gayatri Perlin, Mark Miao, Jianyu Li, Widusha Illeperuma, Canhui Yang, Jiawei Yang, Ruobing Bai, Shuang Zhou, Yecheng Wang, Paul Lefloch, Junsoo Kim, Xavier Morelle (shout out to project members from Wollongong: Charles Hamilton, Shannon Bakarich, and Reece Gately.

My fellow thespians: Cathy Zhang, Raphaël Pestourie, John North Radway, Andrew Bellisari, Effie Gonis, Alexandra van Green, Laila Akhmetova, Zachary Hermann, Ola Friday, René Eber, Talitha Kir, Marissa Grunes, Trisha Banerjee, Ursula DeYoung. Though the days on the stage in Dudley are behind us, I still rehearse scenes in my head and raise a glass (of whiskey) to you all.

To all my friends in the Aikido community that have helped me guide my problems to the ground, I thank you for all the happy tossings. In particular: Dolita Cathcart, Amy Kipp, Daryl Muranaka,

Dya Kaur Levitt, Sharon Kanai, Pao (Kanya) Siangliulue, Ken and Susan Arnold, Sally K. Joyce, Agnes Kamasi, Scott Bennett-Jeffreys, Ken Gareau (may the universe always keep the quota), and Phil Chodrow. I would also like to remember Sioux Hall-sensei, who taught me to face the unknown with both ferocity and kindness (and maybe a bit of snickering along the way).

Folks along the way that helped to revitalize the SEAS Graduate Council and friends I've made at GSAS GSC: Yashraj Narang, Andrea Tokranov, Alperen Degirmenci, Clarke Teeple, Tobias Egle, Siyi Xu, Blakely Bussie O'Conner, Darcy Frear, Masha Bertling, My time at the Harvard Graduate Council has also no shortage of individuals that have made my time there memorable: Peter Dyrud, Simeon Bochev, Marshall Page, Kelly Menjivar, Tracie Gordon, Alvin Tran, Richard Zhang, Nila Devanah, Dolly Amaya, Alexander Rodriguez. I'm also honored to have served on committees with Shannon Rice, Paul Barreira, Patrick O'Brien, and Nancy Turnbull.

To the folks I've met through the HGSLI program, in particular: Amiya Bhatia, Rohan Mascarenhas, Diana Marian, Andrew Kim, and Iulia Alexandra Neagu. Thank you all for your honest and kind friendship during the program and for long after it had all concluded.

To my fellow (former) PhD candidates with whom I've taken on this journey: Lisa Lee, Wanchen (Chickee) Lee, Lauren Hartle, Emily Redston, Rachel Heasly, Christine Zgrabik, Ben Franta, Matheus Fernandes, Bolei Deng, Cindy Hu, Kevin Ma, Janine May, Tina Huang, Gabriele Librandi, Andy Greenspon, Omer Gottesman, Emma Spady, Shoshana Vasserman, Atcha Totachawattana, Simon Fang, Paul Coote. I hope to be toasting with you all as fellow doctors of philosophy, whether it be this May or sometime in the (near?) future!

It'd be a disservice to not recognize everyone in the academic administrative office(s) that have made navigating the program as smooth as it could have been. A shout out to Julie Holbrook, John Girash, Lisa Ann Frazier-Zezze, Ann Greaney-Williams, Robert (Bob) Graham, Kathryn Ann Hollar, and Melissa Majkut at SEAS; and Garth McCavana, Jacqueline (Jackie) Yun, Janet Daniels at GSAS.

To all you CMU alums supporting me from a grand distance, you're certainly in my thoughts: Elaine Lee, Sylvia Lee, Seif Yusef, Kush Mangal, Sophie Zhouzheng, Vani Rajan, Zack (Zackdos) Reagin, Chris Solidum. Of course, I wouldn't even be here getting this degree if it weren't for my professors: Kunal Ghosh, Stephen Garoff, Brian Quinn, Reinhard A. Schumacher, Jiang-Gang (Jimmy) Zhu, and Robert H. Swendsen.

I would also like to thank my brother, George, who's always served as a rational sounding board and fellow "de-stress game" partner. My mother deserves no short praise, for she's always looking for out for me through my many bouts of illnesses and maladies. My father has always been a reliable source of know-how in our household, save for the occasional phone-in-water or forgotten passport.

Last, but not least, I could not forget my dearest Caroline, for whom without this last stretch would have been so terribly dull. I will always be grateful for your limitless patience in handling all the panic and anxiety.

I've been blessed to have had you all touch my life in so many different ways, however brief it may have been. If anyone ever reads this and thinks, "Oh hey, I remember that guy", I welcome you to reach out to me on (insert social media of the future here). That or email me: just conjugate my full name and take out the vowels in my first name at gmail (it's data scrape proof...for now!).

So long, and thanks for all the fish.

0

Introduction

0.1 Hydrogels and Ionotronics

Pierre-Gilles de Gennes first coined the term "soft matter" in 1991, which served to name the fascinatingly complex materials that have only accelerated in their adoption in recent years[1]. Polymers, both natural and synthetic, have advanced much since de Gennes' Nobel lecture of 1991, and

it in this new context that soft materials now being considered for engineering applications previously not thought possible. Hydrogels, which are hydrophilic polymer networks swollen with water, have unique properties imparted by their dual nature of being simultaneously solid-like and liquid-like. The polymer network imbues hydrogels with solid-like mechanical properties, whereas the liquid phase grants the material liquid-like transport properties. Combined with their potential for bio-compatibility, hydrogels have seen rapid development as materials of choice for for tissue engineering and drug delivery systems[2,3,4].

However, recent developments have sufficiently improved the material properties of hydrogels to enable a far wider range of applications than previously thought possible. Mechanically, recent works have drastically increased the range of applications of hydrogels by improving their stretchability and toughness to levels comparable to natural rubber[5,6,7,8] and in some cases comparable to steel[9]. At this point in time, a wide variety of hydrogel toughening mechanisms have been identified and utilized for mechanical reinforcement[10,11,5,8], which has led to the development of novel applications such as fire-resistant fabrics[12]. In addition, studies have also developed methods for hydrogels to engage in self-healing while maintaining high stretchability and toughness[13,14,15].

As applications have turned more towards interactions with biological systems like the human body, this has in turn increased the demand for functional soft materials that can fulfill these needs. A term that is often used to describe these needs is "Stretchable Electronics". For instance, human wearable sensors for biomechanics studies and health monitoring[16,17,18,19], or feedback sensors in soft robotics[20,21,22,23] all require soft, stretchable materials capable of electrical conductivity. Although many stretchable conductors exist, including liquid metals[24,25], nanowires[26,27], nanoribbons[28], pre-stretched elastomer fibers with conductive coatings[29], and micro-cracked metals[30,31], these materials have generally been unable to achieve high levels of optical transparency while maintaining high conductivities and stretchability; a feature that would enable their use in optogenetics[32] or allow optical imaging of the underlying substrate. Conventional strategies of incorporating metallic com-

ponents with elastomers to attain stretchability also yield non-trivial failure modes such as liquid metal leakage[23] and hard-soft material interfacial failure[33].

Hydrogels, with ionic conductivity and favorable mechanical properties, are a viable alternative approach to stretchable electronics. The combination of exceptional toughness, large stretchability, optical transparency, and high ionic conductivity has led to the development of stretchable and transparent ionic conductors[34,35], stretchable electroluminescent devices[36,37], capacitive strain sensors[38,39,36], ionic touch panels[40], soft robotic actuators[41], and chemical/pH sensors[42]. Gel-based ionic circuits thus represent a unique class of devices within stretchable electronics.

From within these developments has come the concept of the "ionotronic device"[43]. Ionotronics devices are formed from the combination of circuity with both types of charge carriers, electronic and ionic. By combining the best of both worlds, one can achieve high-speed signal processes found in the maturity of electronics with the favorable properties of ionic devices such as high stretchability and optical transparency. However, attaining this fusion requires the use of dissimilar materials of all sorts ranging from the hard (metals, semiconductors, ceramics) to the soft (elastomers and gels). Conductors and insulators must both be found within the same manufacturing process. Even for simple ionotronic devices, the bare minimum must include an ionic conductor and a dielectric. Although this can be simply achieved in prototypes with manual assembly, this cannot be scaled for large quantities and small dimensions. Thus, the fabrication of stretchable electronics using hydrogels requires integrating hydrogels with stretchable dielectrics such as dielectric elastomers. So far, few studies have tackled this problem and thus this issue is very much in its infancy. Questions have generally not been asked of the reliability of the materials being manufactured, particularly the interfacial adhesion that is critical to any long-term usage planned for any device. The same is true for composites[44,45], dental material adhesives[46] and in biology[47,48], thus similar efforts need to be made within hydrogel ionotronics. As devices become more sophisticated and complex, crack driving forces may easily scale such that delamination becomes a serious problem. Neither predic-

tive capability nor process optimization is possible without quantification of adhesion. Therefore, as manufacturing processes are adapted for soft materials, soft materials integration challenges in multi-material printing must be addressed[22].

0.2 Manufacturing of Soft Materials

Although a wide variety of materials manufacturing techniques are applicable to soft materials, the class of techniques known as three-dimensional printing (3DP or 3D-printing) has seen a rapid surge in interest in the recent decade. Although 3DP techniques have existed since the 1970s[49], the cost of a particular class of techniques known as "Fused Deposition Modeling (FDM)", whereby a continuous filament of thermoplastic is extruded in a layer-by-layer deposition process, has dropped dramatically due to the 2009 expiration of the Stratasys Inc. patent[50,51]. The subsequent commercial interest in these technologies has generated public fascination with the possibilities of rapid prototyping, though the adaptation of these techniques for materials other than thermoplastics has steadily progressed since the first 3D printers. Generally these types of techniques are referred to as material extrusion printing, or "extrusion 3D-printing".

It is worth briefly mentioning that, although popular due to its low cost, extrusion printing is far from the only additive manufacturing technique available. Although the range of techniques that are compatible with soft materials is more limited, many others have been developed. For instance: Digital projection based techniques or "Stereolithography" (SLA)[52], two-photon polymerization[53], screen printing[54,55], and inkjet[56] are all viable technologies for the soft materials fabrication. However, of all these techniques, material extrusion is the simplest and easiest to adapt for multi-material printing. The remainder of this dissertation will focus on extrusion 3DP.

Research has since expanded the materials roster from thermoplastics to include metals[57], ceramics[58], and soft materials such as hydrogels and elastomers[59,60,61,62,63]. Although studies adapting soft

materials for 3DP are numerous, few consider the fabrication of dissimilar materials within the same procedure[39,64]. Applications for those studies are generally achieved with a single type of material being developed, thus homogeneous materials fabrication currently dominate advanced manufacturing studies for soft materials.

0.2.1 Hydrogel Printing

Research into the materials extrusion of hydrogels has generally focused on several specific areas: primarily their bio-compatibility, mechanical property enhancement, or functionalization. It is not uncommon that the pursuit of one application will cover more than just one of those areas.

For instance, we may begin our considerations with bio-compatibility, as the ability to serve in close proximity to cells or tissue is of great interest to the medical community. This can be something like a cell scaffold that cells are seeded onto in a post-processing step[60,59,65,66], or a more complex and delicate adaptation where cells are suspended in a fluid and printed directly into position (typically called "bioinks")[67,68]. A variety of hydrogels have already been established to be compatible with the materials extrusion process[69], but if a specific type of matrix is required then additional work needs to be put into this verification process. With 3D printing as a platform there is much activity in pursuit of the development of such new biomaterials that are enabled with the spatial precision of the materials extrusion platform[70]. Even so, for any load-bearing application, it is inevitable that improved mechanical properties are necessary. The most typical example is that of cartilage replacement[71], which is difficult due to its outstanding fatigue resistance and load-bearing capacity.

Thus, in addition to being able to print physiologically relevant hydrogels, we also must be able to print tough hydrogels. As discussed earlier, there have been many strategies developed to toughen hydrogels. However, from those strategies we must also be able to adapt them for extrusion printing, as some techniques are not compatible with the materials extrusion process. For instance, in

terms of reinforcement mechanisms, using fabrics and preformed material composites makes for difficult extrusion[11,9]. However, others are more easily adaptable: PAAm-alginate precursors that were toughened by salt solution soaks[8] can be designed for printability and triggered to UV cure the PAAm covalent network, followed by a salt-solution soaking to ionically crosslink[62,72]. Some studies have opted to forsake the triggered curing with a sufficiently high viscosity followed by immediate soaking[73], however, this is not a scalable process for long prints. New tougheners have also been developed, such as one group that utilized a combination of alginate and graphene oxide to produce a 3D printable tough hydrogel[74]. Fiber reinforcement has also been demonstrate to be possible if the fibers are also capable of printability[63]. Hydrogel biomaterials have also been designed such that multiple IPN are formed by the end of the extrusion process[75]. Some groups have also begun to pursue the printing of polyion complex hydrogels[76], which are able to gelate from a sol-gel transition from a dialysis process that occurs in water. Tougheners can also come in the form of printed structures rather than focusing on the printed materials themselves[77]. Another alternative is to take advantage of fast recovering non-covalent crosslinks within the hydrogel, effectively a supramolecular network, as a printable hydrogel material[78,79,80]

Functionality encompasses the many different pursuits that add functions to hydrogels that complement their biocompatibility or toughness. This may include capacity for temporal changes (or "4D" printing)[81,82,83,84], electrical property modification[85,80], drug delivery[86], sensor design[87]. The capacity for gel to self-heal is also quite desirable, and is generally achieved by the introduction of partial or complete hydrogel networks with non-covalent bonding[88,78].

0.2.2 Elastomer Printing

Conventional elastomer printing studies are less extensive compared to those of hydrogel printing, but generally follow the same trends that have been discussed already. Some of the earliest work that utilized silicone elastomers in 3D printing was conducted in 2000[89]. As familiarity with the mate-

rials system was developed[90], applications for elastomers have similarly looked at their applications towards biological systems[91,92] or the monitoring of biological systems[93]. However, elastomer printing has more focused on their potential for stretchable electronics[94] and robotics applications[95,96]. Functionalization has also been explored through printed structures that would be difficult without 3D printing[97,98]. Since the availability of suitable elastomers for 3D printing is more limited compared to hydrogels, other research has looked into developing new materials for the proces[99] or by adapting existing materials like PDMS for the 3DP process[100].

0.2.3 Hydrogel-Elastomer Printing

Conventional hydrogel-elastomer fabrication studies can be broadly divided into two categories of material integration: Physical bonding and chemical bonding. Recent work has suggested that a more detailed consideration involving adhesive topology is possible[101], however current works have not yet developed strategies that warrant these considerations for hydrogel-elastomer material extrusion.

Those that rely on physical bonds for adhesion, such as through hydrogen bonding[64,102] or contact forces from conformation[103,36,39,41], may indicate acceptable integration, but ultimately rely on the lack of significant driving forces at the interface. Adhesive strengths have generally not been measured for systems that have used physical bonding, but for a hydrophillic surface treatment mediated adhesion interfacial toughnesses of up to $\Gamma = 15 Jm^{-2}$ has been observed[102]. Strong integration, which generally is reflected by the presence cohesive failure, has yet to be demonstrated between hydrogel and elastomer through physical bonds.

Techniques utilizing chemical bonds for their integration are predominantly based around the UV photoinitiator benzophenone, with the majority being surface based modifications[104,105,106] and one instance of volume modifications[107]. These techniques use a compound that upon UV exposure generates free-radicals capable of reacting with both hydrogel and elastomer networks in order

to form chemical crosslinks between them; this means that integration occurs simultaneously with network formation. Another chemical bonding strategy involves silane-based chemical coupling agents. Silane coupling agents have been successfully demonstrated to be viable for hydrogels and elastomers[108,109], where a compatible silane coupling agent is co-polymerized into the material bulk and allowed to react independently of the polymerization reaction. However, these studies did not fully explore their viability within the extrusion printing context as a printing-relevant rheology was not tested in conjunction with a silane coupling agent. In addition, the charged surfactant utilized in the hydrogel will not be compatible with the high ionic strength needed for good electrical conductivity. It was also not demonstrated that even with a charged surfactant that appreciable changes in the wetting behaviors of the hydrogel precursor on PDMS, which will significantly affect printing quality. Thus, further work must be completed in order to make realistic claims about the viability of silane coupling agents for the materials extrusion printing of hydrogel and elastomer.

0.3 Outline of Dissertation

This dissertation aims to to develop platforms for the advanced prototyping and manufacturing of soft ionotronic devices, particularly within the extrusion 3D printing context.

Chapter 1 introduces a study on the modification of material properties when a hydrogel is combined with high concentrations of salt at below-freezing temperatures[110]. With this substantial change in mechanical and thermal properties, salt-containing hydrogels prove themselves as viable engineering materials for a variety of applications. In Chapter 2, we further develop salt-containing hydrogels and adapt them for extrusion printability in conjunction with a dielectric/hydrophobic elastomer[64]. This chapter demonstrates the first steps towards the integrated manufacturing of dissimilar materials, which is required for the advanced manufacturing of soft ionotronics. Chapter 3 conducts a detailed experimental study of the interfacial adhesion of the materials system devel-

oped in the previous chapter[102]. Here we discover that the adhesion is stable and that the interface yields unusual macroscopic behaviors. In light of the strength of the adhesion measured previously, Chapter 4 delves into the development of a chemical bonding mechanism, specifically a silane-based coupling agent strategy, for enhancing the adhesive strength of the hydrogel-elastomer interface in the extrusion printing context. The last chapter then concludes with some future outlooks and perspectives on the field.

Whenever you feel like giving up, think of all the people that would love to see you fail.

Anonymous Internet Meme

1

Tough & Salty: Tough gels below freezing

1.1 Introduction

Hydrogels are crosslinked networks of hydrophilic polymer chains dispersed in water. The polymer network gives the hydrogels solid-like mechanical properties, while the aqueous phase enables fast diffusion, endowing the hydrogels with liquid-like transport properties. Along with these at-

tributes, many hydrogels are also biocompatible, making them traditional materials of choice for tissue engineering and drug delivery systems[2,3,4]. Recent works have considerably enlarged the range of applications of hydrogels by improving their stretchability and toughness up to the level of natural rubbers[5,6,7,8]. The combination of exceptional toughness, large stretchability, optical transparency, and high ionic conductivity has led to the development of many new applications in the field of hydrogels, including stretchable and transparent ionic conductors[34], fire-resistant fabrics[12], stretchable electroluminescent devices[36,37], ionic skin and touch panels[38,40], and soft robotic actuators[41]. However, in all these applications, the hydrogels lose their desirable properties once the temperature decreases below the freezing point of water, severely limiting their use in this temperature range. Recently, organic liquids such as propylene or ethylene glycol have been used to synthesize hybrid organo-hydrogels with an improved working temperature range[111]. There are concerns, however, about the environmental impact and health hazard as a result of the toxicity of these liquids[112,113,114,115]. Here, we present another class of hydrogels that retain their stretchability, toughness, and conductivity at temperatures far below $0°C$[116]. These non-freezing hydrogels rely on the colligative property of ionic compounds such as calcium chloride ($CaCl_2$) to depress the freezing point of the aqueous phase[116,117,118,119,120,121]. Freezing point depression is of course a well-known phenomenon with many applications in cold environments. For example, $CaCl_2$ is widely used to prevent roads from icing over[121]. The same phenomenon also allows a number of organisms, including many insects and some wood frogs, to survive extremely cold weather conditions by preventing the formation of ice crystals in their cells[122,123,124]. Electrical conductivity of salt-containing polyacrylamide hydrogels have been measured at temperatures below $0°C$, but their mechanical behavior has not been studied[125]. In the present study, we synthesized a series of polyacrylamide-alginate double network hydrogels, and soaked them in three different aqueous $CaCl_2$ solutions (see Appendix A for experimental details and Figure 1.1). Depending on the concentration of the $CaCl_2$ soaking solution, these hydrogels froze over a range of temperatures from $0°C$ down to approximately $-57°C$. We mea-

sured the mechanical response of these $CaCl_2$–containing double network hydrogels over a broad range of temperatures, from ambient down to $-70°C$, and distinguished three types of behavior depending on the state of the gel: (i) regular hydrogel behavior when the aqueous phase is in the liquid state, (ii) slurry gel behavior when the aqueous phase is in a partially frozen state that consists of a mixture of ice crystals and salt solution and (iii) frozen gel behavior when the aqueous phase is fully frozen. We also characterized the temperature dependence of the fracture toughness of these hydrogels. We discovered that a high fracture toughness ($5000 Jm^{-2}$) can be obtained at temperatures as low as $-50°C$ (see Table 1.2). In particular, slurry gels were found to have the highest toughness in subzero temperature conditions. By focusing on the gradual evolution of the fracture process in the slurry gels, we identified crack pinning and deflection, as well as distributed initiation of microdamage, as additional toughening mechanisms. Finally, we confirmed that $CaCl_2$-containing hydrogels retain good ionic conductivity at low temperatures, and explored potential applications of these non-freezing hydrogels by demonstrating a simple touch sensing ionic panel that works at subzero temperatures.

1.2 Results and Discussion

Figure 1.3 illustrates the three distinct types of behavior observed for hydrogels with different $CaCl_2$ concentrations at the same sub-zero temperature. Despite similar behavior at room temperature, the three hydrogels behave very differently when they are cooled to $-15°C$ and deformed in tension (similar observations in compression are shown in Figure 1.4 in supporting information). While the gel soaked in 30 wt% $CaCl_2$ behaves like a regular hydrogel with good stretchability and transparency at $-15°C$, gels soaked in 0 wt% and 10 wt% solutions behave differently. For the sake of brevity, we will refer to these different gel compositions in the rest of this manuscript by the concentration of their soaking solution, even if the actual ionic content in the gel may be slightly different. At $-15°C$,

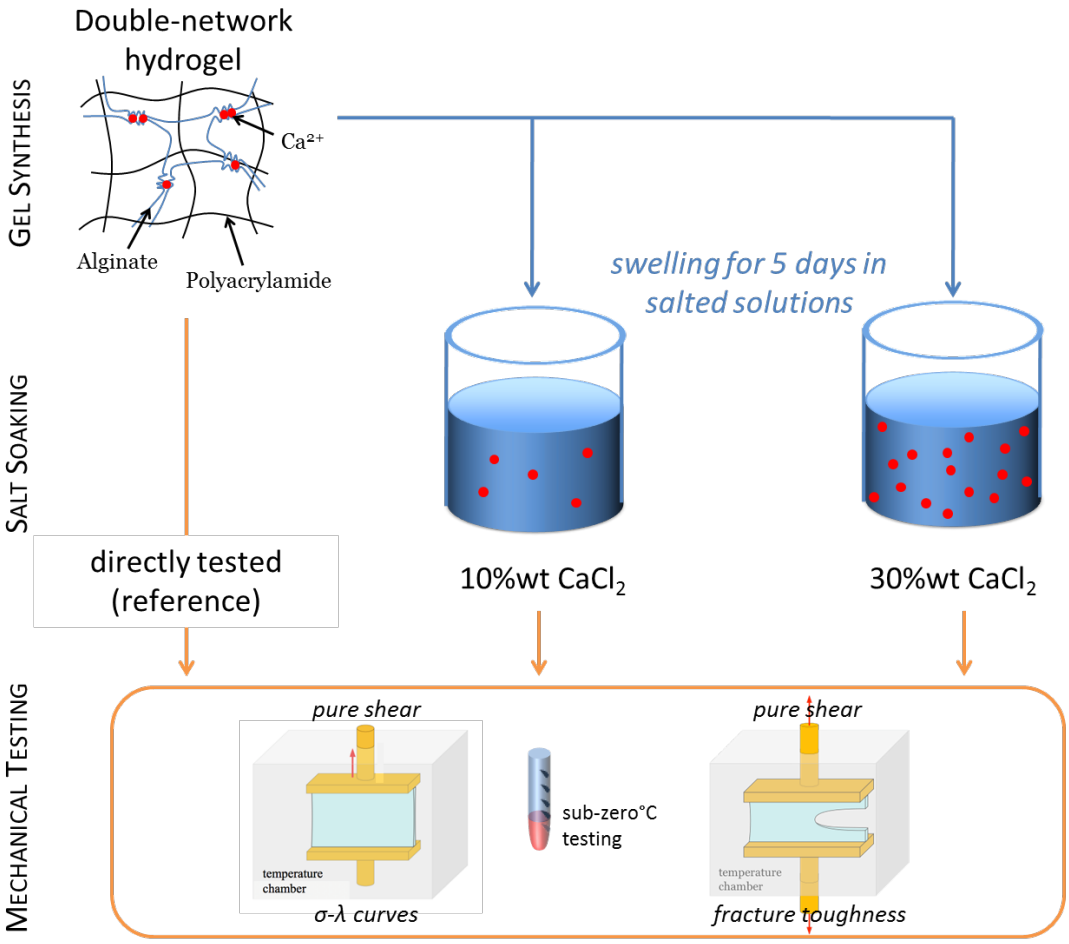

Figure 1.1: Schematics of the preparation and testing of the 3 different batches of gels with different ionic content: 0wt%, 10wt% and 30wt% of $CaCl_2$ respectively.

Temperature	0wt% $CaCl_2$	10wt% $CaCl_2$	30wt% $CaCl_2$
20^0C	9420.6 J/m^2 ± 2166.4	2461.8 J/m^2 ± 108.6	1748.3 J/m^2 ± 494.6
0^0C	6015.1 J/m^2 ± 1553.8	2913.7 J/m^2 ± 787.0	1835.2 J/m^2 ± 253.3
-15^{0}C	2846.1 J/m^2 ± 1090.6	3577.9 J/m^2 ± 455.4	2524.2 J/m^2 ± 253.3
-30^{0}C	542.1 J/m^2 ± 381.2	5127.9 J/m^2 ± 1055.0	3225.3 J/m^2 ± 941.3
-50^{0}C		540.2 J/m^2 ± 301.5	5201.4 J/m^2 ± 549.1
-70^{0}C			58.9 J/m^2 ± 2166.4

Figure 1.2: Average fracture toughness and associated standard deviation for each gel composition over all tested temperatures. A minimum of three (and up to five) specimens of each batch were tested for each temperature.

the hydrogel with 0 wt% $CaCl_2$ is frozen solid, forming an opaque aggregate of ice crystals and polymer chains. The frozen gel is stiff and brittle, and fractures at a relatively small strain (9%). At the same temperature, the hydrogel with 10 wt% $CaCl_2$ is a slurry gel: a gel consisting of a mixture of ice crystals and salt solution embedded in a polymer network. While the gel has lost most of its optical transparency, it remains as stretchable as the 30 wt% gel. The slurry gel behavior occurs over a wide range of temperatures. This observation is consistent with the binary phase diagram of $CaCl_2$ and water (Figure 1.5a), and leads to the experimental phase diagram of the polyacrylamide-alginate double network gel soaked in aqueous $CaCl_2$ solutions shown in Figure 1.5b. The slurry gel state corresponds to the two-phase region in the $CaCl_2$-water phase diagram – both areas are shaded in grey in the respective phase diagrams. As a hydrogel is progressively cooled through the two-phase region, the increasing opacity of the gel reflects the increasing volume fraction of ice crystals.

To construct the phase diagram in Figure 1.5b, we first collected all the experimental observations

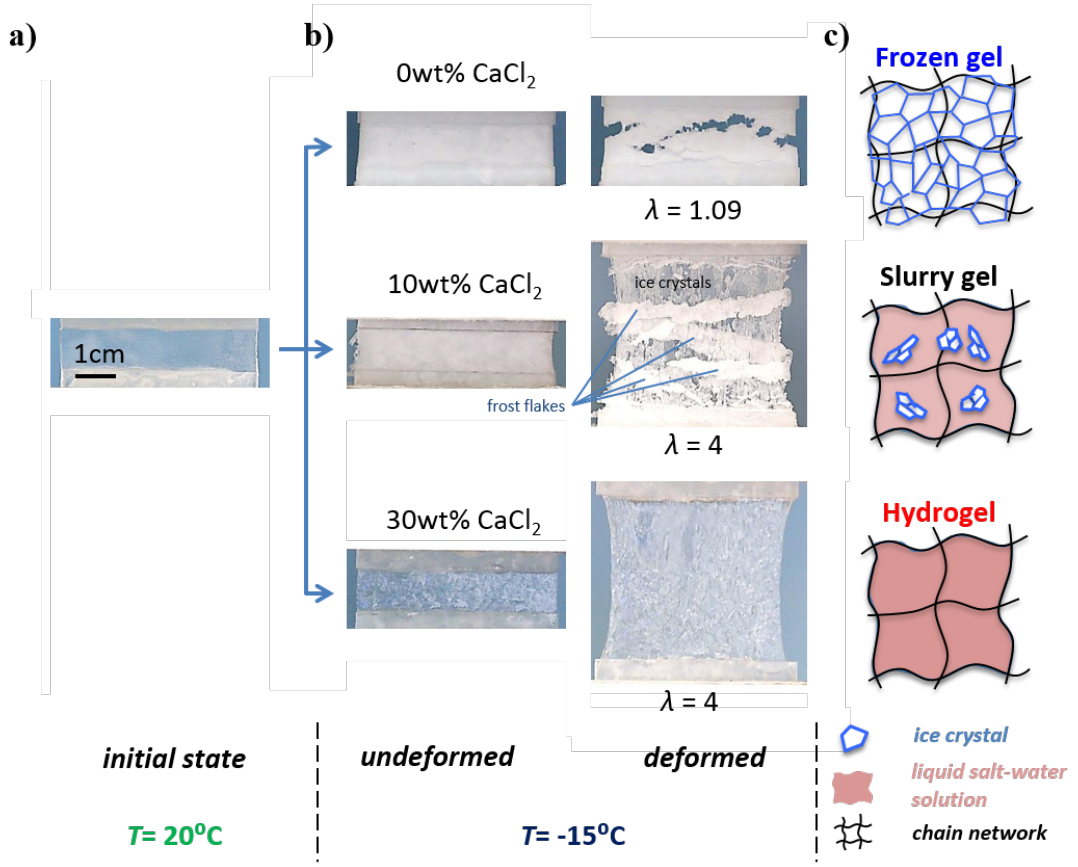

Figure 1.3: Hydrogel behavior in subzero environment illustrated for three different $CaCl_2$-containing gels: a) the initial state at room temperature, b) the undeformed and deformed state at $-15^\circ C$, and c) the corresponding molecular pictures. This illustrates the three physical states for a hydrogel below the freezing point of water: at $-15^\circ C$, the 0 wt% $CaCl_2$ gel is in the frozen state forming an opaque aggregate of ice crystals and polymer chains, the 10 wt% $CaCl_2$ gel is in the slurry state with a mixture of ice crystals and salt solution in a polymer network, and the 30 wt% $CaCl_2$ is in the regular hydrogel state with an aqueous phase in the liquid state. The frozen gel and slurry gel form a frost layer on their surfaces after cooling.

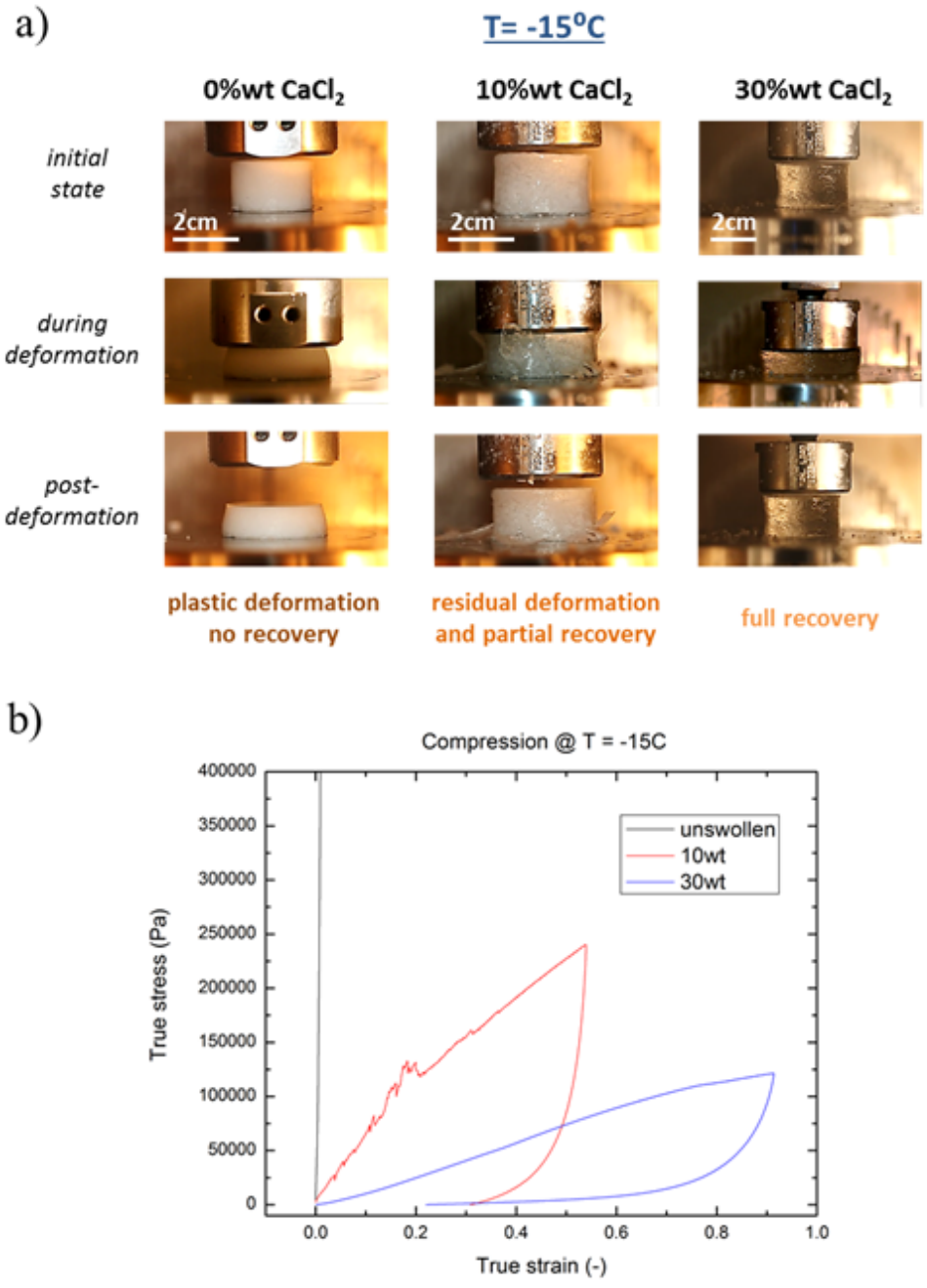

Figure 1.4: Average fracture stretch and associated standard deviation for each gel composition over all tested temperatures. A minimum of three (and up to five) specimens of each batch were tested for each temperature.

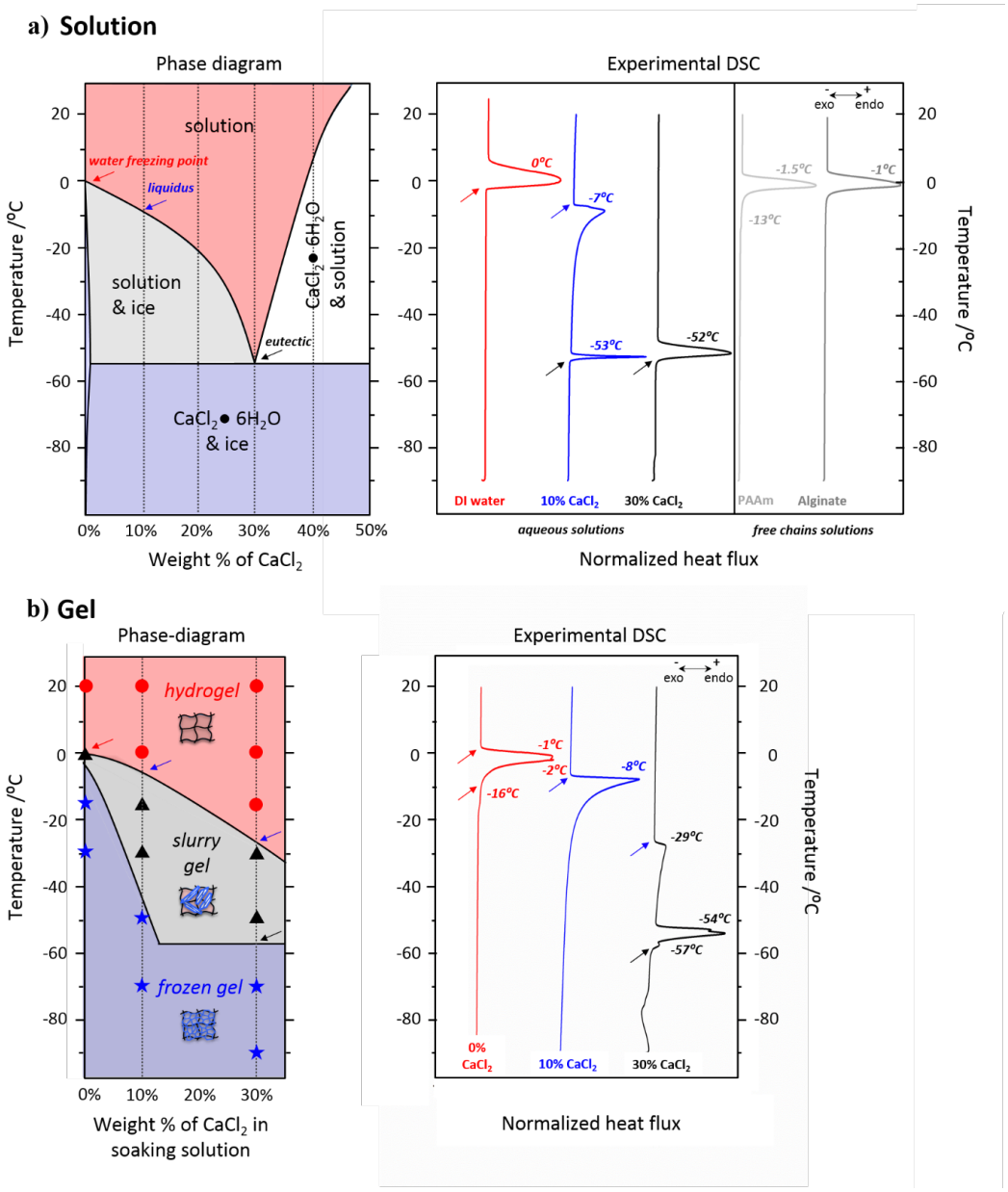

Figure 1.5: Phase diagram and experimental DSC of the aqueous $CaCl_2$ solution and the $CaCl_2$-containing gel. a) aqueous $CaCl_2$ solution case: the theoretical phase diagram (left) is compared to the experimental DSC results (right). b) $CaCl_2$-containing gel case: the experimentally built phase diagram (left) is compared to the experimental DSC results for the three gel compositions (right). The small arrows highlight the correspondence between the phase boundaries in the phase diagram and the fusion enthalpy peaks in the experimental DSC runs.

from the mechanical testing under different temperatures performed on hydrogels soaked in 0wt%, 10wt% and 30wt% $CaCl_2$ solutions, and identified the state of each gel based upon its mechanical response and optical transparency. These observations provided a discrete sampling of the phase diagram, depicted by the symbols in Figure 2b. In a second step, we characterized each gel composition and its various components using differential scanning calorimetry (DSC) from $-90^{\circ}C$ to room temperature to obtain a more accurate measurement of the boundaries of the various phase regions. We also performed DSC analyses on aqueous $CaCl_2$ solutions to identify the phase boundaries for the aqueous system, which were found to be consistent with the reported phase diagram[117] with only minor experimental deviations. Aqueous solutions of polyacrylamide and alginate were independently thermally characterized (Figure 1.5a right) to assess the effect of the polymer chains on the freezing point of the solutions. Comparison of Figures 1.5a and b demonstrates that the DSC curve for the 0 wt% $CaCl_2$ gel can be regarded as the superposition of the curves for its constituents, with a double peak, a small shoulder, and a small shift of the liquidus to lower temperature. These peaks in the DSC curve indicate that the hydrogel behaves like a ternary system rather than a simple binary. The calorimetry data in Figure 1.5b shows that the slurry region of the hydrogel is shifted to significantly higher $CaCl_2$ concentrations compared to the two-phase region of the aqueous $CaCl_2$ solution. Indeed, it is clear from the two distinct and separate peaks of the DSC curve that the 30 wt% $CaCl_2$ gel has not yet reached the eutectic composition. We hypothesize that this shift is the result of interactions of $CaCl_2$ with the alginate and polyacrylamide polymer chains in the gel and an indication that the equilibrium concentration of $CaCl_2$ inside the gel is lower than in the aqueous solution. Indeed, by weighing the fully dried residue of the different gel compositions, we estimated the actual concentration of $CaCl_2$ inside the 10 wt% and 30 wt% $CaCl_2$ gel batches respectively as 5-7 wt% and 20-23 wt% of $CaCl_2$.

Figures 1.6a-c show the evolution of the stress-stretch curves with decreasing temperature for the 0 wt%, 10 wt% and 30 wt% $CaCl_2$ gels, respectively (for complete experimental data, see Figure

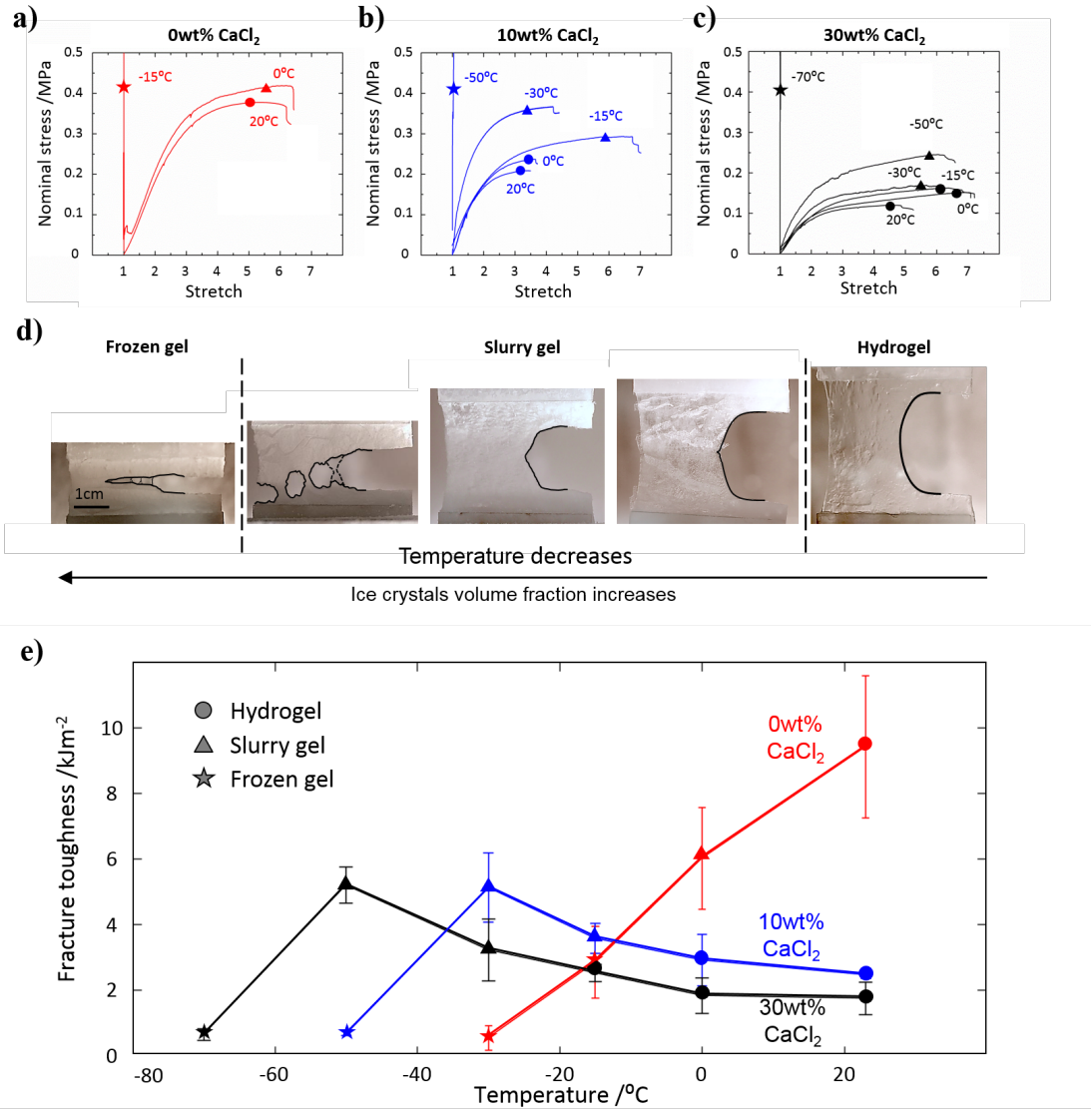

Figure 1.6: Mechanical characterization and fracture patterns of gels with different $CaCl_2$ content as function of temperature. The stress-stretch curves is measured at different temperatures for the three gels: a) 0wt% $CaCl_2$, b) 10wt% $CaCl_2$, and c) 30wt% $CaCl_2$. d) The evolution of crack propagation profile in different $CaCl_2$ containing gels as the temperature decreases, and thus as the volume fraction of ice increases. Gel type and associated testing conditions from left to right are: (i) 30 wt% at $-70^\circ C$, (ii) 30 wt% at $-70^\circ C$ (undercooled), (iii) 10 wt% at -50° (undercooled), (iv) 0 wt% at $0^\circ C$, (v) 30 wt% at $-30^\circ C$. e) The fracture toughness of the three gels is characterized as a function of temperature. For each testing condition, symbols (circle, triangle and star) indicate the corresponding physical state of the gel (hydrogel, slurry and frozen state respectively).

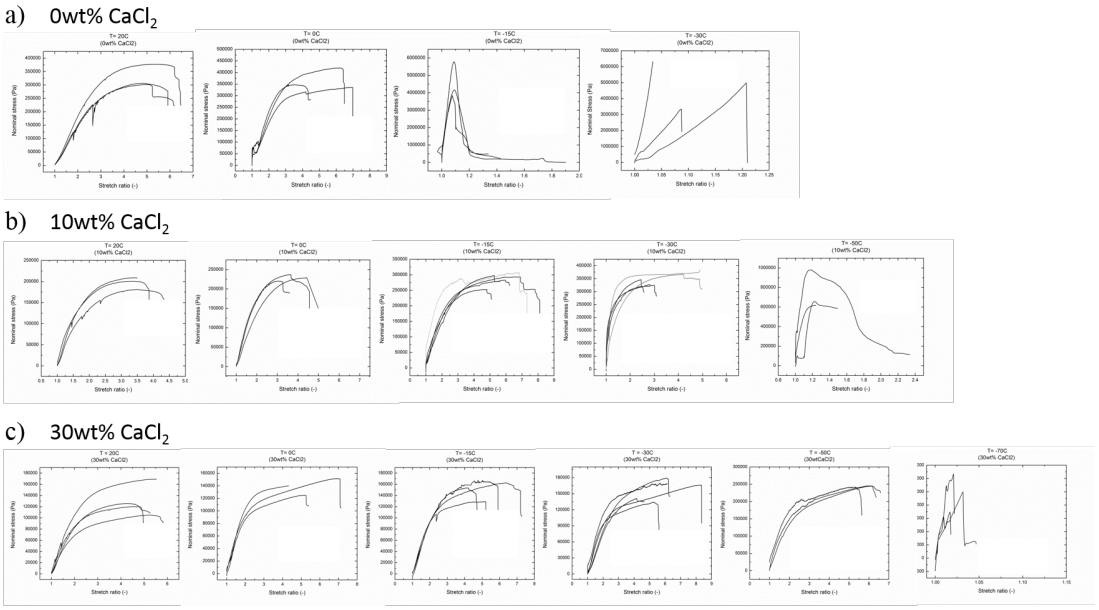

Figure 1.7: The complete experimentally measured stress-stretch curves for each gel composition as a function of temperature: (a) 0wt%, (b) 10wt%, and (c) 30wt% CaCl2.

1.7). At room temperature, the 0 wt% $CaCl_2$ gel has the highest strength and stretchability. When the temperature is reduced to $-15^\circ C$, however, this gel becomes stiff and brittle. The 10 wt% and 30 wt% $CaCl_2$ gels, on the other hand, retain their stretchability at temperatures down to at least $-30^\circ C$ and $-50^\circ C$, respectively. For all gels, both the elastic modulus and the strength gradually increase as the temperature decreases. This stiffening effect can be explained by the gradual increase of the volume fraction of ice crystals in the slurry gel (Figure 1.6d). The ice crystals stiffen the gel, while still allowing large deformation to occur through shear yielding between them, similar to the toughening of polymer nanocomposites[126,127,128,129]. Interestingly, the presence of ice crystals tends to improve the stretchability before the gels become brittle (see evolution of fracture stretch in Table 1.8). A careful inspection of post-mortem specimens showed a large number of micro-sized cavities dispersed throughout the specimens (Figure 1.10). These micro-cavities may nucleate due to the triaxial state of stress that builds up around stiff ice crystals. A similar mechanism of cavitation and fracture

has been reported in adhesively bonded elastic and viscoelastic layers[130,131,132]. From the study of adhesively bonded materials, cavitation first appears when the hydrostatic stress is approximately ten times larger than the shear modulus of the elastic layer[132]. The cavities grow and eventually coalesce, leading to catastrophic cohesive failure of the adhesive layer[130,131]. Growth of these cavities provides an additional energy dissipation mechanism that may explain the increased stretchability observed in the slurry state. This mechanism leads to the apparent "ductile" failure mode mechanism with macroscopic void growth and coalescence observed experimentally in specimens with large volume fractions of ice in the slurry state (see Figure 1.6d). Further investigation showed that the nucleation of these micro-cavities is also facilitated by the application of repeated cooling cycles to very low temperature. Indeed, repeated formation of ice crystals eventually leads to a permanent weakening of the gel network, creating local defects that facilitate the nucleation of cavities upon deformation. To characterize the fracture toughness of the gels as a function of temperature, we measured the stress-stretch curves of notched specimens and determined the critical stretch at which fast fracture takes place (Table 1.8). We calculated the corresponding energy release rate by integrating the area under the nominal stress-stretch curve of a pure shear specimen without a pre-crack (from Figure 1.6a, b and c) up to the critical stretch of the notched specimens, following the method devised by Rivlin and Thomas[8,133]. The results show the temperature dependence of the fracture toughness for each gel (Figure 1.6e and Table 1.2). As expected, the fracture toughness of the 0 wt% $CaCl_2$ gel reduces dramatically as the temperature is lowered below $0°C$. By contrast, the fracture toughness of the 10 wt% and 30 wt% gels increases as the gels enter the slurry state. The fracture toughness of these gels eventually drops as the gels are fully frozen. For all gels, the slurry state exhibits a relatively high toughness, ranging from 3000 to 6000 Jm^{-2}. In practical applications, the amount of salt added to a hydrogel can be adjusted to fulfill the requirements in terms of modulus, stretchability, and fracture toughness depending on the targeted temperature range.

In order to better understand the toughening mechanism associated with the slurry gels, we com-

Temperature	0wt% $CaCl_2$	10wt% $CaCl_2$	30wt% $CaCl_2$
20^0C	5.03 ± 0.25	3.42 ± 0.10	4.86 ± 0.62
0^0C	5.55 ± 1.79	3.70 ± 0.71	5.48 ± 1.33
-15^0C	1.08 ± 0.01	5.88 ± 0.86	5.03 ± 0.73
-30^0C	1.07 ± 0.03	3.39 ± 0.95	5.93 ± 1.53
-50^0C		1.16 ± 0.03	5.75 ± 0.59
-70^0C			1.08 ± 0.10

Figure 1.8: Average fracture stretch and associated standard deviation for each gel composition over all tested temperatures. A minimum of three (and up to five) specimens of each batch were tested for each temperature.

pare the crack propagation and failure scenarios in the three states of the hydrogel (Figure 1.9). A regular hydrogel fails through the propagation of a large blunted crack (Figure 1.9c). Slurry gels and frozen gels, however, exhibit significantly different failure mechanisms. In the frozen gel, a sharp crack propagates rapidly through the specimen once it is loaded, following the straightest and weakest path between ice crystals, resulting in a relatively low fracture toughness (Figure 1.9a). The fracture behavior of slurry gels varies depending on the amount of ice crystals in the gel, but is typically characterized by crack pinning and deflection as the crack path encounters stiff ice crystals. Such features, observed in all slurry gels, lead to a discontinuous crack propagation, and sometimes a less blunted crack tip compared to the regular hydrogel state (Figure 1.9b right). The final fracture path in a slurry gel tends to zigzag and creates rough crack surfaces. The amplitude of that zigzag and the degree of roughness of the crack surface varies depending on the ice volume fraction (i.e. the higher the volume fraction, the larger the zigzag). More specifically, in some slurry gels with a large volume

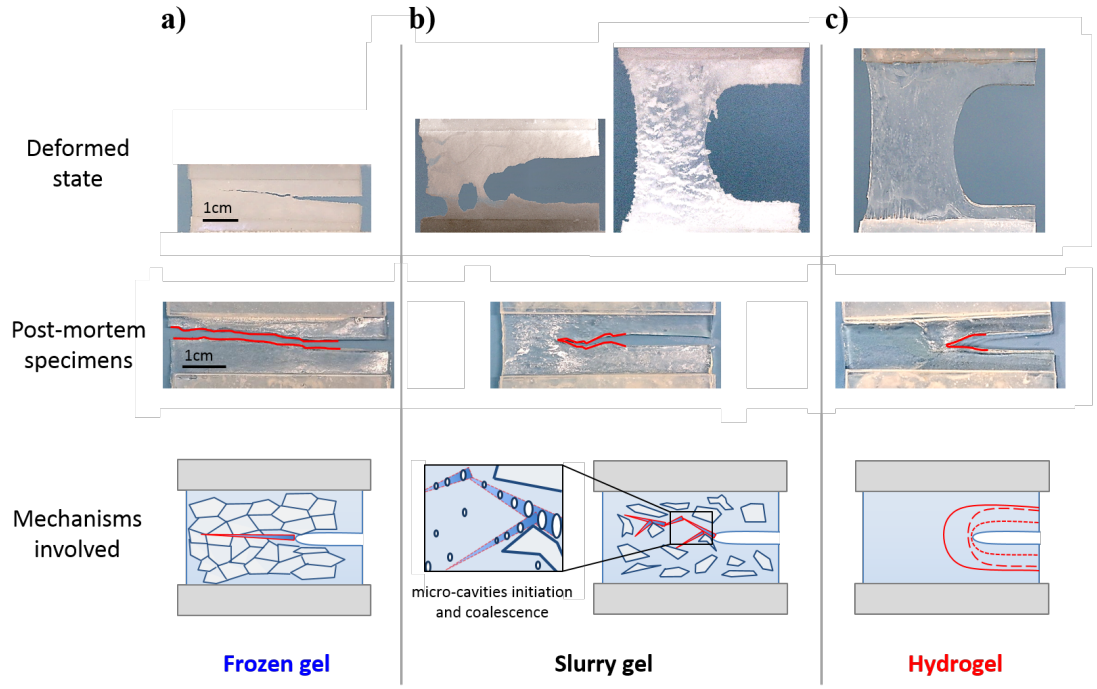

Figure 1.9: Different failure scenarios and the associated fracture mechanisms in the three states of a gel. a) For a frozen gel, brittle fracture occurs by fast propagation of a sharp crack following the straightest and weakest path between ice crystals. b) For a slurry gel, the fracture varies with the volume fraction of ice crystals, but typically shows a stick-slip propagation following a zig-zag path. A relatively large not fully blunted crack opening is observed (the middle and top right picture). Crack pining, crack deflection and micro-cavitation have been identified as associated toughening mechanisms, sometimes leading to the coalescence of multiple macro-cracks in some samples (top left). c) For a regular tough hydrogel, a large blunted crack is observed during the crack propagation. The gels shown here to illustrate the fracture scenario of each of sub-water-freezing state of gels have been tested with the following conditions, from left to right: (a) 0 wt% $CaCl_2$ at $-50^\circ C$, (b-left) 30 wt% $CaCl_2$ at $-70^\circ C$ (undercooled), (b-right and crack path) 10 wt% $CaCl_2$ at $-30^\circ C$, and (c) 30 wt% $CaCl_2$ at $-30^\circ C$.

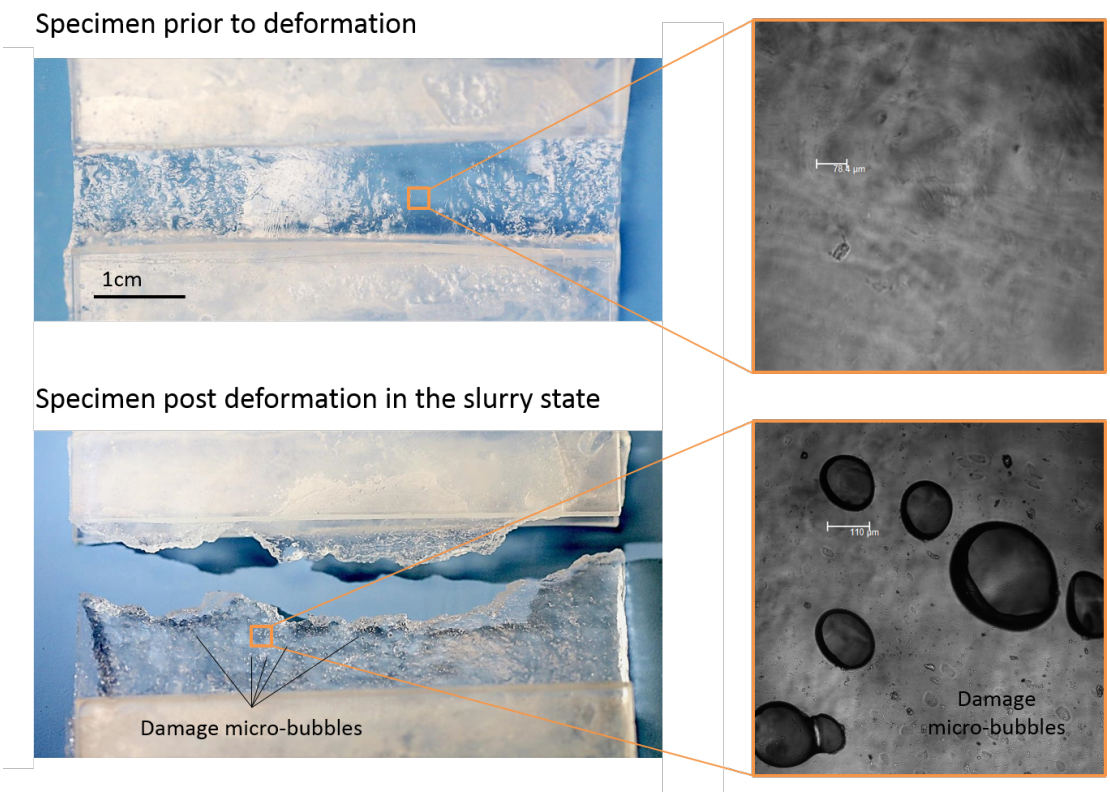

Figure 1.10: Illustration of dispersed micro-damage bubbles observed ahead of the crack tip after deformation of a 0wt% $CaCl_2$ gel at $0^\circ C$ in the slurry state. After deformation (and fracture) in the slurry state (see phase diagram of Figure 2b), we observed many micro-bubbles dispersed all over the post-mortem specimen, highlighting the important micro-cavitation occurring during deformation as a result of the triaxial state of stress between ice-crystals. We used a confocal microscope (Leica TCS-SP5) with an Argon laser of 488nm band to capture the micro-sized cavities in the gel after deformation.

fraction of ice, multiple macro-cracks grow upon loading, and eventually coalesce (Figure 1.9b left). These macro-cracks are assumed to initiate at the dispersed micro-cavities observed ahead of the crack tip (Figure 1.10) as mentioned earlier.

During the experiments, we observed significant undercooling of the slurry gels below the eutectic temperature, which can have a significant impact on the stability of subzero mechanical behavior of hydrogels. As shown in Figure 1.11, a 30 wt% $CaCl_2$ gel can stay in an undercooled slurry state, and exhibit high stretchability and fracture toughness at temperatures as low as $-70^\circ C$ if it is not

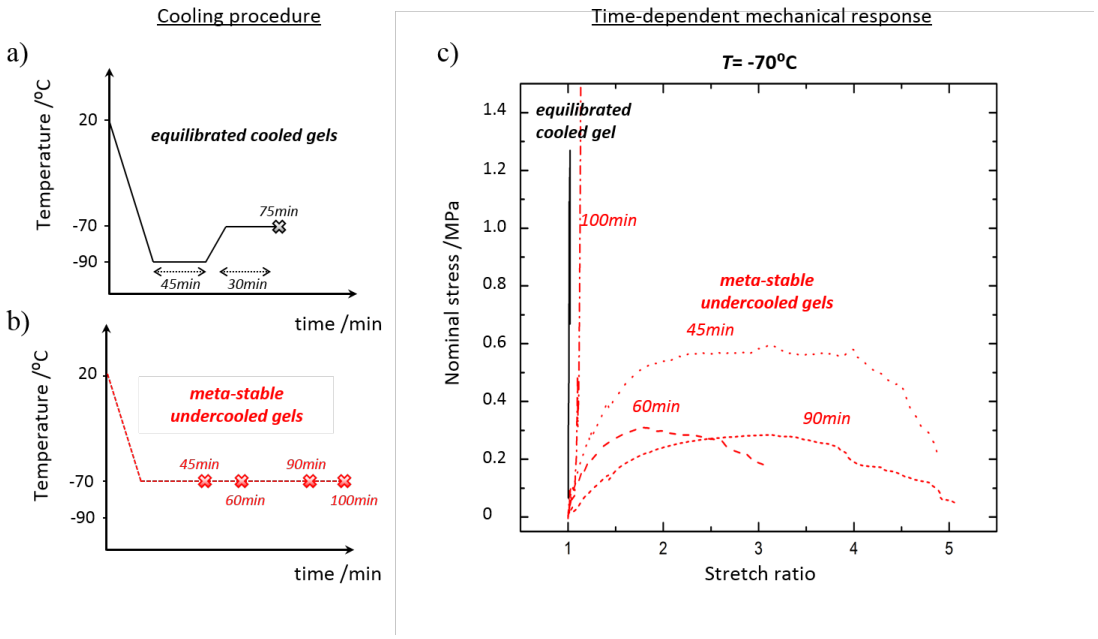

Figure 1.11: Time dependent stress-stretch curves of metastable undercooled 30wt% $CaCl_2$ gels at $-70^\circ C$: (left) two different temperature profiles for the cooling procedures of (a) equilibrated cooled gels versus (b) metastable undercooled gels with different cooling time at $-70^\circ C$ before testing; (c) the corresponding stress-strain curves, showing inconsistent and variable mechanical response for undercooled specimens. Waiting long enough at $-70^\circ C$ will eventually make the gel reach the equilibrated gel response.

cooled down long enough to reach thermodynamic equilibrium. The undercooled gels are thermodynamically unstable, and consequently have stress-stretch curves that vary inconsistently with the storage time at -70°C (see Figure 1.11c). To avoid this undercooling effect, all the testing specimens in this study were first cooled to $-90^\circ C$ for 45 minutes before heating them to the target testing temperature. To conclude, the slurry state of $CaCl_2$-containing hydrogels at subzero temperatures can indeed provide unforeseen mechanical property improvements, but caution must be taken to ensure that the material is not in a thermodynamically unstable state due to a kinetic delay of the crystallization process.

The $CaCl_2$-containing gels maintain their ionic conductivity at temperatures well below the freezing point of water (Figure 1.12a). This ability, together with their high stretchability and toughness

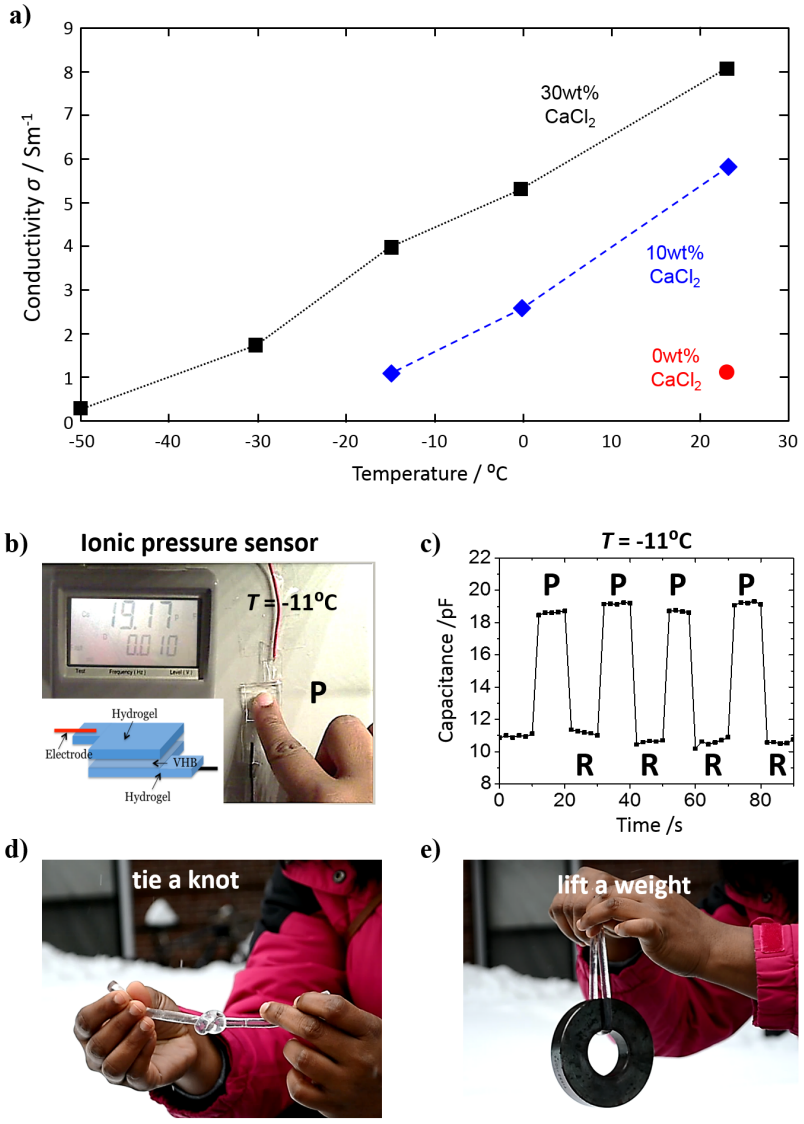

Figure 1.12: Applications of the stretchable, tough and anti-freezing hydrogel at low temperature. a) The conductivity as a function of temperature for the 0wt%, 10wt% and 30wt% $CaCl_2$ gels. b) A stretchable ionic touch sensor is fabricated by sandwiching a layer of dielectric elastomer (3M VHB) between two layers of 30wt% $CaCl_2$ gels. c) The capacitance changes at $-11^{\circ}C$ by a finger press and release. 'P' denotes finger press and 'R' denotes release. d) and e) demonstrate the good stretchability and strength of a 30wt% $CaCl_2$ gel in outdoor snowing conditions. The weight used is 2.5lbs (1.13kg).

at low temperatures, opens up a range of applications in low-temperature environments. Here, we demonstrated a simple ionic touch sensor that takes advantage of both attributes. The touch sensor consists of a dielectric elastomer layer sandwiched between two hydrogel layers (Figure 1.12b). The hydrogel layers consist of 30 wt% $CaCl_2$ hydrogels, while the elastomer is VHB 4905 (3M, Maplewood MN). The architecture of the touch sensor is based on a sensor described previously by Sun et al.[38] Figure 1.12c illustrates the response of the sensor when operated at a temperature of $-11°C$. The capacitance of the sensor changes reversibly by approximately 50% upon touching, which is readily measured using a capacitance meter. The response of the sensor does not degrade when cycled repeatedly at subzero temperatures. One can readily envision use of this sensor in applications under a broad range of environmental conditions, including stretchable and rollable keypads and pressure sensors for soft robotics.

1.3 Conclusion

In summary, we have developed a class of hydrogels that retain high stretchability, high fracture toughness and good conductivity at temperatures far below the freezing point of water. We adopted a well-known strategy for depressing the freezing point of water and applied it to a tough hydrogel by soaking the gel in various aqueous solutions of $CaCl_2$. The experimental phase diagram of the $CaCl_2$-containing hydrogel differs slightly from that of the aqueous $CaCl_2$ solution due to the presence of the polymer network. Depending on the temperature and the $CaCl_2$ content, the gels can be classified into three types: regular hydrogel, slurry gel, and fully frozen gel. We measured the stress-stretch curves and fracture toughness of the hydrogel as a function of temperature and $CaCl_2$ content. Slurry gels exhibit the highest toughness at a given temperature. We attributed this observation to the introduction of additional toughening mechanisms in the slurry gels, which include crack pinning, crack deflection, and energy dissipation through micro-cavitation. Finally, we

demonstrated a stretchable ionic touch sensor that functions at temperatures well below the freezing point of water. We anticipate that this class of hydrogels will enable a broad range of applications under low-temperature conditions.

1.4 Acknowledgements

This chapter was based on work that has been published in a scientific journal[110].

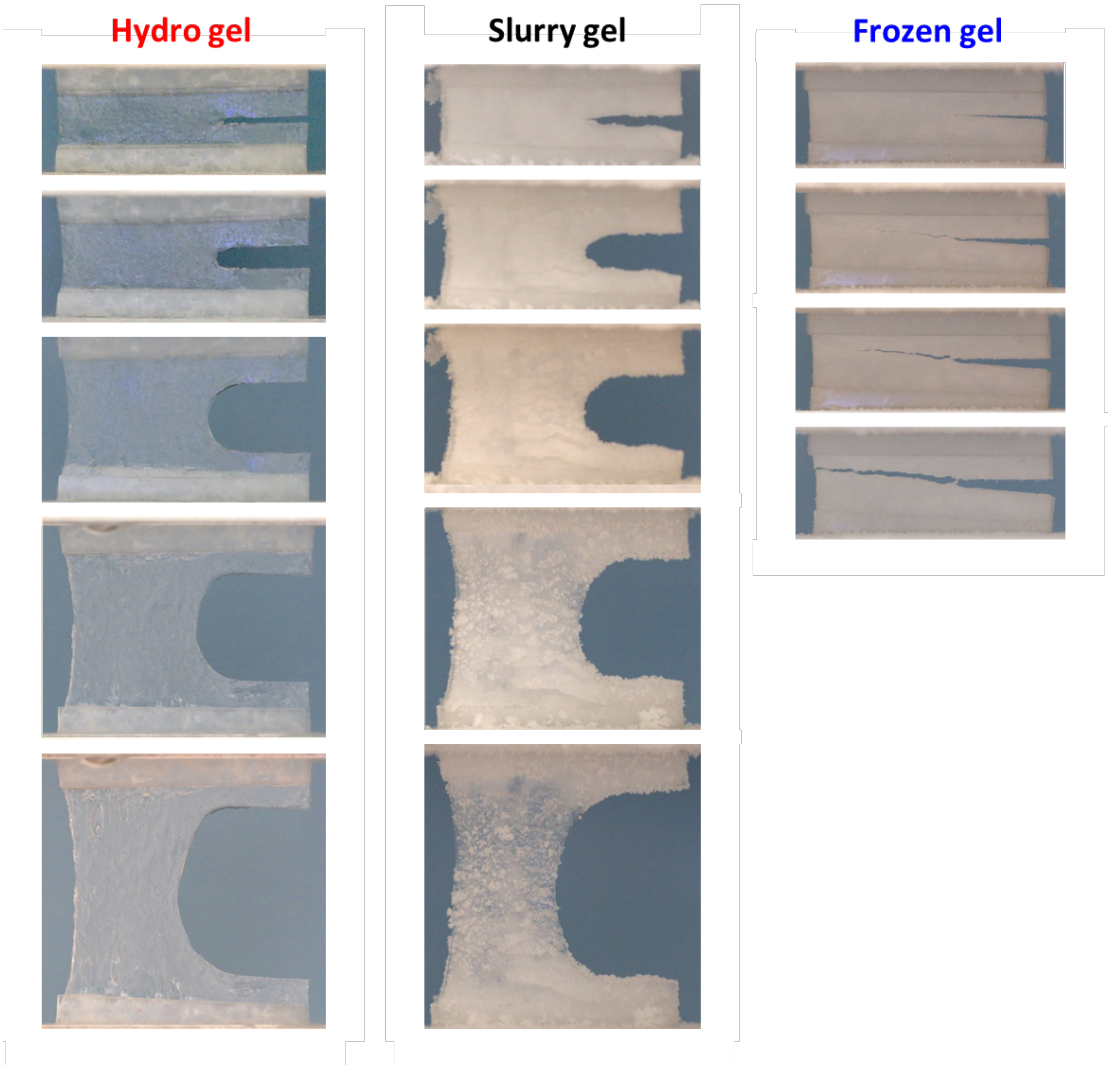

Figure 1.13: The progressive crack propagation in the 3 different states of gels below water-freezing temperature: (a) Hydrogel (10wt% $CaCl_2$ gel at $0^\circ C$); (b) Slurry gel (30wt% $CaCl_2$ gel at $-50^\circ C$); (c) Frozen gel (0wt% $CaCl_2$ gel at $-30^\circ C$).

A journey of a thousand miles begins with a single step.

Laozi

2

Adapting Salt-hydrogels for 3D Printing

2.1 Introduction

Interest in stretchable electronics has grown significantly in recent years, driving a need for soft and stretchable materials that can sustain high strains and still fulfill their function in applications such as human wearable sensors for biomechanics studies and health monitoring[16,17,18,19], or feedback sensors in soft robotics[20,21,22,23]. Although many stretchable conductors exist, including liquid met-

als[24,25], nanowires[26,27], nanoribbons[28], pre-stretched elastomer fibers with conductive coatings[29], and micro-cracked metals[30,31], these materials have generally been unable to achieve high levels of optical transparency while maintaining high conductivities and stretchability; a feature that would enable their use in optogenetics[32] or allow optical imaging of the underlying substrate. Conventional strategies of incorporating metallic components with elastomers to attain stretchability also yield non-trivial failure modes such as liquid metal leakage[23] and hard-soft material interfacial failure[33]. The use of gels as conductors, where ions are the charge carriers instead of electrons, represents an entirely different approach that has gained popularity recently. Their high stretchability and transparency, when combined with recent improvements in toughness and stiffness[8,7], have already enabled their use as stretchable electrical conductors,[34,35] capacitive strain sensors[38,39,36], and chemical/pH sensors[42]. Gel-based ionic circuits thus represent a unique class of devices within stretchable electronics. Conductive gels can be generally divided into those where the ions are provided by solvated salts[36,125] (hydrogels) or by ionic liquids[39,134,135] (ionogels). Although immune to dehydration, ionogels have comparatively lower conductivities than hydrogels. Ionic liquids also interfere with some gel polymerization reactions, limiting the range of polymers that can be used to synthesize ionogels.[136] By contrast, hydrogels are generally easier to synthesize, but they are susceptible to dehydration. Solvated hygroscopic salts may serve the dual purpose of increasing both their ionic conductivity and water-retention properties,[125] though a balance must be struck between maximizing water-retention and ionic conductivity due to non-idealities of the electrolyte solution that reduce molar conductivity at high salt concentrations.[137]

Fabrication of stretchable electronics using hydrogels requires integrating hydrogels with stretchable dielectrics such as dielectric elastomers; a process thus far primarily achieved via manual assembly of cast segments. If the field is to progress, advanced manufacturing techniques that integrate dielectric elastomers and hydrogels need to be developed.[22] Fabrication techniques specific to hydrogels have already been developed, including extrusion three-dimensional (3D) printing,[39,69,62,63,60]

digital projection based techniques,[52] and screen printing[54,55]. Extrusion printing techniques in particular are most easily capable of multi-material printing at high resolution and low costs.[62,63] Recently, Robinson et al. fabricated a soft sensor with an ionic-liquid based gel and a silicone elastomer by combining soft lithography with extrusion printing.[39] Although recent studies have successfully fabricated stretchable electronics consisting entirely of soft materials, conductive hydrogels and dielectric elastomers, thus far these fabrication techniques have relied on casting or a combination of extrusion printing with other methods.[34,35,38,39,36]

Here, we describe a simple approach to 3D extrusion printing of soft, stretchable electrical devices integrating a conductive hydrogel and a dielectric elastomer with sub-millimeter resolution. We show that both types of materials can be integrated into a single device using a single fabrication process. We characterize the mechanical and electrical performance of the printed hydrogel and demonstrate the technique by printing a soft strain sensor. The device was fabricated using poly(acrylamide) (PAAm) hydrogel and poly(dimethylsiloxane) (PDMS) because of their widespread use, as well as their favorable electrical and optical properties. The hydrogel precursor consisted of a concentrated aqueous solution of a hygroscopic salt, a compatible rheological modifier, and UV-initiated polymerization/cross-linking compounds. Lithium chloride (LiCl) was selected as the hygroscopic salt in a compromise between vapor pressure and ionic conductivity, and its concentration (7 mol L-1) was set above peak conductivity, but below saturation in an aqueous solution.[138] The PDMS was a UV curing formulation to allow for rapid setting during the printing process (KER-4690, courtesy of Shin-Etsu Silicones).

2.2 Methods

Printing was performed using an extrusion 3D printer comprised of a precision positioning system, an ink extrusion system, and a hardware/software interface to control location and rate of material

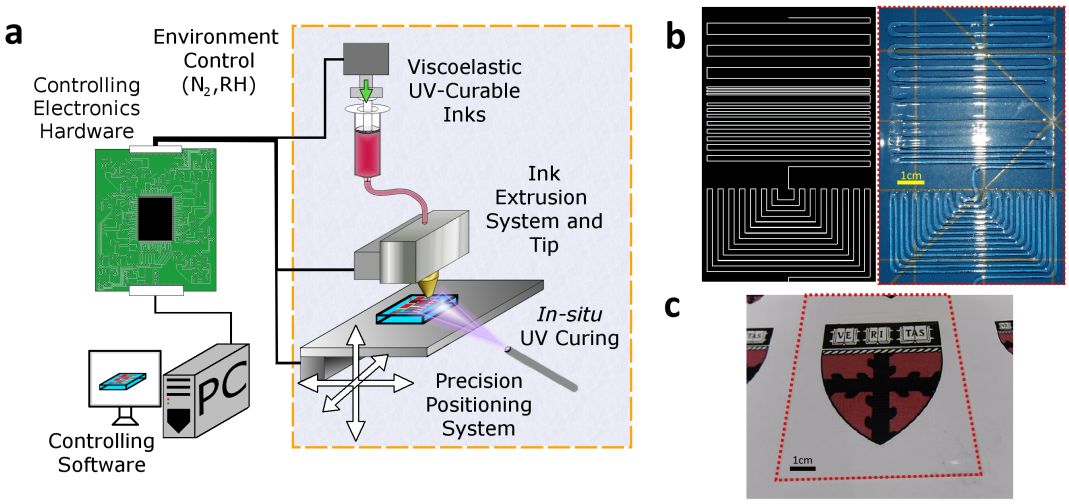

Figure 2.1: a) Overall schematic of the 3D printing extrusion system used in this study. b) A side-by-side comparison of a patterned design and the final printed hydrogel-on-PDMS sample. c) The same printed sample placed over an image to demonstrate its complete optical transparency.

extrusion relative to the sample stage (Figure 2.1).[62] The entire system was housed inside a nitrogen environment. The relative humidity (RH) of the environment was fixed at 43% by bubbling nitrogen through a saturated solution of potassium carbonate.[139] Significant variations in RH during the fabrication process can lead to elastic instabilities in the hydrogel surface as a result of hydrogel swelling,[140] which can happen very quickly because of the high surface area to volume ratio of sub-millimeter features. Oxygen displacement was needed to prevent inhibition of the free-radical polymerization in the hydrogel precursor. In situ UV curing was used to partially set the extruded ink and prevent extensive spreading. This process is further elaborated during the discussion of rheological characteristics of the hydrogel precursor. Figure 2.1b demonstrates our printing capabilities of complex hydrogel-elastomer designs by comparing the final printing shape to its printing trace and Figure 2.1c highlights the optical transparency of the printed devices.

Selecting materials for extrusion printing requires the consideration of their rheological properties, since these properties dictate extrusion pressure, post-extrusion shape retention, and printing

resolution. A shear-thinning characteristic is particularly desirable for extrusion, allowing for lowered viscosity under the high shear rates involved in extrusion and a higher viscosity post-extrusion for shape retention. Shear thinning is usually achieved through the addition of a rheological modifier, of which many are commercially available.[141] For this particular application, where the elastomer serves as a bulk dielectric as opposed to finer features, the resolution requirements for the extrusion printing of the PDMS are not as stringent as for the hydrogel. Consequently, the UV-curing PDMS formulation could be used without modification, despite its almost Newtonian behavior with viscosities of $4.8 Pa\,s$ at $10^{-1}\ s^{-1}$ and $4.5 Pa\,s$ at $10^{2}\ s^{-1}$. For applications where a higher resolution is required, many techniques and products are available to adjust the rheological behavior of the PDMS precursor.[20,39,142,143,144,145,146]

The development of the hydrogel precursor for our extrusion printing was more demanding and required a balance between conductivity, stability, and rheological characteristics. A significant proportion of rheological modifiers used in extrusion printing are sensitive to the ionic strength of the precursor,[62,63,147,61] and may lead to precipitation[148,149,150] or flocculation[151] of the rheological modifiers at the high salt concentrations necessary for good electrical conductivity and water retention. This requirement excludes many of the modifiers that are routinely used for hydrogel printing. High-molecular weight polymers, however, are insensitive to the ionic strength of the precursor and have been used successfully in hydrogel extrusion printing.[39,60] In this study, we use high-molecular weight PAAm as a rheological modifier, because of its transparency and compatibility with the precursor formulation.

2.3 Results and Discussion

The rheology of the PAAm / LiCl solution used to modify the flow characteristics of the precursor was characterized by measuring its viscosity (η), yield stress (σ_y), and viscoelastic moduli (G, G). The

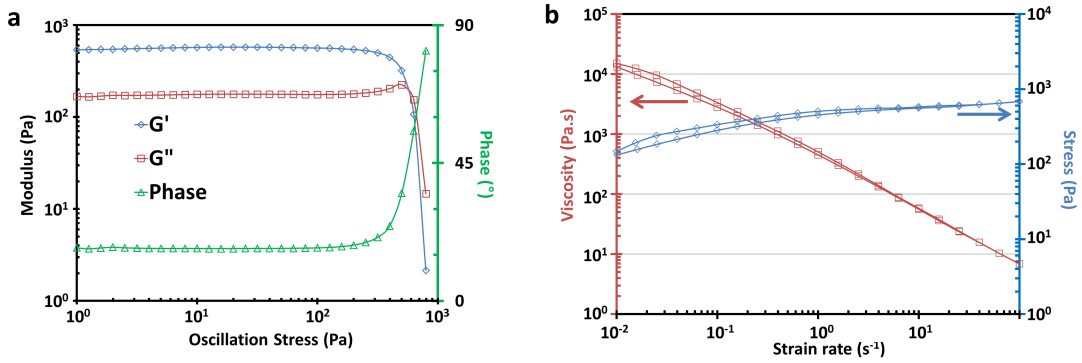

Figure 2.2: Rheological analyses of the rheological modifier for the hydrogel precursor. a) Typical oscillatory rheology results showing shear storage (G') and shear loss (G") moduli evolution of inks used over increasing shear stress. b) Typical viscometry results showing stress and viscosity against shear rate. Tests were begun at low shear rates and swept up, then back down to demonstrate a mild thixotropic effect.

precursor rheology is dominated by the PAAm; all other components in solution do not affect the viscosity significantly at their respective concentrations. We performed both viscometry and oscillatory rheology (Figure 2.2) at 25 *C*. The storage modulus (G) plateaus at a modulus of 558.5 ± 4.6 *Pa* and exceeds the loss modulus (G) at shear stresses below 570 *Pa*, indicating solid-like behavior up to this stress level (Figure 2.2a); at stresses greater than 570*Pa*, G exceeds G and the precursor behaves more like a viscous liquid. Thus, the precursor has an apparent oscillatory yield stress of 570 *Pa*. Figure 2.2b depicts the stress and viscosity as a function of shear rate obtained from viscometry measurements. The viscosity shows clear shear-thinning behavior with $\eta \sim 15000$ *Pa s* at low shear rates ($10 - 2\ s^{-1}$) and $\eta \sim 5$*Pa s* at high shear rate ($10^2\ s^{-1}$). Extrapolating the linear portion of the stress-shear rate curve back to zero shear rates provides a Bingham yield stress of 458 *Pa*, which agrees well with the cross-over between G and G.

We estimate the shear-rate during extrusion using the generalized form of the Rabinowitsch-Mooney equation (Equation 2.1) for a power-law fluid flowing through a cylindrical tube of radius r,[152]

$$\gamma = \frac{3n+1}{4n}\frac{4Q}{(\pi r^3)} \tag{2.1}$$

where Q is the volumetric flow rate and n is the exponent of the power-law describing the shear stress as a function of shear-rate, $\tau = K\gamma^n$, where K is the consistency index. By performing a power-law fit of the data in Figure 2.2b, we obtain a value of 0.148 for the shear-thinning exponent n in the high-strain rate region ($\gamma > 1\, s^{-1}$). For a volumetric extrusion rate of $1\, mm^3 s^{-1}$ and a 0.337 mm syringe tip diameter, the shear rate $\dot{\gamma}$ of the hydrogel precursor is $\sim 81\, s^{-1}$, with a corresponding viscosity of $\sim 7\, Pa\, s$. Immediately after extrusion, the viscosity increases to approximately $1300 Pa\, s$, assuming a shear rate of $0.1\, s^{-1}$. Other studies have achieved extrusion printing with viscosities of $10\, Pa\, s$ at $10^2\, s^{-1}$ and $10^2 10^3\, Pa\, s$ at $0.1\, s^{-1}$ strain rates[39,62,60,61]. Typical values for oscillatory rheological parameters in hydrogel extrusion printed inks place $G \sim 3503000\, Pa$ and $\sigma y \sim 500 - 3000\, Pa$.[39,60] Our precursor hydrogel compares favorably with these other systems in terms of rheological performance. However, the precursor viscosity/G' values are insufficient to ensure printed shape retention over long periods of time. Since the hydrogel is UV curable, the simplest solution is to implement in situ UV curing during the extrusion printing process to partially cure the inks as they are extruded from the syringe tip (Figure 2.1). Various hydrogel line geometries were generated by printing line stacks in both the lateral and vertical directions (Figure 2.4a), specified as the x and z-directions respectively, at constant extrusion rate, stage velocity, and lateral/vertical center-to-center spacing ($6.0\, mm^3 s^{-1}$, $7.5\, mms^{-1}$, $S_x = 0.3\, mm$ and $S_z = 0.15\, mm$ respectively). To precisely design 3D structures of hydrogel printed directly on PDMS, we characterized the geometry of the printed hydrogel structures in terms of the number of lines (N_x and N_z) in the x and z-directions, respectively (Figure 2.4b-c). We note that the degree of spreading in the x-direction increases with N_z, but that the spreading saturates once three layers have been printed, indicating that building up stable 3D structures is possible. The spreading of the hydrogel precursor post-extrusion is governed by a balance between capillary, viscous, and inertial forces acting on the extruded geometries. We may determine the dominant force using the Ohnesorge number,[153] $Oh = \eta/\sqrt{\varrho\gamma L}$, where, γ is the surface energy, ϱ is the mass density, and L the characteristic length

scale. Using conservative values, $\eta \sim 10^3\ Pa\,s, \gamma \sim 0.1\ Jm^{-2}, \varrho \sim 10^4\ kgm^{-3}$, and $L \sim 10^{-3}\ m$, we observe that $Oh \sim 10^3 \gg 1$, indicating dominance of the viscous forces, as expected by the rheological design of the hydrogel precursor. The minimum level of lateral spreading was 0.8 *mm*, which can be observed by extrapolating Figure 2.4c to the y-intercept. This value can be decreased further by tuning the precursor rheology, increasing the in situ UV curing intensity, lowering the extrusion rates (Figure 2.3), increasing the stage speed, or by utilizing a smaller size of syringe tip. Optical micrographs of multi-layer gel patterns showed smoothly merged surfaces (Figure 2.4d-f) and the formation of what are believed to be residual wetting layers on the hydrogel edges. Optical profilometry was used to obtain cross-sectional profiles of the printed hydrogel lines (Figure 2.4g-h), which demonstrate that these profiles are nearly identical, indicating the reproducibility necessary for us to design and build 3D hydrogel structures.

Electrical testing of bulk cast hydrogel samples was conducted using a four-point probe configuration to establish the baseline electrical conductivity of the hydrogel. As shown in Figure 2.5a, we observed Ohmic conduction with a conductivity of $10.39 \pm 0.31\ S\,m^{-1}$, which is comparable to the conductivity of the corresponding aqueous salt solution.[138] By contrast, the conductivity of the printed lines, measured under conditions of controlled humidity at RH 43%, was found to be $2.90 \pm 0.40\ S\,m^{-1}$. This value is markedly lower than the bulk conductivity, but is most likely due to water loss post-extrusion. Although hydrogel water loss in open air will not be entirely avoided without the use of a sealant, such as by coating the hydrogel in an elastomer, the LiCl will allow the hydrogel to remain stable at a RH determined by the salt species and concentration. An aqueous LiCl solution increasing in mass percentage from 20% to 30% suffers a conductivity loss of 14%[138] and the volumetric change from water loss alone would cause a 62% decrease in cross-sectional area, which together approximates conductivity loss to be at least 48%. We characterized the resistance change of printed hydrogel lines printed on PDMS upon application of uniaxial tensile strain. The ideal case can be reasoned as follows: we let R and L, respectively be the resistance and length of

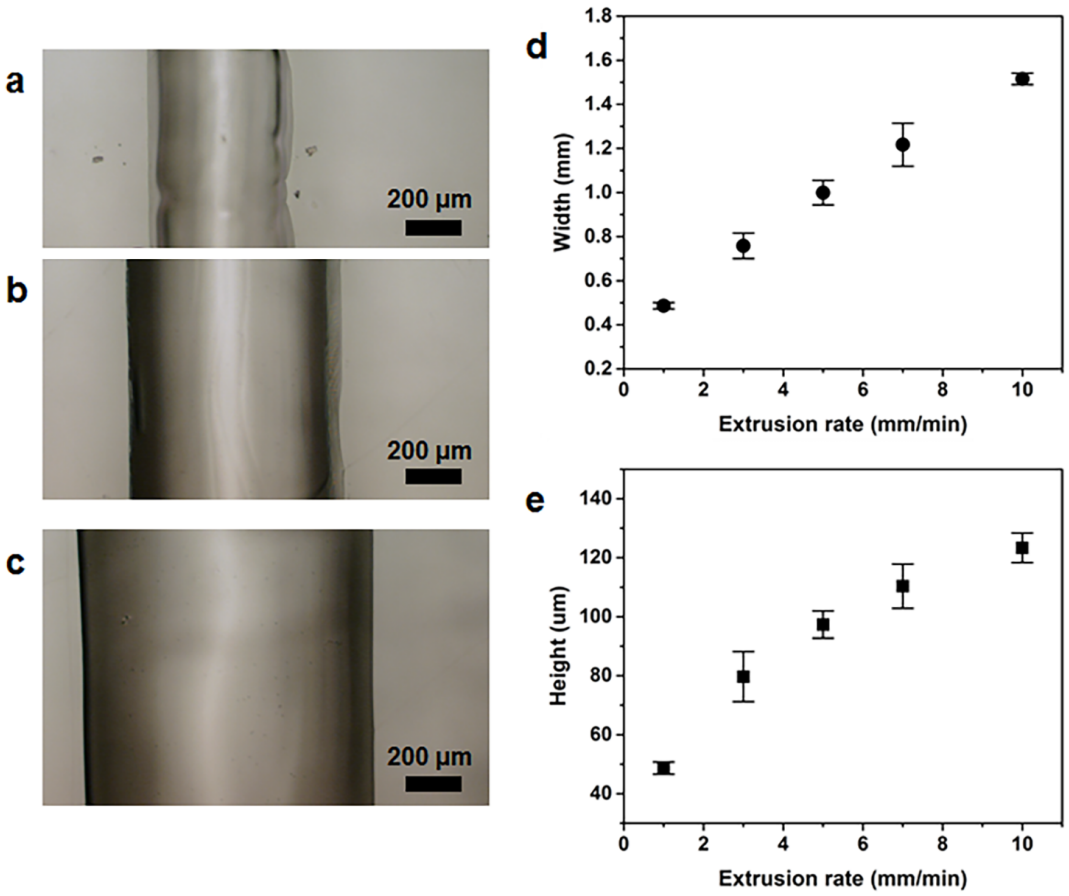

Figure 2.3: Variations in hydrogel geometry by only nominal extrusion rate variation, keeping stage velocity (450 mm/min), extrusion height (300 μm) and extrusion tip diameter (337 μm) constant. We illustrate gel geometry with optical micrographs of the printed hydrogel on top of PDMS substrate at (a) 1, (b) 3, and (c) 5 $mm\ min^{-1}$ extrusion rates. (d) shows a plot of the relationship between extrusion rate and final line width, with what appears to be a linear correlation. (e) A similar plot for final gel height versus extrusion rate.

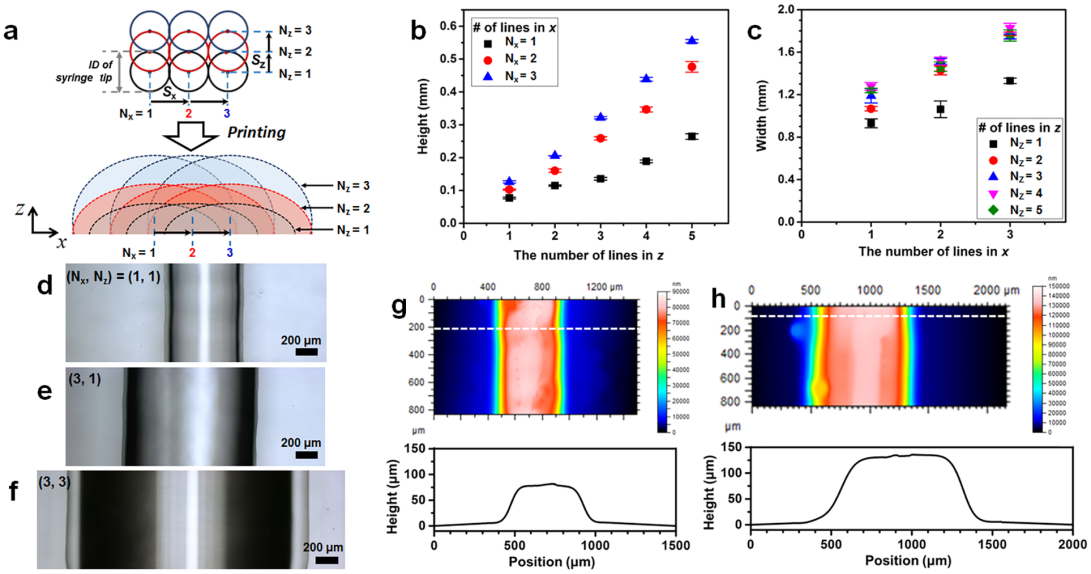

Figure 2.4: a) Schematic illustration of the extrusion trace and the resulting geometry of multiple lines separated both laterally, by S_x in the x direction, and vertically, by S_z in the z direction. The number of lines in x and z is (N_x ,N_z) = (3, 3), respectively. b) Height of gel lines as a function of N_z. c) Width of gel lines as a function of N_x. Optical micrographs of stacked layers of gel lines with. d) (N_x, N_z) = (1, 1), e) (3, 1) and f) (3,3). Optical profilometry images and the cross-sectional profiles of gel lines with multiple hydrogel layers of g) (1, 1) and h) (3,1).

a hydrogel line, and indicate their initial values with a subscript zero. We assume that the hydrogel is incompressible and the resistivity is independent of stretch. These assumptions predict that the ratio of resistance of the stretched hydrogel over the initial, unstretched resistance is given by $R/Ro = (L/Lo)^2$. When the printed hydrogel lines are stretched by mechanically loading the PDMS, their resistance values obey this relationship up to rupture of the samples at 50% strain (Figure 2.5b). This result suggests that the hydrogel lines are intact up to this strain, since damage in the hydrogel would cause a deviation from this expression. Tensile tests on freestanding hydrogel samples show that the printed gel is capable of stretching up to 150% strain before rupture, further supporting the notion that the PDMS is the mechanically limiting component in this case. One could feasibly substitute PDMS with an alternative commercially available silicone elastomer for greater stretchability; silicone elastomers are generally compatible with the surface and rheological modification techniques used in this study. We also performed a fatigue test on a PDMS-hydrogel sample over the strain range from 0% to 20% for one thousand cycles, and measured the resistance of the hydrogel at logarithmic time intervals. Remarkably, there were no observable changes to the resistance of the device, nor were there visible signs of delamination (Figure 2.5c). We believe that the adhesion is primarily physical in nature; no chemical bonding between the two networks is possible given the lack of active sites. While PDMS surface oxidation treatments are known to degrade over time, this hydrophobic recovery is significantly inhibited by contact with water.[154,155,156] Given the high water content of hydrogels, their direct contact with PDMS should impart a similar protection of the surface treatment.

To demonstrate transmission of AC electrical signals, we fabricated a simple analog to the ionic cable:[35] two parallel ionically conductive hydrogel wires were extruded onto a printed PDMS substrate, with the two terminals at either end serving as either an electrical input or output. The transfer function of the device was measured and fitted to a simple RC circuit model. Yang et al. demonstrated that the transmission of signals through an ionic conductor can be described using a special

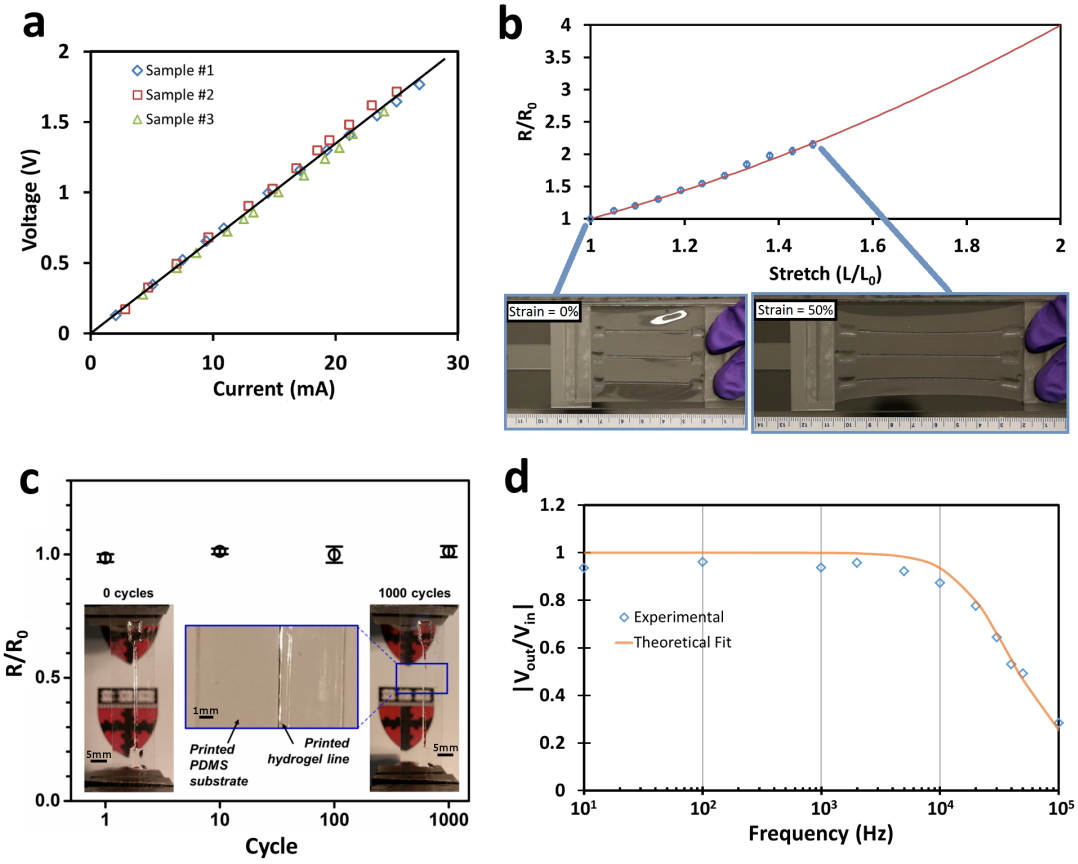

Figure 2.5: Electrical characterizations of the hydrogel in bulk and printed state. a) $I-V$ curves obtained from 4-point probe measurements performed on bulk hydrogel samples. Sample dimensions were on average 30 cm long, 4.2 mm wide, and 3.5 mm in height, with an average measured resistance of $67.3 \pm 2.4\Omega$; this corresponds to a conductivity of $10.39 \pm 0.31\, S\, m^{-1}$. b) The normalized resistance of printed hydrogels on a PDMS substrate is measured as a function of stretch, plotted against the ideal geometric behavior. Photos illustrate the sample in the initial (strain = 0%) state and the fully stretched (strain = 50%) state with the mechanical load applied only to the PDMS. c) The normalized resistance of printed hydrogels on a PDMS substrate as a function of fatigue cycle number. Uniaxial tensile strain cycles of 20% strain were performed for up to 1000 cycles. No significant change to the resistance vs. strain behavior was observed during our tests. Comparing images both before and after fatigue tests illustrate the lack of visible damage or delamination d) The transfer function of an ionic cable design is plotted against frequency. We perform a theoretical fitting of our results using a simple RC circuit model for the ionic cable and can observe a reasonable level of agreement between experimental results and theory.

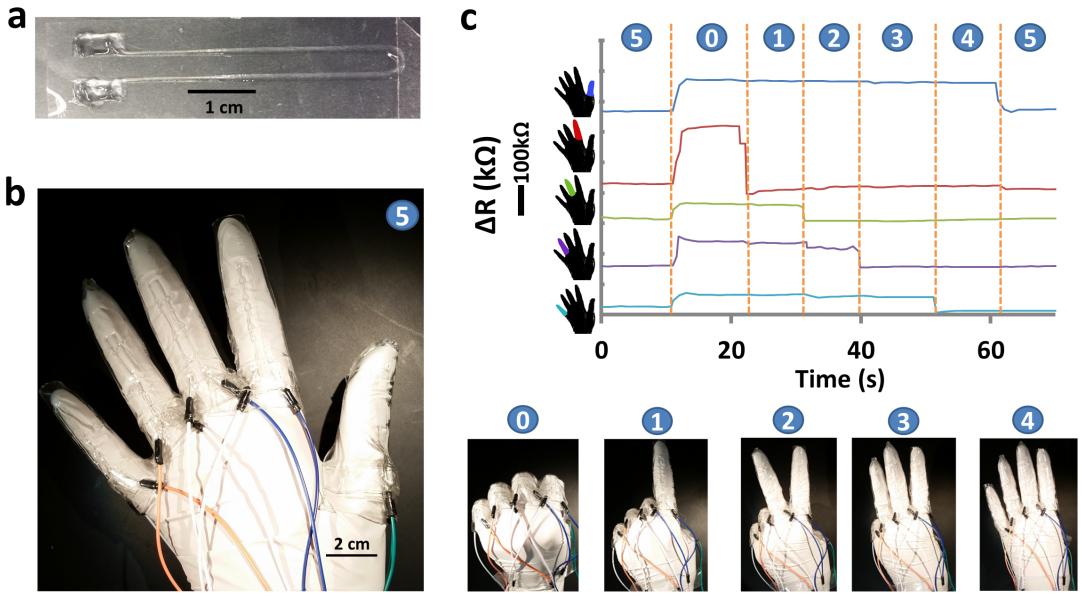

Figure 2.6: An example of a printed hydrogel-elastomeric type device, where fairly arbitrary shapes and designs can be easily integrated into the system by virtue of the printing process. In this case a) a simple resistance-based strain gauge is replicated using the hydrogel as the conductor and PDMS as the encapsulating substrate. b) By attaching the sensor to a flexible glove and flexing the digit we are able to observe a change in resistance up to 30% of its initial value at maximum finger bending and c) illustrate this process for a variety of hand gestures for each digit's strain sensor resistance change over time.

case of a transmission line model.[35] According to the theory of ionic cables, the condition for negligible decay of the signal is

$$\frac{2\omega\alpha\varepsilon l}{(bd)} \ll 1, \tag{2.2}$$

where ω is the signal frequency, l is the cable length, b and α are the thickness and resistivity of the ionic conductor, and d and ε are the thickness and permittivity of the dielectric, respectively. Using representative values, $\varepsilon = 2 \times 10^{-11}\, Fm^{-1}$, $\alpha = 10^{-2}\, \Omega m$,$l = 10\, mm$, $b = 50\, \mu m$, $d = 50 \mu m$ and let $\omega = 10^{5}\, s^{-1} \approx 15\, kHz$, we evaluate the expression to be 0.08, indicating negligible signal decay. Using a printed ionic cable with similar dimensions, we have successfully demonstrated signal transmission of AC signals up to 15 kHz in frequency (Figure 2.5d).

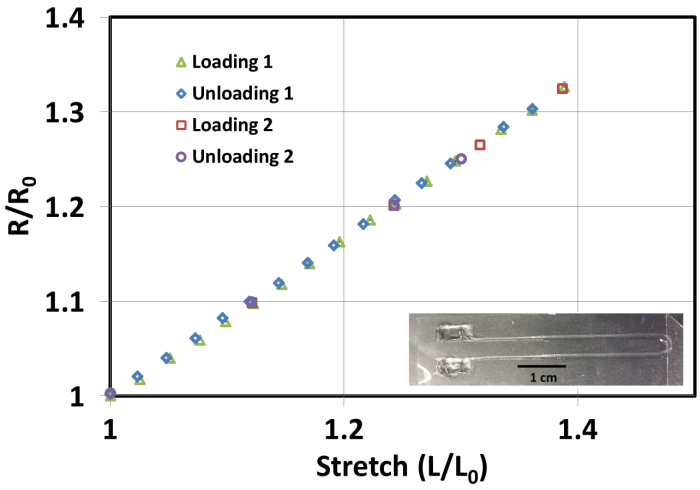

Figure 2.7: Resistance change of a stretched strain gauge sample, demonstrating a linearity of the resistance change response for this design up to 40% strain.

To demonstrate the capabilities of the printing process, we have extrusion printed a single-loop resistive strain gauge of hydrogel embedded within PDMS (Figure 2.6). The sensor has a gauge factor of 0.84, and remains linear up to 40% strain (Figure 2.7). The strain sensor was attached to the index finger of a nitrile glove using a thin layer of VHB adhesive tape (3M) and connected to a multimeter to measure the resistance of the sensor as it underwent varying degrees of strain as a result of the bending/flexing of the digits of the glove (Figure 2.8). This sensing capability was extended to all five digits of a human hand (Figure 2.6). It can be observed that the strain gauge is sensitive enough to detect inadvertent finger motions of the ring finger in position two (Figure 2.6c), as well as intermediate positions between being fully bent and fully straightened (Figure 2.8b). We observed changes up to 30% in the strain gauge resistance at maximum finger bending, corresponding to an average strain of 36%. No delamination or fracture was observed during the experiment, verifying our previous results on the durability and stretchability of the printed laminates.

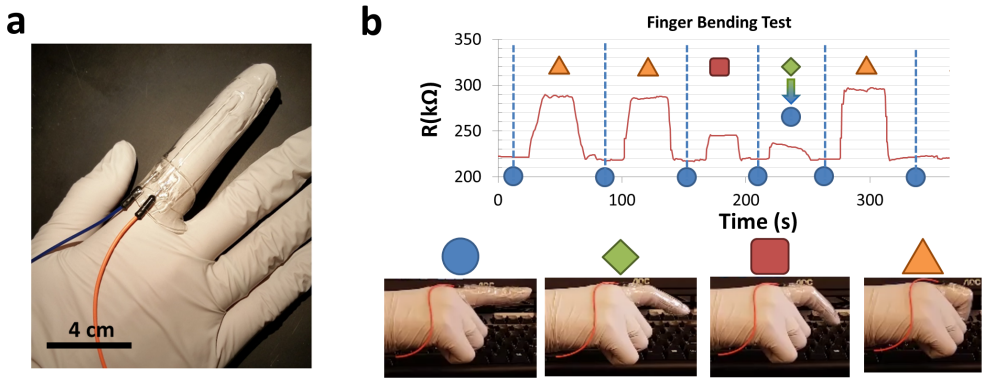

Figure 2.8: A single strain gauge is mounted onto the index finger and held in various positions while the resistance is recorded. (a) Illustrates the mounting of the strain gauge using VHB tape and leads connecting the gauge. (b) Illustrates the various positions alongside the time-trace of the gauge's resistance. The mildly bent position (green diamond) is gradually straightened to the default position, whereas others were more rapidly transitioned from straight to bent positions.

2.4 Conclusions

In conclusion, we have described a method for the 3D extrusion printing of an ionically conductive PAAm hydrogel and a PDMS dielectric elastomer to fabricate soft ionic devices. By tuning the rheological behavior of the hydrogel precursor and performing oxygen plasma treatments of PDMS surfaces, it is possible to print and integrate hydrogels directly with PDMS at sub-millimeter resolution. This capability was demonstrated by the fabrication and functional verification of an ionic cable and resistance-based strain sensor. More complex geometries are readily designed and printed. The flexibility of the process allows one to replicate the design in an array or to print stacked devices for multi-axial strains. The strategies employed here to obtain the desirable printing resolution can be used for any hydrogel-PDMS material system. The PDMS may also be substituted with other commercially available silicone elastomers, since silicone elastomers are compatible with both the surface treatment and the rheological modification strategy used in this work. This study provides a simple pathway to the fabrication of hydrogels and dielectric elastomers in an integrated fashion for

stretchable electrical devices and soft robotics applications.

2.5 Acknowledgements

This chapter was based on work that has been published in a scientific journal[64].

Luck is the residue of design.

John Milton

3

Adhesion between Hydrophobic Elastomer and Hydrogel

3.1 Introduction

Soft materials have recently risen in popularity for a wide variety of engineering applications, particularly in the areas of soft-robotics[157,23], stretchable electronics[158,104], and biological research[20,59,60]. Most designs require the integration of dissimilar soft materials into a single device. For instance, ionic devices have seen several suites of functionalities developed from combinations of hydrogels and elastomers[38,37,35,34,43]. These devices illustrate materials dissimilarity as a functional necessity: a hydrogel serves as an electrical conductor and a hydrophobic elastomer serves as a dielectric. As these devices become more sophisticated, more care must be given to their manufacture. Although great progress has been made in the extrusion-based fabrication of stretchable electronic[158,104] and ionic[39,36,64] devices, less attention has been devoted to a more subtle but equally important problem: how reliable are these manufacturing techniques for dissimilar materials? In this context, the interfacial adhesion is critical to the reliability of a broad range of materials, including composites[44,45], dental adhesives[46], and biological organisms[47,48]. Recent forays into soft-materials extrusion printing have acknowledged adhesion as important, but have rarely quantified the adhesion between dissimilar materials within printed systems[39,64]. As devices become more sophisticated and complex, crack driving forces may easily scale such that delamination becomes a serious problem. Nei-

ther predictive capability nor process optimization is possible without quantification of adhesion. Therefore, as manufacturing processes are adapted for soft materials, studies that quantify the adhesion between dissimilar materials must be conducted. One area of manufacturing that has seen particularly rapid development is 3D extrusion printing, as research has expanded the materials roster from thermoplastics to include metals[57], ceramics[58], and soft materials such as hydrogels and elastomers[59,60,39,64,61,62,63]. In our previous work, we identified hygroscopic-salt-containing polyacrylamide (PAAm) hydrogel and polydimethylsiloxane (PDMS) as suitable materials that can be integrated in an extrusion printing process for ionic devices[64]. The hygroscopic salt served to maintain water content while enhancing electrical conductivity[125]. The fabrication process developed utilized rheological tuning combined with surface energy matching of PDMS via plasma oxidation to allow for consistent submillimeter extrusion printing of a hydrogel precursor onto PDMS. Controlling the rheological behavior of the precursor is essential to achieving 3D extrusion printable hydrogels[69]; an established method for this is by adding a rheological modifier to the hydrogel precursor such as uncrosslinked PAAm[60,39,64], alginate[62], or synthetic-clay[61]. As part of the fabrication procedure, the PAAm hydrogel precursor contained a PAAm-based rheological modifier to tune its extrusion behavior. Incidentally, the use of uncrosslinked PAAm chains as a rheological modifier enables the printed hydrogels to be optically transparent, which is significant to some devices[34,43]. To ensure good wetting of the PDMS by the hydrogel precursor, the PDMS surface was treated with oxygen plasma. However, since PDMS plasma-based surface treatments are known to be transient[159,160,161,162,163], the long-term stability of the adhesion between a hydrogel and PDMS remains in question. As these materials are common within stretchable electronics/ionics, the adhesive interactions at the interface of hydrogel and hydrophobic elastomer are of broad interest.

The general strategy of plasma oxidation treatments for improving adhesion and wetting is well established for a wide variety of materials, including polycarbonate[164], oxides[104], glass[165], and silicon wafers[166]. When PDMS is exposed to an oxygen plasma, surface methyl groups are converted

into silanol groups[162,165] (Figure 3.1A). The silanol groups are capable of hydrogen bonding with water, and thus render the surface of the plasma-oxidized PDMS hydrophilic. However, PDMS also exhibits a hydrophobic recovery of its surface chemistry that is almost always dominated by the migration of residual siloxane oligomers towards the surface[160,161,162,167,168,169]. If exposed to the atmosphere, plasma-oxidized PDMS reverts back to a hydrophobic state in a matter of hours[160,167,170,171] (Figure 3.1B). A similar instability of plasma-based surface treatments is observed in other materials, although the timescale of recovery is extremely material dependent[164,172]. Even though methods exist for mitigating hydrophobic recovery, such as thermal aging[160], solvent extraction[163], and chemical grafting[159], these processes are generally incompatible with 3D extrusion. This would suggest that, within the context of extrusion printing, the interfacial adhesion between hydrogel and plasma-treated polymer may degrade due to hydrophobic recovery.

On the other hand, the absence of delamination in fatigue tests in our previous work suggests that the PDMS/hydrogel interface may be stable[64]. Since suppression of hydrophobic recovery has been observed with PDMS in contact with an aqueous medium[155,173](Figure 3.1C), we hypothesize that the water in the hydrogel suppresses hydrophobic recovery through formation of hydrogen bonds with the silanol groups in the PDMS surface (Figure 3.1D). A hydrophilic surface, by definition, physically binds with water in an energetically favorable manner and thus must contain polar functional groups with which water may interact. It is therefore reasonable that such a surface would also bind with other polar groups and improve the adhesion with another material. For instance, silanol groups on a plasma-treated PDMS surface could form hydrogen bonds with polar groups in a hydrogel network enhancing the adhesion between both materials. The presence of water molecules and polar groups at the interface would also reduce the driving force for the diffusion of hydrophobic species in the PDMS to the interface and impede hydrophobic recovery. We therefore posit that the hydrogen bonding interaction includes polar species such as water, as well as the acryloyl and amide functional groups present in both the hydrogel network and the rheolog-

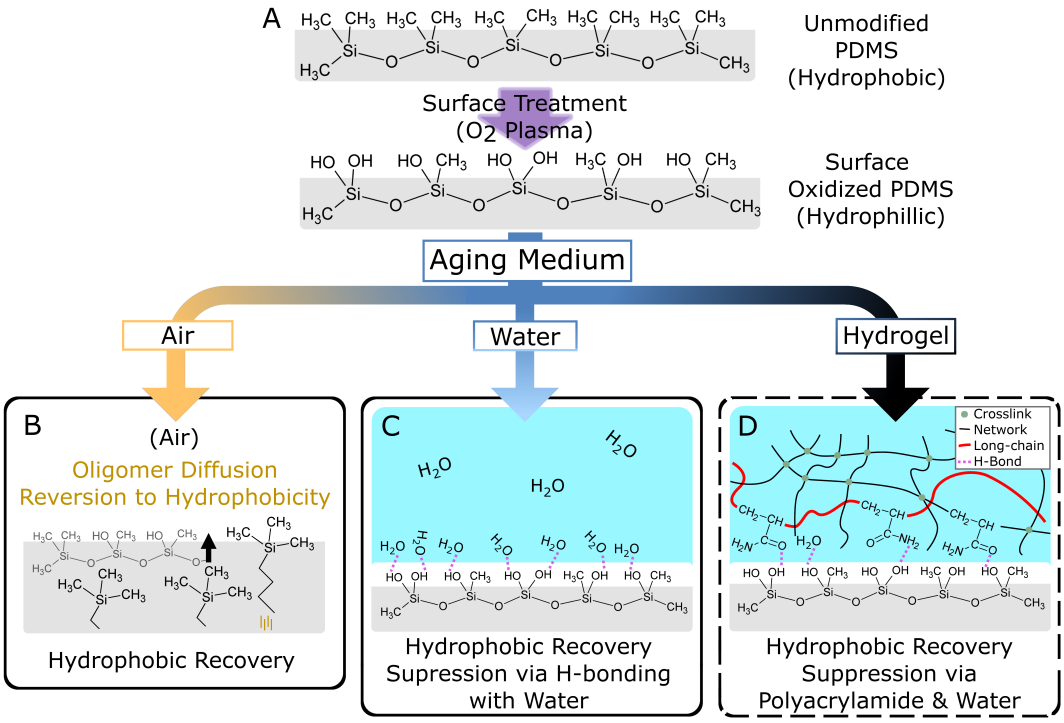

Figure 3.1: A) Illustration of the change in surface chemistry of a PDMS sample upon exposure to an oxidizing surface treatment. B)-D) Illustration of the possible fates for a surface oxidized PDMS sample, where the surface silanol groups are either B) dominated by hydrophobic recovery while exposed to atmosphere or C) hydrogen bonded with a polar solvent and suppresses hydrophobic recovery. D) This work proposes an alternative method of preserving the hydrophilic surface of PDMS through direct contact with a hydrogel, which also enables the preservation of the interfacial adhesion between hydrogel and PDMS.

ical modifier. This mechanism establishes the possibility that hydrogels are capable of stabilizing the adhesion with plasma treated PDMS, with possible extensions to other polymers or elastomers. Therefore, the aim of this paper is to quantify the adhesion between plasma-treated PDMS and hydrogel over an extended period of time.

Interfacial adhesion has been characterized by a wide variety of methods[174], including angled peeling[175], lap shear[176], scratch[177], and flexure[178,179] testing. The applicability of these methods to very soft materials capable of large deformations is, however, not well established. For instance, peeling tests have problems with hysteresis due to bending induced plasticity in the samples, while most other tests are either invalid beyond small-strain assumptions or are ill-suited for soft materials[178]. Even so, there exist several techniques that are suitable for evaluating the adhesion of hydogels, including bilayer shear-based tests[180] and 90°-peeling tests[158,104]. We selected the 90°-peeling test (Figure 3.4A,B) because it is both compatible with the samples of interest and because it is a simple and standardized method for which adhesion energies are readily compared.

This study reports on the stability of the interfacial adhesion in materials systems that consist of printable hydrogels and PDMS. During this investigation, we were able to verify the long-term reliability of the adhesion, but also observed segregation of a viscous phase to the interface, which had a significant impact on the adhesive behavior. We demonstrate that this segregation is directly related to the surface treatment of the PDMS and the presence of the rheological modifier in the hydrogel precursor. This finding suggests that long-chain polymer additives, which were originally added to tailor the viscosity of the hydrogel precursor, also aid in the long-term reliability of the PDMS/hydrogel interface, and possibly of other materials systems.

3.2 Methods

3.2.1 Sample Preparation and Processing

The hydrogel precursor formulation as described by Tian et al.[64] contains lithium chloride (LiCl) salt and uncrosslinked PAAm. The materials used in this study were chemically identical to those used by Tian et al.[64], but the samples were cast instead of printed. To facilitate the casting process, the viscosity of the hydrogel precursor was decreased by reducing the amount of rheological modifier to 36.7% of the network polymer (see Appendix A for exact weight percentages). This amount of modifier still yields a rheology that is suitable for extrusion printing (3.3), although with reduced resolution. The modification in the hydrogel formulation was driven by the need to fabricate macroscopic samples in a reasonable amount of time so that a statistically significant number of samples could be tested with peeling forces that were large enough to be measured accurately with available load cells. The interfacial adhesion of the cast samples and the underlying mechanisms are not expected to differ significantly from samples that were printed beyond potential effects of shear deformation during extrusion. This shear could cause some degree of polymer alignment, which, if we use the rubbing shear-alignment of polystyrene (PS) as a proxy, may slightly reduce adhesion[181]. This alignment may also result in some anisotropy in the interfacial toughness, which is not considered in this study.

However, such history dependency of the polymer can be partly observed through crystallinity of the sample. Measurements were made of the hydrogel in order to determine if this was the case (Figure 3.2). As can be observed, there are no thermal peaks associated with the presence of crystalline regions in the sample. There is only one broad endothermic peak centered around 100°*C*, which we may attribute to the evaporation of water. The absence of crystalline regions is in agreement with the literature on solid polyacrylamide. Polyacrylamide is generally understood to be an amorphous polymer for free-radical based polymerization methods[182,183,184], although crystalline forms of the

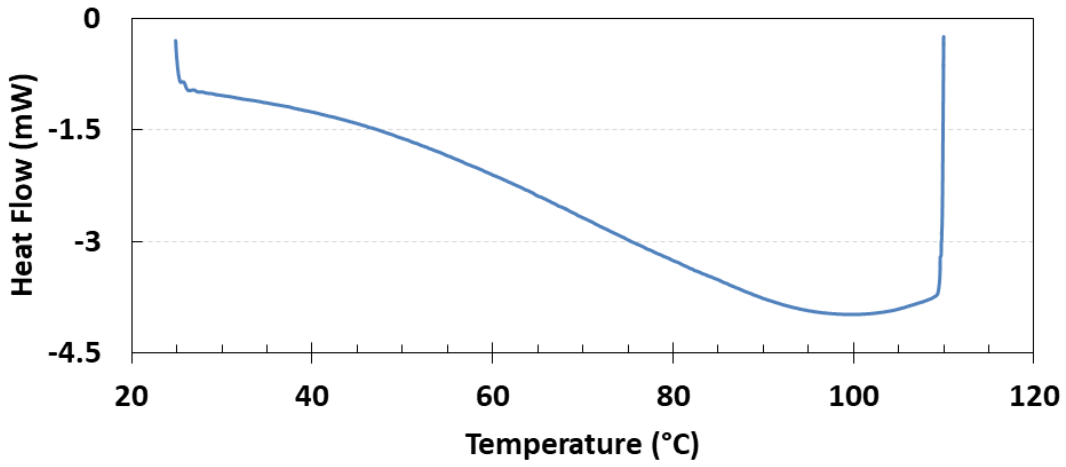

Figure 3.2: Differential Scanning Calorimetry (DSC) measurement of a bulk hydrogel containing rheological modifier, with endothermic being negative on this scale. Measurements made on a DSC Q200 (TA Instruments). A heating sweep from $25^{\circ}C to 110^{\circ}C$ is made and we notice only a broad peak centered around $100^{\circ}C$. Samples were contained in a Tzero Low Mass Aluminum pan. The DSC was operated under a $40L\ min^{1}$ nitrogen flow rate, $5^{\circ}C/min$ temperature ramp and data captured at a rate of $1Hz$.

polymer are possible with different polymerization mechanisms[185]. Studies that have used commercial or free-radical synthesized PAAm appear to find nothing remarkable in DSC measurements of the material[183,186].

Samples were fabricated using a split mold that allowed removal of the samples from the mold without applying any forces perpendicular to the bilayer interface (Figure 3.4C,D). This procedure was used for all samples, even though it was strictly only necessary for samples with very weak adhesion. Once the hydrogel precursor and PDMS were cured in contact, samples were aged in a controlled environment with 42% relative humidity between 18 and 408 hours. The environmental control during aging was necessary to ensure that the swelling ratio of hydrogel would not change during aging. A 90°-peel test setup was then used to quantify the adhesive energy of the hydrogel-PDMS bilayers, whereby the PDMS was peeled off from the hydrogel layer affixed to a glass substrate (Figure 3.4A). Data from the 90°-peel tests consisted of peeling force against peeling extension. All tests were initiated by making a pre-crack of less than $5mm$ and were performed at a con-

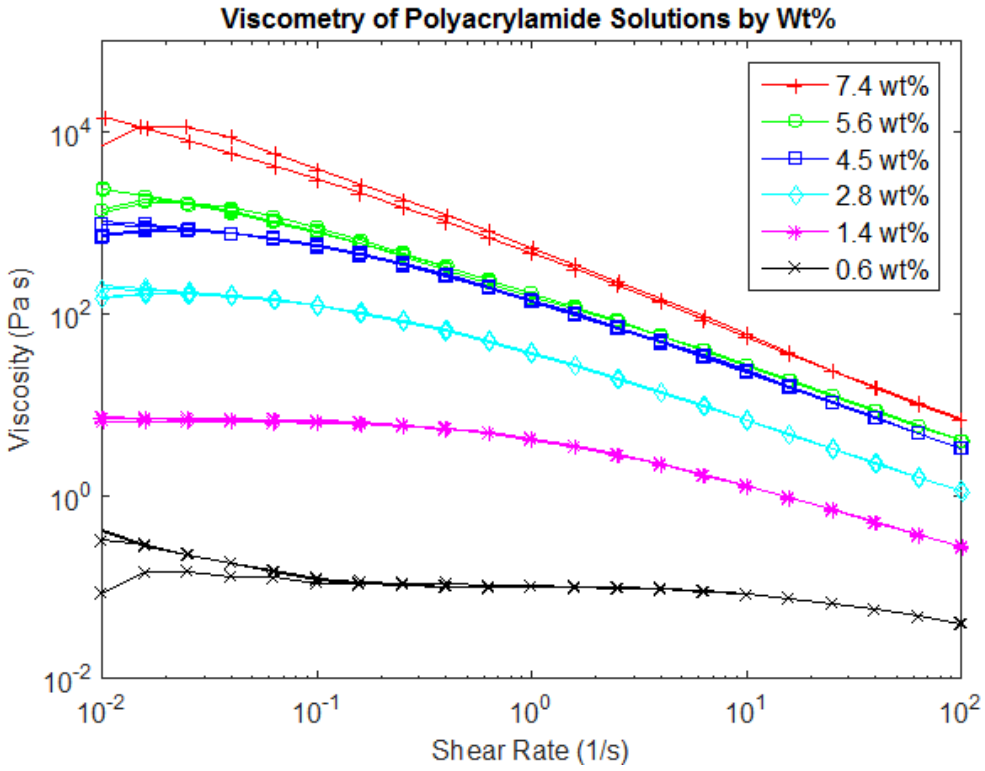

Figure 3.3: Viscometry data on various weight-percentage solutions of the rheological modifier polyacrylamide. A previous study utilized a 7.4wt% PAAm solution, whereas this study used an equivalent 5.6wt% PAAm solution. Our internal tests suggest that extrusion printing with solutions as low as 2.8 wt% are possible.

stant peeling rate of $50mm/min$ for a length of at least $100mm$. After the crack began to propagate through the bilayer, the peeling force eventually settled into a steady-state regime. The expression for the strain energy release rate during peeling[187], is $G = \frac{F}{b}(1 - cos\vartheta)$ for peel angle ϑ, peel force F, and sample width b. For 90° peeling, this expression simplifies to $G = F/b$. Under steady-state crack propagation, the interfacial fracture energy Γ is equal to G, so that Γ is given by the plateau peeling force divided by the width of the specimen.

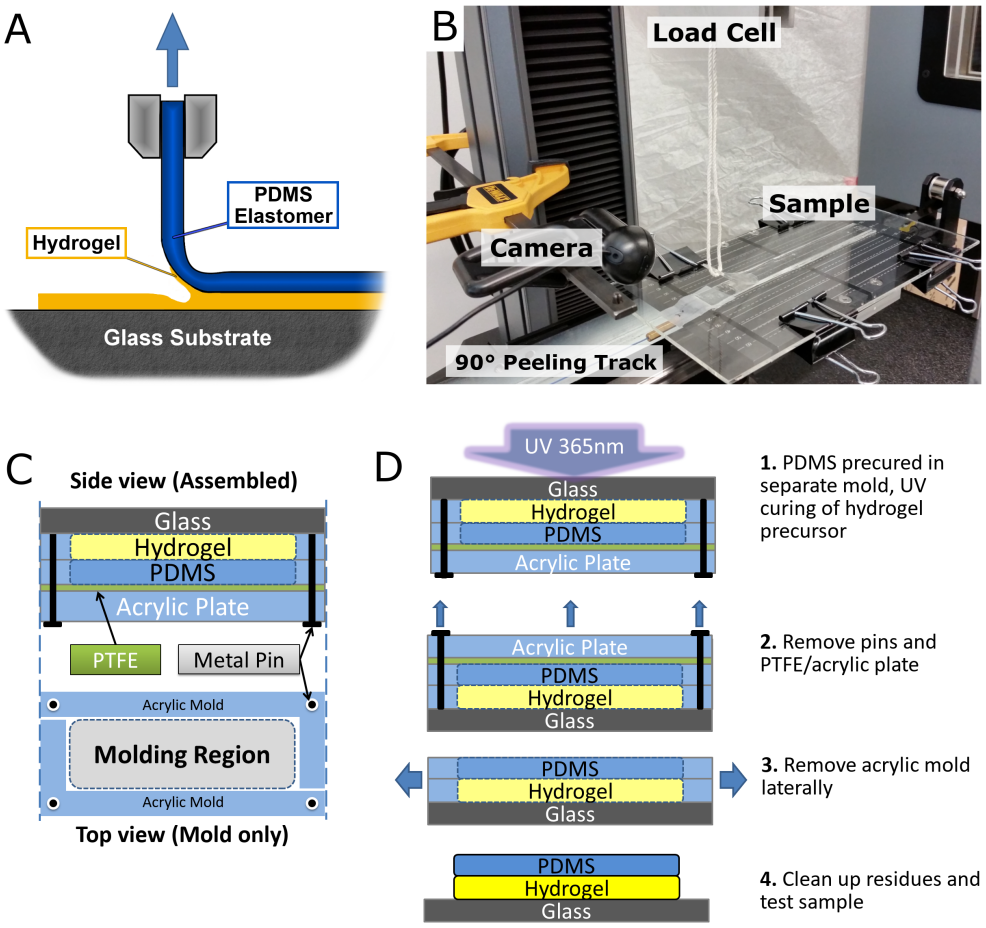

Figure 3.4: A) Illustration and B) Photograph of the experimental setup for adhesion measurement using a 90° peeling setup. C) A schematic overview of the segmented mold developed to preserve sample interface integrity. D) The sequence of sample fabrication, assuming a fully assembled mold stack.

3.3 Results and Discussion

3.3.1 Hydrophobic recovery and interfacial adhesion

The contact angles of water on various PDMS surfaces are shown in Figure 3.5A as a function of aging time. The contact angle on untreated PDMS was initially measured to be $\vartheta = 109.9^\circ \pm 2.8^\circ$ (Figure 3.5B), consistent with the extreme hydrophobicity of untreated PDMS, and remained unchanged during aging. A plasma-treated PDMS surface that was aged under atmospheric conditions only retained its hydrophilicity for a short period of time (Figure 3.5C) and reverted to a hydrophobic state within 10 hours. The behavior of untreated and treated PDMS during aging matches that reported in the literature[162,188,154] and is thus not particularly remarkable. On the other hand, plasma-treated PDMS surfaces aged in contact with a hydrogel were able to retain their hydrophilicity, $\mathfrak{F}30^\circ$, for a period of at least 408 hours, although the average values of the contact angle were slightly higher than the initial contact angle of treated PDMS, $\vartheta = 23.5^\circ \pm 6.9^\circ$. This result suggests that there is an interaction between the hydrogel and the silanol groups on the PDMS surface that suppresses hydrophobic recovery. The graph shows clearly that even a brief exposure to the atmosphere degrades the contact angle on treated PDMS. It is now necessary to relate these changes in contact angle relate to interfacial adhesion before any conclusion can be drawn.

Figure 3.6 shows the results of the peel tests as a function of interface aging time. As illustrated in the figure, the measured adhesion energy changes significantly with aging: it increases from an initial value of $\Gamma = 4.69 \pm 0.53 J\,m^{-2}$ to $\Gamma = 14.63 \pm 0.75 J\,m^{-2}$ after 73 hours, i.e., a three-fold enhancement in adhesion. Although this behavior is not explained by any mechanism based on the hydrophobic recovery hypothesis, it is clear that the adhesion is stable at its plateau value of $15 J\,m^{-2}$ for up to 408 hours after the initial aging period. If hydrophobic recovery had occurred during aging, the adhesion would have degraded due to the reduction in physical bonding between hydrogel and elastomer or a reversion of the contact angle of the PDMS surface back to a hydrophobic state. Since neither of

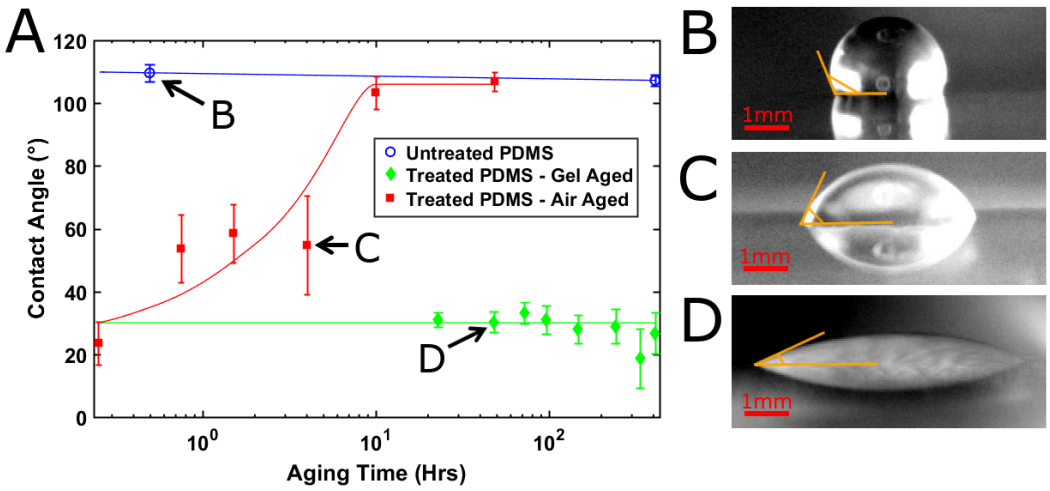

Figure 3.5: Contact angle stability of plasma-treated PDMS and Hydrogel interface. A) Contact angle measurements over a period of 400 hours of untreated PDMS and plasma-treated PDMS aged in contact with hydrogel (green diamond) or exposed to atmosphere (red square), with all lines to act as a guide to the eye; samples were all stored under RH control of 47%. Images illustrating B) hydrophobic (at 109.9°), C) weakly hydrophilic (at 54.8°) and D) hydrophilic (at 30.3°) regions of the behavior are shown.

these effects were observed, the surface treatment must be preserved, verifying the hypothesis that hydrophobic recovery of plasma-treated PDMS is inhibited by the presence of a hydrogel. This new form of hydrophobic recovery suppression may be useful for preserving the surface treatments of PDMS and polymers in general, both within the context of printed soft materials and beyond.

3.3.2 Viscous dissipation at the hydrogel-elastomer interface

During adhesion testing, a viscous fingering instability developed at the interface between the hydrogel and the PDMS. In controlling for the rheological modifier (Figure 3.8A and B), it became apparent that this phenomenon is directly related to the presence of the rheological modifier in the hydrogel. A hydrogel without any rheological modifier was cast and aged for a period of 336 hours, but no fingering was observed (Figure 3.8A), while a hydrogel with modifier showed extensive fingering at approximately 73 hours (Figure 3.8B,C). With aging, a viscous layer develops at the

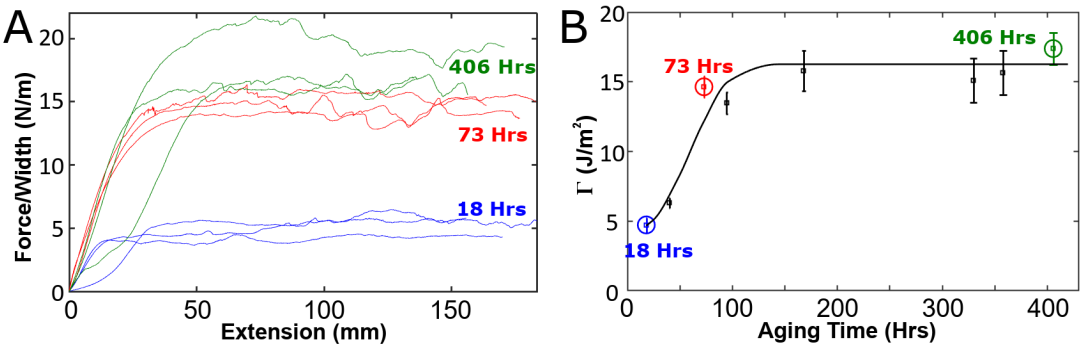

Figure 3.6: Peeling data for interfacial toughness of PDMS-Hydrogel interface. A) An example of the hydrogel-elastomer bilayer interfacial peeling data used to calculate the plateau peeling force, presented as a plot of peeling force divided by sample width against peeling extension. B) A plot of the interfacial toughness of the plasma-treated PDMS and PAAm hydrogel interface observed over a 408 hour time period, with black line as a guide to the eye. Highlighted in blue, red, and green are data points at 18, 73 and 406 hours represented by the peeling data illustrated in A).

hydrogel-PDMS interface leading to fingering during delamination. We believe that energy dissipation in this viscous layer contributes to the interfacial adhesion, consistent with models of the adhesive failure of visco-elastic solids[189], and is in fact the reason why the adhesion improves with aging. The only other time-dependent phenomenon expected in this context is hydrophobic recovery of the PDMS, which is readily ruled out since this mechanism would lead to a decline in adhesion. Visually, the phenomenon appears similar to the fingering instabilities first observed in the study of viscoelastic adhesion[190]. They have also been observed in elastic systems[191], such as when peeling rigid plates from elastic adhesive films[192] and the elastic instabilities present during the peeling of pressure sensitive adhesives[193]. That these instabilities remain after peeling suggests that the material responsible for the fingering is extremely viscous, which is indeed the case for the rheological modifier.

The viscous layer leaves a visible residue on the PDMS surface, as well as filaments on the hydrogel surface, indicating that the interfacial fracture propagates within the viscous layer rather than at the interface of hydrogel or PDMS. A consequence of this viscous residue is that it allows for com-

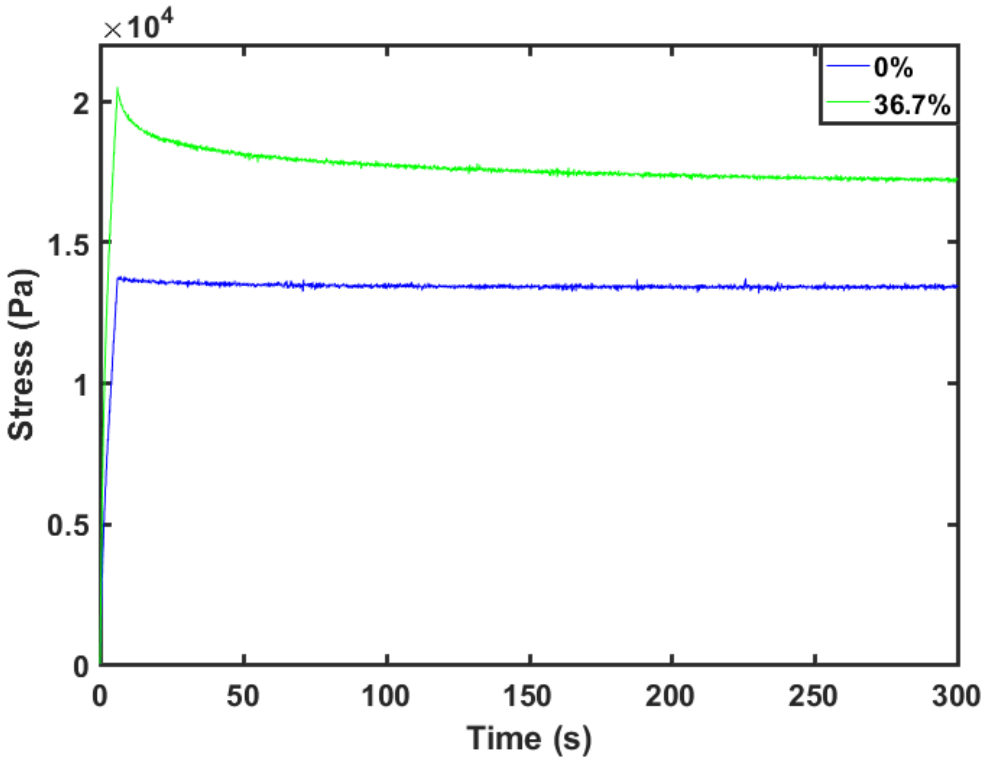

Figure 3.7: Stress-relaxation tensile testing of bulk hydrogel samples with varying ratios of uncrosslinked to crosslinked PAAm within the network. This illustrates the small effect of uncrosslinked PAAm on the bulk hydrogel mechanical properties.

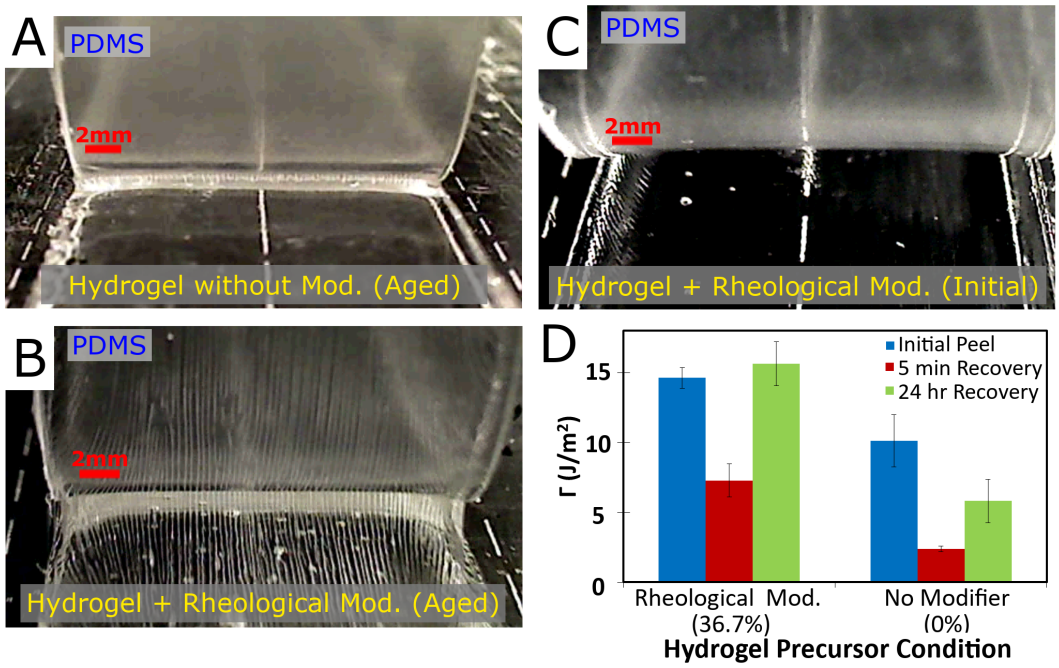

Figure 3.8: Peeling of PDMS-Hydrogel interface and Adhesion Recovery. A) A representative image of a peeling test after 336 hours of aging for a hydrogel containing no rheological modifier cured in contact with oxygen plasma-treated PDMS. B) & C) These representative images illustrate peeling tests of PDMS off hydrogels containing rheological modifier at aging time of 73 hours and 18 hours respectively. D) Plot of the adhesion recovery at different waiting times, 5 min and 24 hrs, of the plasma-treated PDMS-hydrogel interface for hydrogels both with and without the rheological modifier.

pletely reversible adhesion between the hydrogel and PDMS, as illustrated in Figure 3.8D. The figure shows a simple experiment in which a hydrogel-PDMS bilayer was first aged for at least 96 hours to ensure full development of the viscous layer, then delaminated and re-adhered without additional applied pressure (i.e. only gravity), and finally delaminated again after the specified amount of time. At each delamination step the adhesion energy was measured. The observation is that the adhesion in the final delamination recovers $107 \pm 11\%$ of its previous value after 24 hours if the hydrogel has the rheological modifier, but only $57 \pm 33\%$ without the modifier. We believe that the reduced adhesion in the latter case is due to partial hydrophobic recovery. When the plasma-treated PDMS surface is exposed to the atmosphere for approximately ten minutes after delamination, it undergoes hydrophobic recovery. This does not happen for the samples with the rheological modifier because the viscous residue that is left on the surface of the PDMS acts as a medium with which silanol groups in the PDMS can form hydrogen bonds. The adhesion is then dominated by the dissipation that the viscous layer affords, i.e., the viscous layer acts as a pressure-sensitive adhesive binding the bilayer together.

Since the viscous layer significantly alters the behavior of the interface when loaded under mainly mode I conditions, we also evaluated the effect of the viscous layer when the interface is loaded mainly in shear. We thus conducted a mode II dominated delamination test to evaluate if the failure mode was different from previously observed hydrogel-elastomeric bilayer systems[180] (Figure 3.10A). As Figure 3.10B illustrates, the crack front only propagates a small distance despite the stiff backing layer applied to the hydrogel to drive the bilayer towards delamination. Instead of steady-state crack propagation, the PDMS substrate fails and proceeds to slide across the hydrogel surface; this can be inferred from the lack of apparent flow or motion in the central region where the fractured PDMS and hydrogel remain in contact. There is a significant amount of viscous residue remaining on both hydrogel and PDMS, as observed in the 90° peel tests. The critical energy release rate, G, for this geometry can be determined using the method described by Tang et al.[180] and is approximately

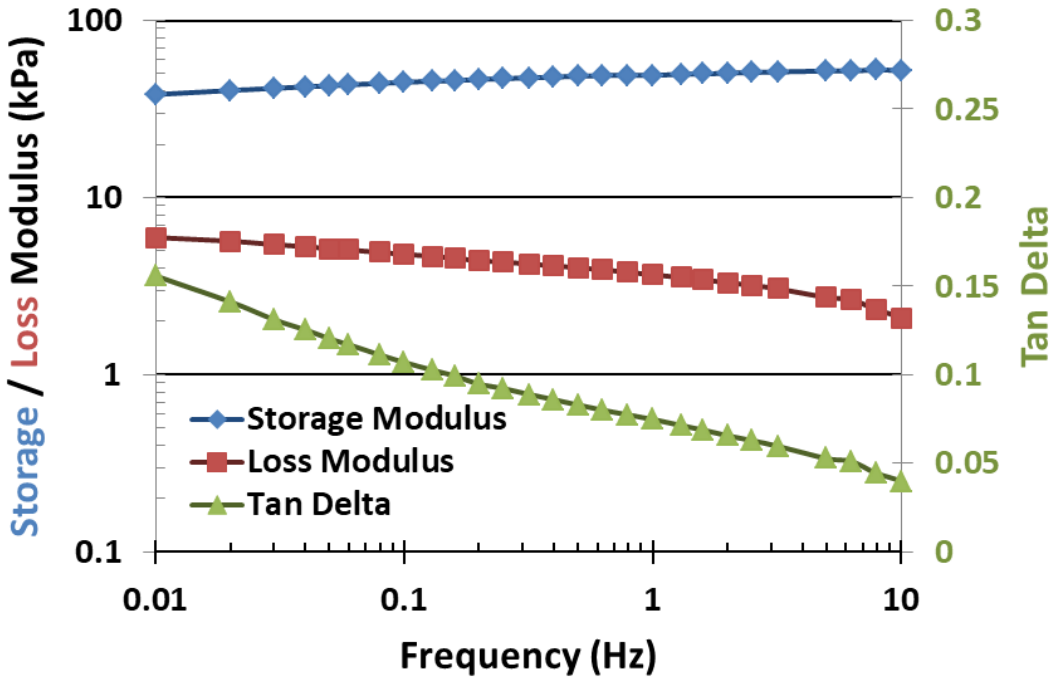

Figure 3.9: Dynamic Mechanical Analysis (DMA) data on bulk hydrogel containing rheological modifier using a DMA Q800 (TA Instruments). The test was performed under compression at maximum oscillatory strain of 3% on a cylindrical sample at $25^{\circ}C$ and an initial contact force of $0.01N$.

$G = 29.88 J\,m^{-2}$ shortly prior to substrate failure (see Figure 3.9 for hydrogel viscoelastic moduli). We note that the crack front of the sample propagated a small amount, but then stopped even after the PDMS substrate failed and began sliding back (Figure 3.10B). This behavior is due to the flowing of the viscous layer as the sample is deformed in shear (Figure 3.10C). Contrary to the mode I scenario where the two materials are separated perpendicularly, in mode II the materials are kept in contact with the viscous layer at all times.

Several possibilities were considered regarding the origin of the viscous layer. For instance, the viscous layer could be the result of incomplete curing caused by the presence of oxygen in the PDMS given the high gas permeability of the material[159,194]. However, the lack of viscous fingering in a hydrogel cured without rheological modifier suggests otherwise (Figure 3.8A). Separate combina-

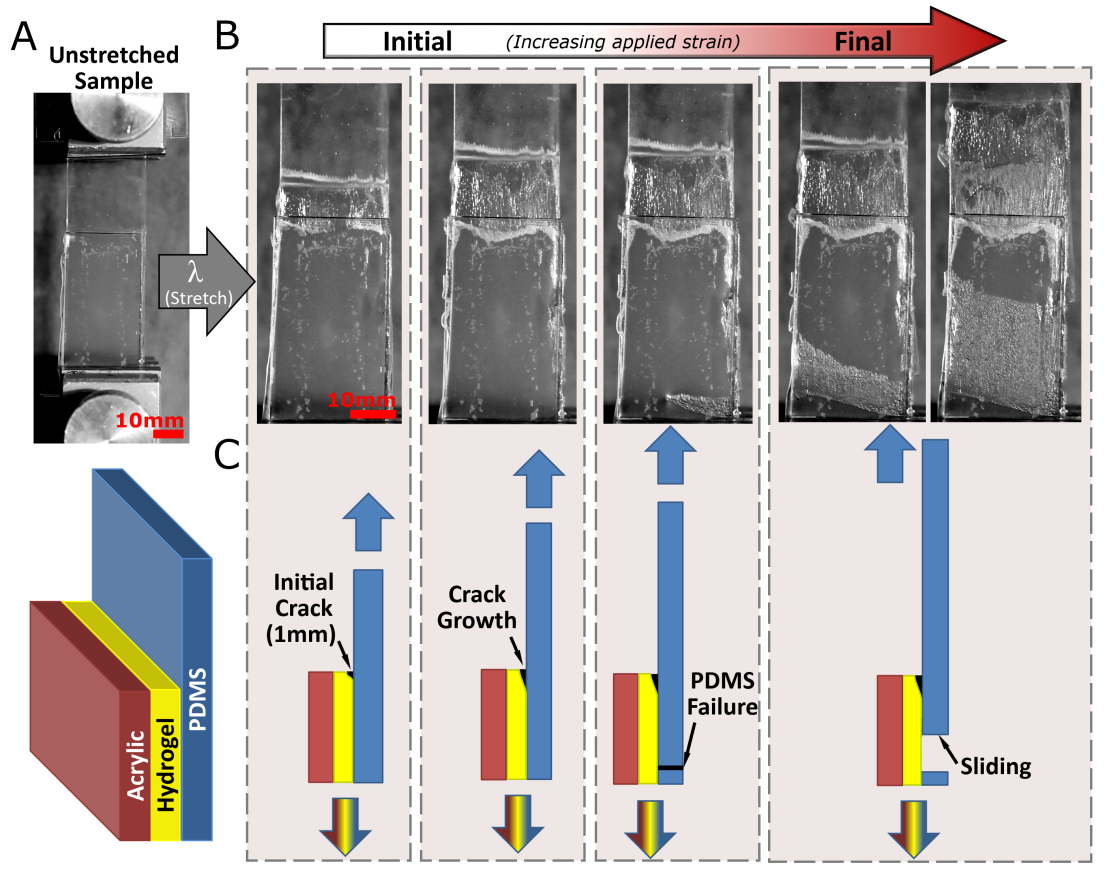

Figure 3.10: Bilayer shear testing performed on an aged hydrogel-PDMS interface. Photos have been decolorized for clarity. A) shows the sample and a representative schematic of the un-stretched sample (schematic not to scale). Acrylic, hydrogel, and PDMS layers had thicknesses of 1.6mm, 0.5mm, and 1.6mm respectively, all had a width of 25mm. B) As the sample is stretched at a rate of 10mm/min, the PDMS portion is deformed while the thinner hydrogel layer, bonded to a stiff acrylic plate, is constrained. With increased strain the PDMS eventually fails and displays a slide/relaxation phenomenon that is readily explained by the presence of a viscous layer at the hydrogel-PDMS interface. C) An equivalent schematic representation of the previously described sample as it is stretched.

tions of hydrogel-PDMS curing tests showed that viscous fingering occurred only when both the PDMS was plasma-treated and the rheological modifier was present in the hydrogel. Both hydrogels with and without rheological modifier were found to have negligible adhesion and no viscous fingering after peeling from untreated PDMS. Furthermore, it was impossible to reproduce the effect even after 350 hours of aging if the rheologically modified hydrogel was cured separately and subsequently placed in contact with plasma-treated PDMS. These observations suggest that the hydrogel must be cured in contact with the treated PDMS surface to reproduce the segregation. Since the uncrosslinked PAAm used as rheological modifier has a high molecular weight and is quite viscous, this requirement may arise from the difficulty of the PAAm chains diffusing to the surface in the presence of a fully formed network. We further note that hydrogen bonding as a driving force acts equally on both the hydrogel network and the rheological modifier, given that they are chemically indistinguishable aside from the low-density crosslinks, but only the rheological modifier is mobile. Since hydrogen bonding is typically a short-range driving force, we suggest that a fraction of the rheological modifier is able to migrate to the PDMS interface pre-gelation, which partially anchors these chains to the interface via hydrogen bonding. Once anchored, these polymer chains may continue their migration to the interface post-gelation through a pull-out process.

The segregation phenomenon was further confirmed by means of fluorescence confocal microscopy using fluorescently tagged un-crosslinked PAAm chains as rheological modifier. Figure 3.11 makes it abundantly clear that the PAAm chains are in fact aggregating as a macroscopic, 30 μm thick layer at the interface between the hydrogel and PDMS and that this layer is present as early as 18 hours after sample fabrication. As the bilayer is aged beyond 18 hours, we observe that 1) the thickness of the layer continues to increase from an initial $30\mu m$ to $50\mu m$, and that 2) visible levels of un-crosslinked PAAm remain within the hydrogel network. This result strongly suggests that this phenomenon is indeed a bulk-to-interface segregation of the rheological modifier within the PAAm hydrogel. Although recent studies have described how bulk-to-interface viscous flows can contribute

to hydrogel adhesion[195], there are no previous reports of fluids in hydrogels undergoing macroscopic phase separation from bulk to interface. Furthermore, the observation that no segregation occurs if the hydrogel is cured separately from the treated PDMS suggests the need for an initial "seed layer" at the interface that forms during the network curing stage and that allows continued segregation after the hydrogel is fully cured. That this layer continues to grow in thickness at a slow rate could be explained as a diffusion-driven process[196], whereby the uncrosslinked polymer chains are drawn from the network to the interface; however it is difficult to establish whether this is due to chain-anchoring or some other driving force in the system. The adhesion enhancement that comes with the migration of the viscous layer must arise from the entanglement that is inevitable for long polymer chains contained within a cross-linked network. This entanglement allows viscous dissipation at the interface, greatly enhancing the adhesion. The fact that significant amounts of residue remain on the PDMS surface signifies that the hydrogen bonds between the viscous layer and the PDMS are not readily severed, making the situation a viscoelastic analog to the classical tethered polymer melt at the interface between two polymers[197]. The introduction of this rheological modifier changes the nature of the adhesion from simple physical bonding into one where polymer chains are pulled out of their entangled state, albeit one where the chains are not chemically anchored to either surface[197,198].

3.4 Conclusions

Evaluation of the interfacial adhesion as well as contact angle measurements demonstrate that a hydrogel is capable of stabilizing PDMS surface oxidation treatments for extended periods of time while in direct contact. Furthermore, we have discovered that a macroscopic viscous layer segregates to the interface of a hydrogel-PDMS system if the hydrogel precursor contains a long-chain rheological modifier and the PDMS surface has been plasma treated with oxygen. This viscous layer

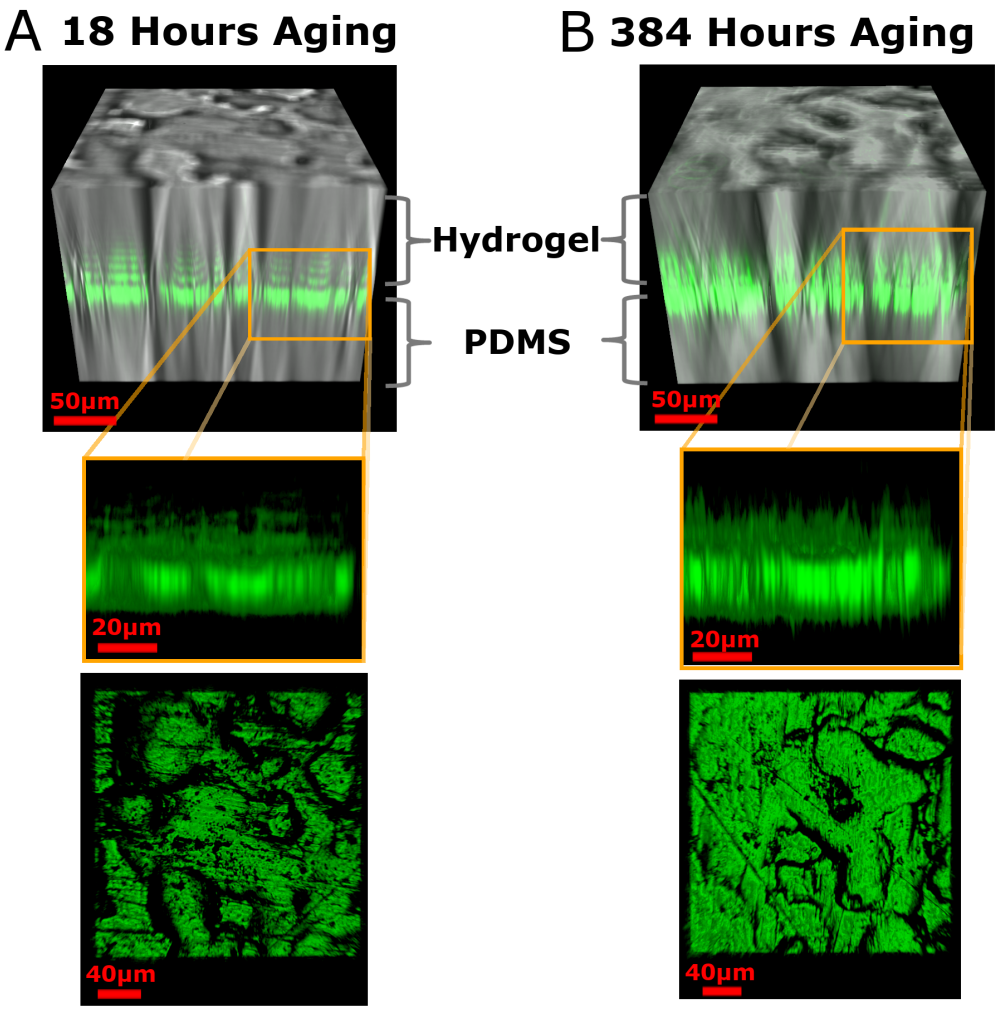

Figure 3.11: Fluorescence confocal imaging of the PDMS-hydrogel interface, having containing tagged the uncrosslinked PAAm chains with fluoroscein-o-acrylate and aged for A) 18 hours or B) 384 hours. 3D reconstruction utilized scans centered on the interface $\pm 100 \mu m$ and included both bright field and fluorescence channels for the perspective view; top and side views of the reconstruction used only the fluorescence channel.

enhances adhesion by increasing energy dissipation during delamination, a picture that is consistent with accepted models for interfacial failure in adhesives[189] and earlier studies on adhesion enhancement through viscous dissipation[199,200,201]. The presence of the viscous layer also results in fully reversible interfacial adhesion. This result highlights a simple method for improving the fabrication by printing of integrated systems of soft materials using preexisting techniques and materials that are readily available. Since the surface modification strategy employed here is applicable to polymers in general, the combination of rheological modifiers and plasma treatments may be an effective method for improving the adhesion for any printed heterogeneous material system consisting of a hydrogel and an elastomer.

3.5 Acknowledgements

This chapter was based on work that has been published in a scientific journal[102].

Luck is not chance-

It's Toil-

Fortune's expensive smile

Is earned-

Emily Dickinson

4

Exploring Hydrogel-Elastomer Adhesion Enhancement Mechanisms

4.1 Introduction

As the field of stretchable electronics matures, hydrogel-based ionotronics stand well poised to fulfill many applications that require softness, stretchability, transparency, and biocompatability[43]. However it has only been recently that developments have been made towards the advanced manufacturing of heterogeneous soft materials devices. Prior to these developments casting and manual assembly has been the dominant means of making these devices, which range from skin-like sensors[38,36,202,158], ionic cables[35], optical wave-guides[203], touch panels[40], actuators[204], and electroluminescent sources[36,37]. Some studies have begun to move beyond manual assembly by combining casting with other techniques like sewing[205,109]. However, in terms of single-step processes a variety of manufacturing techniques have been applied towards hydrogel device fabrication, including stereolithography[206], two-photon polymerization[53], and inkjet printing[207,208]. Materials extrusion (also known as extrusion printing[209], 3D plotting[210], direct ink writing[211], etc.) has the advantage of technological simplicity, ease of adopting multiple materials, and low commercial costs[51].

Multi-material printing or the fabrication of devices with dissimilar materials is important as these are what will ultimately give the most functionality. In the same way that electrical circuitry relies on dissimilar materials in order to function, such as between conductors and dielectrics, hydrogel-

based circuitry requires the integration of elastomers both hydrophilic and hydrophobic. Without proper integration, long-term reliability of such devices will inevitably become suspect leading to failures such as delamination. Unfortunately, although there are an abundance of studies that have looked at the extrusion printing of soft materials independently, such as for hydrogels [62,59,60,212,213,214,215,76] or silicone elastomers [20,21,143,146,216,217,91,100], those that have looked at hydrogel-elastomer device fabrication are far fewer in quantity.

Hydrogel-elastomer fabrication studies can generally be divided into several categories. Those that rely on physical bonds for adhesion, such as through hydrogen bonding [64,102] or contact forces from conformation [103,36,39,41], may indicate acceptable integration, but ultimately rely on the lack of significant driving forces at the interface. Strong integration, which generally is reflected by the presence of cohesive failure, has yet to be demonstrated between hydrogel and elastomer through physical bonds. Techniques utilizing chemical bonds for their integration are predominantly based around the UV photoinitiator benzophenone, with the majority being surface based modifications [104,105,106] and one instance of volume modifications [107]. These techniques use a compound that upon UV exposure generates free-radicals capable of reacting with both hydrogel and elastomer networks in order to form chemical crosslinks between them; this means that integration occurs simultaneously with network formation. Silane-based chemical coupling on the other hand has been successfully demonstrated to be viable for hydrogels and elastomers [108,109], where a compatible silane coupling agent is co-polymerized into the material bulk and allowed to react independently of the polymerization reaction (Figure4.1). However, previous works using silane coupling agents with hydrogels did not fully explore their viability within the extrusion printing context as a printing-relevant rheology was not developed and used in conjunction with a silane coupling agent. In addition, modifications to the system described are necessary in order to adapt them for hydrogels of high ionic strength as needed for good electrical conductivity. Since silane coupling represents a potentially different pathway towards achieving dissimilar materials integration for extrusion 3D-

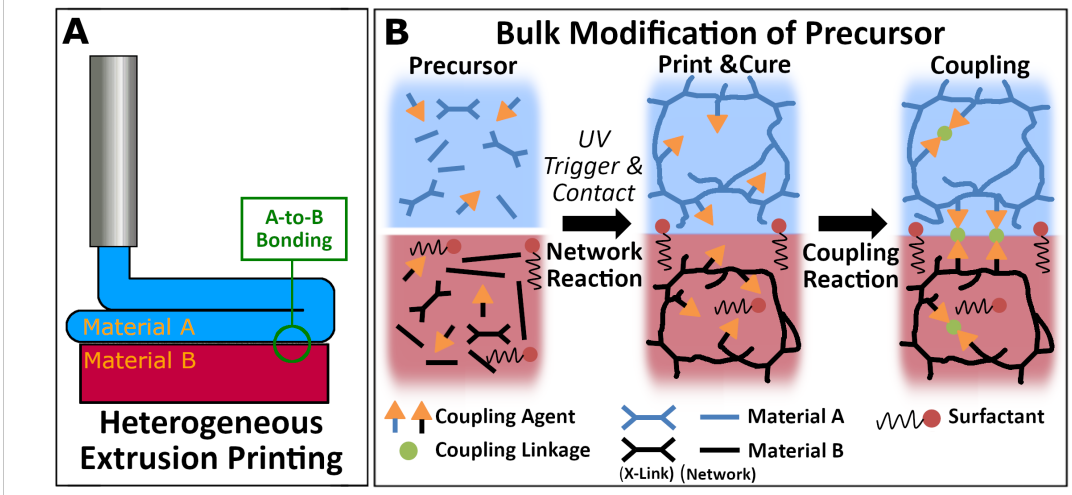

Figure 4.1: In heterogeneous printing, one must account for the integration of materials across materials interfaces. In this work, we highlight the use of coupling agents that can be integrated into the bulk of the materials being printed, but can subsequently bond across the materials interface even after the networks have been formed.

printing, validating its viability is worth exploring.

This work studies the viability of silane coupling agents as a strategy for adhesion enhancement for the extrusion 3D printing of high ionic strength hydrogel and silicone elastomer. Polyacrylamide (PAAm) hydrogel and polydimethylsiloxane (PDMS) hydrophobic elastomer have been selected as a model system for their simplicity, ease of fabrication, and ubiquity in hydrogel ionotronic devices. As the foundation for the extrusion printability of these materials, we build upon existing work in the extrusion 3D-printing context[64].

4.2 Methods

Figure 4.2 highlights the chemical reaction schematic that underlies the silane-based coupling agent strategy we have employed.

Because of the maturity of the silane chemistry, there is already a pre-existing library of com-

pounds that are available for commercial purchase[218,219]. As a result, there are a wide variety of networks that are capable of being adapted to the strategy we utilize here. For this study we have adopted 3-(trimethoxysilyl)propylmethacrylate (TMSPMA) and triethoxyvinylsilane (TEOVS) as the coupling agents for the PAAm hydrogel and PDMS networks respectively. Co-polymerizing these agents into their respective networks (Figure 4.2) effectively modifies the entire network so as to be potentially capable of coupling together. The hydrolysis step then activates the silane compounds by converting methyl groups into hydroxyl groups, a process which occurs more readily under acidic conditions[220]. It is vital to note that this step readily occurs in the hydrogel due to its high water content, provided the pH is of sufficient acidity. However, hydrolysis does not naturally occur in the PDMS elastomer[108], presumably due to its hydrophobic nature. Hydrolysis in the PDMS can be initiated by making contact with acidic water or hydrogel and potentially accelerated through the use of surfactants, effectively causing a surface activation of the silane coupling agent. It is important to note that condensation is a reaction that readily occurs under high pH conditions and the kinetics are significantly reduced at low pH[220]; in order to preserve condensation sites during processing, but still maintain a reasonable rate of condensation during curing, the pH was tuned to 3.5 and was not otherwise modified.

Coupling in and of itself is not sufficient for extrusion printing and several other factors need to be addressed. Wetting is crucial for material printability of the extrusion 3D-printing process. Previous studies have indicated that integrating surfactants into the PDMS is a viable strategy for improving wetting behaviors[221,222,223]. By integrating surfactants into the bulk we may simultaneously accelerate the coupling reaction and achieve satisfactory wetting behaviors without the need for additional processing such as plasma-oxidation[64]. In line with previous work, we opt to integrate the surfactant into the PDMS, though integration into the hydrogel precursor is possible. In order to avoid incompatibilities due to the high ionic strength of the hydrogel precursor, a non-charged surfactant was selected for use (Brij®L23).

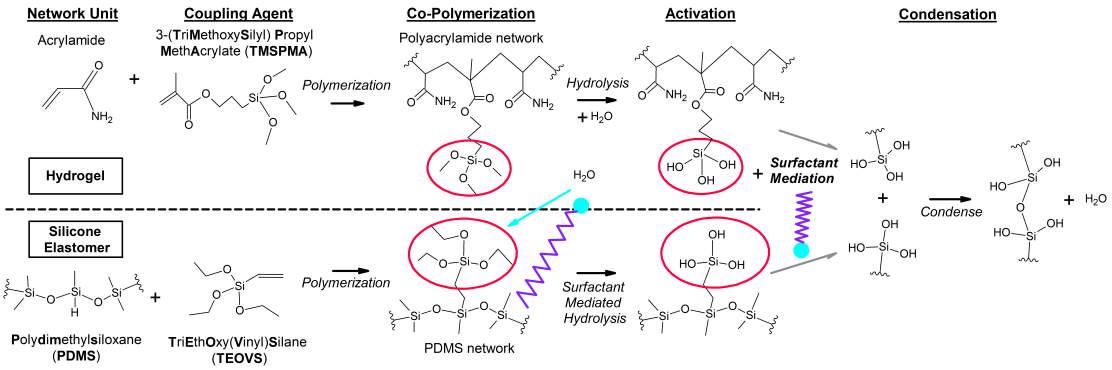

Figure 4.2: Chemical reaction schematic for the incorporation of coupling agents into hydrogel and silicone elastomer networks and their subsequent activity leading to materials integration. Coupling agents are incorporated into their network through reactions with the network unit. After co-polymerization into the network, the coupling agents undergo activation via hydrolysis; this process readily occurs in the hydrogel but requires mediation to occur in the PDMS. After activation, the coupling agents are able to condense across the material interface to form chemical linkages between the two networks.

The hydrogel precursor formulation as described by Tian et al.[64] contains lithium chloride (LiCl) salt for its conductivity and hygroscopic properties, and uncrosslinked PAAm for rheological modification. The materials used in this study have been modified from this formula to incorporate the silane coupling agents and other necessary compounds. As illustrated by Figure 4.3, the rheological properties of the modifier are suitable for printing and minimally differ from those observed previously for the same concentration of polymer in aqueous solution[64]. Initial testing was performed using casting rather than printing for throughput and experimental reasons. Though clear differences exist, a previous study has supported the idea that the underlying mechanisms of adhesion are not expected to differ significantly beyond shear-induced printing effects on the material properties[102].

In particular, we highlight the role of several compounds in the hydrogel and PDMS elastomer. In the hydrogel precursor: TMSPMA serves as the coupling agent; Acetic acid was used to adjust the pH of the precursor to 3.5 in order to control hydrolysis/condensation[220,108]; since the reaction kinetics of the silane coupling agents are sensitive to pH and UV curing rate is tied to

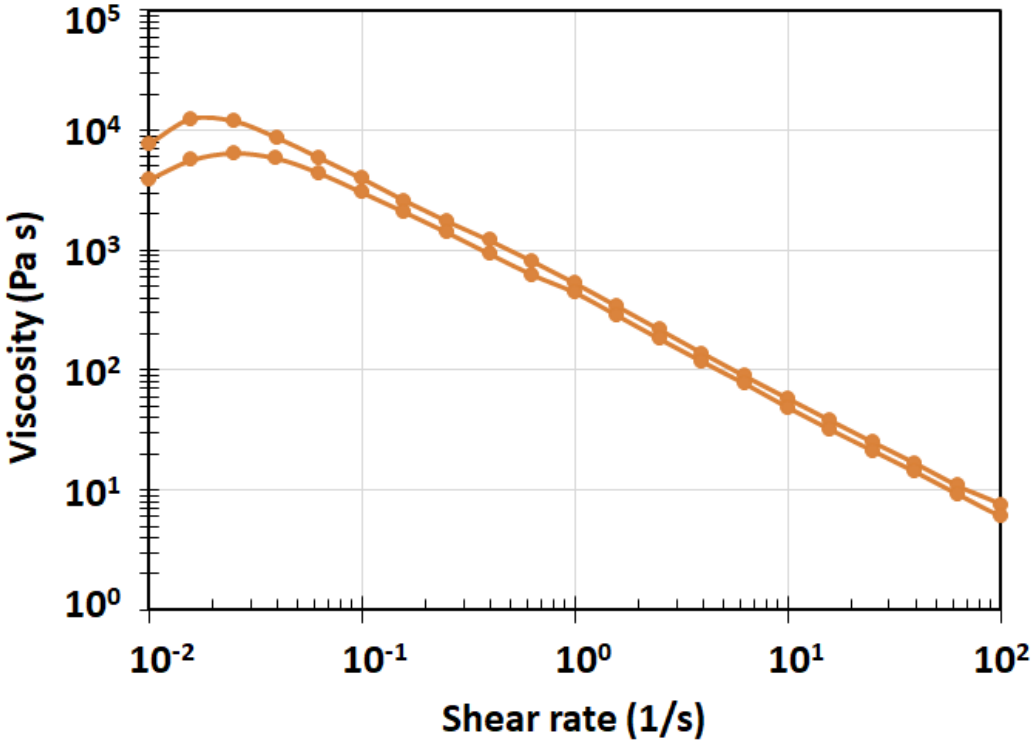

Figure 4.3: Viscometric data for the rheological modifier used in this study, uncrosslinked PAAm chains polymerized at 8% w/v monomer concentration using Irgacure 2959 as UV initiator. The rheological behavior does not appear appreciably different from that observed previously[64], thus this modifier will be suitable for extrusion printing.

initiator concentration, the UV initiator was changed from α-ketoglutaric Acid to Irgacure 2959 in order to avoid coupling pH to UV curing rate. In the PDMS precursor: TEOVS serves as the coupling agent; Brij®L23 acts as the surfactant (Chemical name: Polyoxyethylene(23) lauryl ether, $CH_3(CH_2)_{10}CH_2(OCH_2CH_2)_{23}OH$).

The TEOVS concentration was kept constant for experimental simplicity in the following study, however we note that due to the integration strategy we have utilized, the crosslinking density of PDMS is adversely affected by the addition of higher concentrations of TEOVS. At [TEOVS]=5% w/w, it was observed that the final material after 24 hours of $65^\circ C$ curing was significantly softer and readily underwent plastic deformation. When even higher concentrations of TEOVS were used, the resulting material did not cure into a solid, presumably due to the consumption of available crosslinking sites by the silane coupling agent. This places a limitation on the Sylgard 184 PDMS recipe, and potentially other similar elastomers, without additional modifications to introduce more crosslinker. Exact recipes used in this study have been specified in the experimental section (Appendix A).

It is worth mentioning that due to the silane coupling agent's bonding capabilities, particularly given the UV exposure used in this study, it is crucial that during the sample removal process that care be given towards the materials in contact with the hydrogel precursor, as these will strongly bond together. This results in the need to apply additional pressure to the bilayer in order to maintain interfacial integrity prior to testing; this can be achieved by designing a mold with externally accessible ports to apply said pressure.

A 90°-peel test setup was used to quantify the adhesive energy of the PAAm hydrogel-PDMS bilayers. By peeling off the PDMS from the hydrogel layer affixed to a glass substrate, traces of the peeling force against peeling extension were obtained. All tests were initiated by making a pre-crack of less than $5mm$ and performed at a constant peeling rate of $50mm/min$ for a length of at least $60mm$. After the crack begins propagating through the bilayer, the peeling force eventually

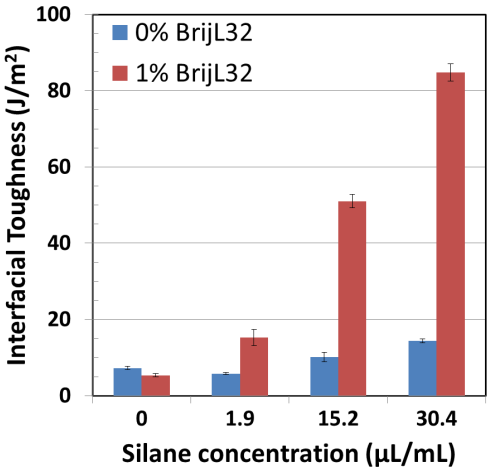

Figure 4.4: Cast hydrogel-PDMS bilayers with varying hydrogel silane concentration (TMSPMA) and PDMS surfactant content (Brij®L23). PDMS silane concentration (TEOVS) was kept constant at 2% w/w relative to PDMS mass. It can be observed that the presence of both surfactant and high amounts of silane are required in order to obtain good adhesive strength of the materials interface.

settles into a steady-state regime. Strain energy release rate during peeling, G, can be described[187] as $G = \frac{F}{b}(1 - cos\vartheta)$ for peel angle ϑ, peel force F, and sample width b. This expression simplifies to $G = F/b$ for $\vartheta = 90°$. Under steady-state crack propagation, the interfacial fracture energy or toughness $\Gamma = G$, such that Γ is given by the measured plateau peeling force divided by the width of the specimen.

4.3 Results and Discussion

The peeling tests reveal a clear difference in adhesive behaviors depending on the compositions that are used in the hydrogel and elastomer. In all of the discussed tests, the silane concentration in the PDMS was kept constant at 2% w/w of the net PDMS content. As Figure 4.4 shows, increasing the coupling agent concentration corresponds to an increase in the adhesive strength of the interface. However this trend only seems to hold for cases where surfactant is incorporated into the PDMS

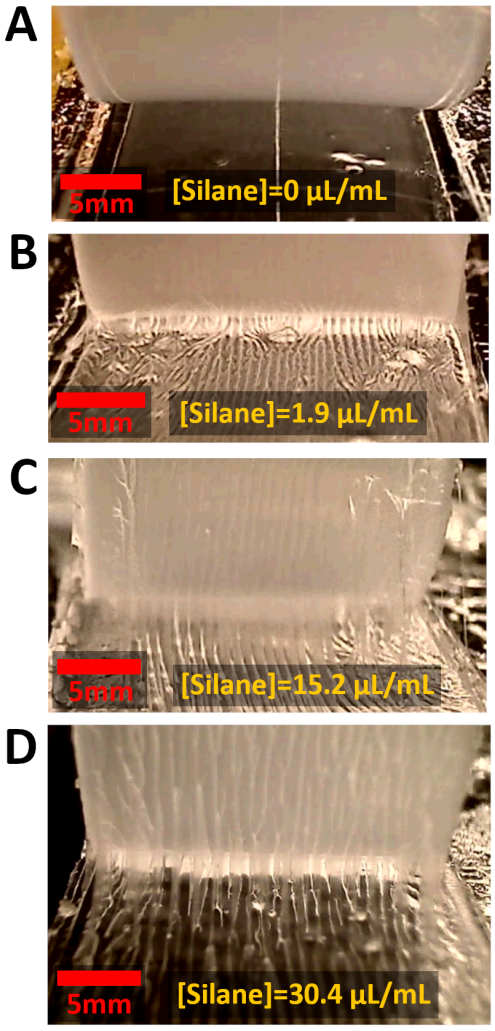

Figure 4.5: As the silane concentration of the hydrogel is varied, it can be observed that the peeling behavior of the hydrogel-PDMS interface varies as well. TMSPMA concentration: A) 0 $\mu L/mL$, B) 1.9 $\mu L/mL$, C) 15.2 $\mu L/mL$, D) 30.4 $\mu L/mL$. In A) and B) we observe interfacial failure, as no permanent damage is sustained by either material. In C) and D) we begin to see cohesive failure of the hydrogel, as solid residues are left on the PDMS surface and permanent damage is observed on the hydrogel. We note that clear ligaments can be observed in C) and D).

(1% BrijL23 condition). Within these conditions, the highest interfacial toughness we were able to achieve was $\Gamma = 84.74 \pm 2.25$ at [TMSPMA]=30.4 $\mu L/mL$ and 1% BrijL23.

For the surfactant containing conditions, experimental observations indicate a shift from interfacial failure of the interface to cohesive failure of the hydrogel occurs around [TMSPMA]=15.2 $\mu L/mL$, as permanent damage can be seen in the hydrogel after peeling and solid residues remain on the PDMS. The fingering instabilities that form during peeling (Figure 4.5) begin to form clearly defined ligaments with more silane coupling agent (Figure 4.5 C and D, Figure 4.6). This behavior is consistent with previous studies of soft materials adhesion[102] and may be attributed to either elastic[191,192,193] or viscoelastic effects in the adhesive[190]. These instabilities only temporarily remain after peeling for the lower silane concentrations, but are permanent for the higher concentrations (above [TMSPMA]=15.2 $\mu L/mL$). Previous studies have indicated that some mechanisms allow for the participation of the rheological modifier in the formation of these peeling instabilities[102], however, it is possible there is a combined effect at play. The aforementioned mechanism requires a degree of hydrophilicity of the PDMS surface before occurring, which coincides with the introduction of the surfactant. Further investigation would be required to firmly establish to what extent the rheological modifier affects the peeling.

It is expected that the positive correlation between TMSPMA and interfacial toughness continue above the tested range of TMSPMA, however [TMSPMA]=60.8 $\mu L/mL$ hydrogel precursors were attempted and resulted in a phase-separated mixture that was unable to properly UV-cure under standard conditions. TMSPMA was still incorporated into the gel mixture, as the hydrogel does eventually crosslink due to the self-condensation action of the silane over the course of several days; this indicates that the initiator was likely affected in some way, however we were unable to determine the root cause. Even so, observations for the 1% BrijL23 and [TMSPMA]=30.4 $\mu L/mL$ condition suggest that the interfacial toughness is more likely bounded by the toughness of the hydrogel rather than the hydrogel-PDMS interface. Modifying the recipe by halving the amount of

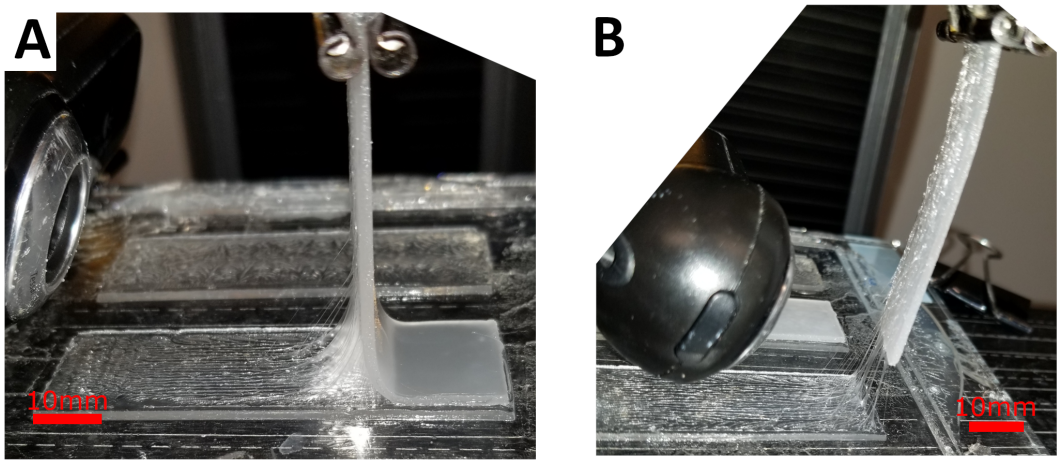

Figure 4.6: These two cropped images grant a different perspective to Figure 4.5D, in order to highlight the well-defined ligament structures that coincide with cohesive failure of the hydrogel. A) is a photograph taken during peeling, while B) is taken at the end of the same peeling test.

UV crosslinker (corresponding to the N,N'-methylenebis(acrylamide) or MBAA) and keeping all other factors constant, we are able to achieve a stronger interface with peak peeling forces indicating $G = 127 Jm^{-2}$. According to the Lake-Thomas model[224], reducing the crosslinking density of the hydrogel network leads to a greater capacity for elastic energy dissipation. This increase in energy dissipation would lead to a corresponding increase to the overall interfacial toughness, provided the inter-network bonding is of sufficient strength to allow for such deformation[106]. Further improvements to the toughness will likely need to explore toughening mechanisms for the materials being printed. In addition, since it is well known that the TMSPMA will act as a secondary crosslinker within the material bulk, designing materials recipes should factor in the ultimate materials properties after both the standard copolymerization process and coupling reactions have occurred[108]. We note that unless the pH is modified to an alkaline environment, complete condensation will likely take a significant period of time due to kinetics[220].

In the condition where no surfactant was used (0% BrijL23), minimal changes were observed in the peeling behavior with increasing [TMSPMA]. Fingering instabilities were present as soon as

TMSPMA was introduced, in line with the 1% BrijL23 and [TMSPMA]=1.9$\mu L/mL$ condition, however only interfacial failure was observed for the entire range of surfactant/silane explored. This suggests the surfactant is a necessary mediator of the coupling reaction for the range of compositions that we have explored. However, previous experiments have demonstrated that surfactant is not necessary for satisfactory hydrogel-elastomer bonding outside printing-relevant contexts[108], which suggests that some form of inhibition is occurring within the system we are studying.

To investigate this, we have examined all components and processing steps that may differ between Liu et al.[108] and the present system. This investigation has led to the hypothesis that the presence of the rheological modifier has a detrimental effect on the final adhesive strength that can be attained at lower concentrations of TMSPMA. This has been observed even for reduced rheological modifier concentrations, down to 1/4 of quantities reported in the experimental methods. It was initially suspected that the centrifugal mixing process may have exhausted silanol sites prior to interfacial condensation. Though the rheological modifier is too viscous to mix using a vortex mixer and centrifugal mixing must be used, Figure 4.7 indicates that there is no appreciable difference between the two processing techniques. Hydrogel precursor formulations that do not utilize any rheological modifier achieve similar levels of adhesion and are all observed to experience cohesive failure. Inserting a waiting time at room temperature does little to affect the adhesive strength, and additional tests verified that inserting a waiting time at elevated temperatures of $65^{\circ}C$ also has minimal effect. Temperatures of the mixtures during centrifugal mixing were observed to be elevated up to $41-45^{\circ}C$, with the rheological modifier contributing to a $4^{\circ}C$ increase in stable temperature during mixing; this we determined was too small of a difference to warrant further consideration. However, the introduction of the rheological modifier immediately results in poor adhesion.

Other possible explanations for this were explored, but unfortunately none yielded a concrete mechanism of action. Another proposed parameter was the precursor viscosity, where the high viscosity required for printing may have adverse affects on the kinetics of condensation. Though this

would appear to make sense of the results, internal tests and previous work[108] without rheological modifier have both shown that cohesive failure can still be obtained by having fully-cured hydrogel and PDMS making contact and cured at elevated temperatures. A solid network would be a sufficiently close approximation to a liquid with infinitely high viscosity, thus the hypothesis appears to fail by an experimental *reductio ad absurdum*. Another possibility considered was an interaction between the monomer (acrylamide) and the silane coupling agent, however repeated internal tests confirmed that cohesive failure was still achieved with hydrogel precursors of the equivalent network monomer content as monomer and rheological modifier combined. Although some batch consistency issues arose from moisture sensitivity of the TMSPMA, even after handling procedures were standardized the presence of the rheological modifier consistently failed to achieve appreciable adhesion at lower silane concentrations. TMSPMA was also pre-hydrolyzed prior to addition to the rest of the hydrogel precursor by vortex mixing it with an acidic aqueous solution (pH=3.0, Acetic Acid) for 10 minutes, however this also did not induce any change to the adhesion with rheological modifier present. Regarding PDMS processing, modifying the mixing order of its components (base, surfactant, silane, and curing agent) was considered, but failed to yield any significant results. While we were unable to determine the mechanism underlying this phenomenon, we have observed that the rheological modifier appears to necessitate significantly more TMSPMA and the presence of a surfactant to achieve good interfacial toughness of the hydrogel-PDMS interface.

In order to explore the effects of the surfactant on the adhesive strength, we maintain a constant concentration of the TMSPMA ([TMSPMA]=30.4 $\mu L/mL$) and vary the surfactant concentration (Brij®L23) in the PDMS. Figure 4.8 shows that there is an optimal amount of surfactant to be used, which is approximately at the 1% BrijL23 concentration. Too little surfactant (0.5% and less) yields interfacial failure, suggesting that insufficient levels of condensation occurs in that condition. Whether this is due to insufficient hydrolysis or condensation was not able to be determined. Too much surfactant (2% Brij®L23) still yields cohesive failures, but adhesive strength is lower than

RheoMod	Mixing Condition	Γ (J/m^2)	±	n
0	30s vortex + no wait	35.91	5.36	3
0	30s vortex + 1hr wait	27.96	1.54	2
0	30s vortex + 2hr wait	27.13	3.76	6
0	1hr centrifuge + 1hr wait	40.19	4.53	3
8% w/v	1hr centrifuge + no wait	6.00	0.76	3

Figure 4.7: Different mixing methods and time were tested for their achievable interfacial toughness and to isolate the effects of the rheological modifier on the silane coupling agent kinetics. All tests were performed at [TMSPMA]=1.9$\mu L/mL$ and [TEOVS]=2% w/w to PDMS mass. No surfactants were utilized and fabrication procedures are otherwise identical to those stated in the experimental section. Rheological modifier was introduced at the same printing-relevant level as indicated and was unable to achieve reasonable adhesion. n indicates the number of tested samples in each condition.

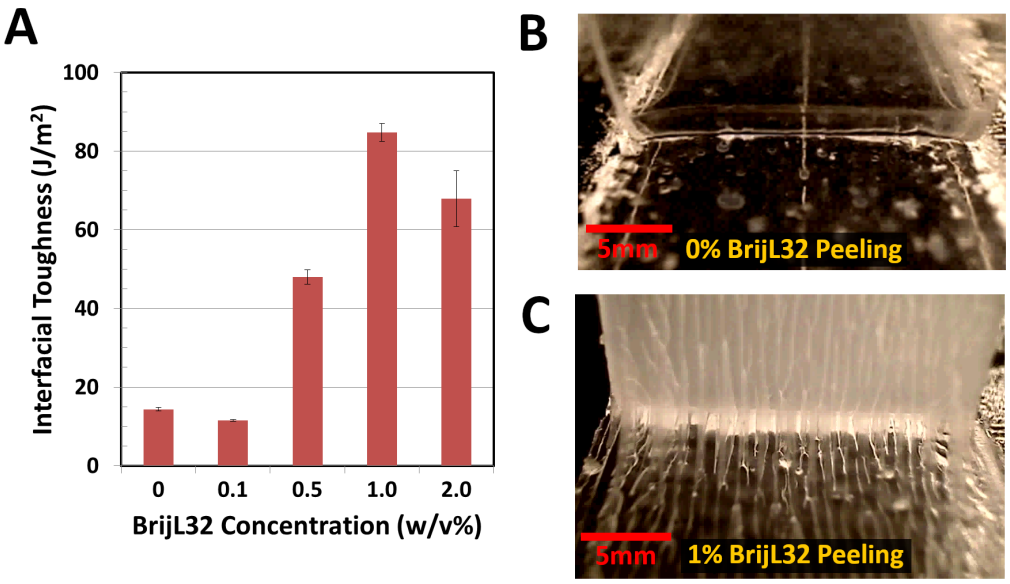

Figure 4.8: A) By fixing hydrogel TMSPMA concentration at 30.4$\mu L/mL$ and PDMS TEOVS concentration at 2% w/w, we can clearly see the effects of varying the surfactant concentration (Brij®L23) on the interfacial toughness. Too little surfactant yields minimal improvement to the adhesion, whereas too much can cause degradation of the adhesion. B) & C) illustrate the peeling behavior differences between having 0% and 1% surfactant, which shows interfacial and hydrogel cohesive failure respectively.

at 1% Brij®L23. The results are consistent with previously reported results[108], however due to the time-sensitive nature of silane kinematics it is difficult to disentangle the hydrolysis from the condensation process. A previous report suggests that a crowding out of the silane functional groups may be occurring at higher surfactant concentrations. While our results do not shed further light on precise mechanism of action, they do confirm the general trend of a local maximum of effectiveness for surfactant action.

Nevertheless, experimental observations suggest that the surfactant plays a role at both the hydrolysis and condensation stages of the coupling. First being that in all cases, both with and without surfactant, the PDMS surface after peeling and DI water rinsing are more hydrophilic in their wetting behavior even when no cohesive failure has been observed; this suggests that (at least partial) hydrolysis of the TEOVS has occurred in the time the PDMS has been in contact with the PAAm hydrogel irrespective of the presence of the surfactant. Secondly, the fact that excess surfactant causes poorer adhesion to occur only makes sense if we consider condensation stage related activity in addition to those in hydrolysis. Surfactant participation in silane hydrolysis only explains the poor adhesion observed at lower concentrations of surfactant.

In order to validate the study that we have performed using materials casting, we then fabricated samples using an extrusion printer with methods as described by[64]. As Figure 4.9A illustrates, a $500\mu m$ barrel was used to extrude a UV-curable formulation of PDMS, which was then fully cured prior to extrusion of the hydrogel precursor directly on top. A glass plate was then placed on top of the hydrogel with spacers prior to a complete UV cure within a nitrogen purged container, which then allows for a rigid peeling substrate to cure in contact with the hydrogel and develop strong bonding. A peeling test was then performed using bilayer sheets of material that were printed in this manner, which as Figure4.9 demonstrates, good bonding between hydrogel and PDMS elastomer is achieved with $\Gamma = 192.79 \pm 6.26 Jm^{-2}$. It is worth noting that the failure mode observed was primarily that of the hydrogel-glass interface, despite an initial crack at the hydrogel-PDMS inter-

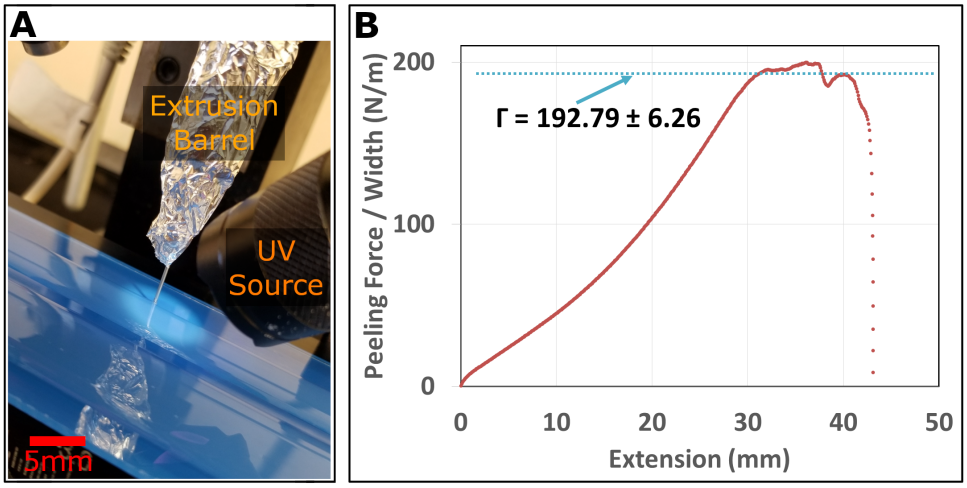

Figure 4.9: A) Samples are fabricated via materials extrusion from syringe barrel in a customized extrusion printing machine for the peeling test shown in B). PDMS was printed first and cured to completion prior to hydrogel extrusion. Both hydrogel and PDMS were printed as a 20mm x 70mm sheet with a 500μm ID syringe tip. B) Peeling tests indicate adequate adhesion and failed primarily at the hydrogel-peeling substrate interface despite initial crack at the hydrogel-PDMS interface.

face, which suggests that the actual interfacial toughness may be different from or larger than the observed value.

4.4 Conclusions

In summary, we have successfully demonstrated that, with the appropriate modifications, a silane coupling agent strategy is viable for the extrusion printing of hydrogel onto PDMS elastomer. Although there appears to be some form of condensation inhibition due to the presence of the rheological modifier, the combination of a non-charged surfactant and increased coupling agent concentration is sufficient to overcome this barrier to cohesive failure. Evidence suggests that the interfacial adhesion that we have achieved is bounded by the material toughness, not the interfacial toughness. Therefore further enhancements to the adhesion must investigate mechanical toughening mechanisms for the hydrogel and PDMS materials. Although further work needs to be done in order to establish full compatibility of the coupling agent strategy for the extrusion printing of high ionic strength hydrogel and elastomer, this work serves as an important step in verifying the potential of silanes to serve well in this task.

This is the way the world ends

This is the way the world ends

This is the way the world ends

Not with a bang but a whimper.

"The Hollow Men", by T.S. Eliot

5

Conclusion

Hydrogels have undergone a rapid series of developments over the last several decades and have proven their potential, not only for its bio-compatibility, but as a powerful and complex engineering material. Though the field surrounding hydrogel-elastomer ionotronic fabrication is nascent, many contributions towards proper materials integration in extrusion printing have been made through the course of this dissertation. We summarize these contributions:

- A new class of hydrogels that retain high stretchability, high fracture toughness and good conductivity at temperatures far below the freezing point of water was developed by using an alginate-PAAm tough gel soaked with $CaCl_2$. Three new hydrogel states below freezing were characterized: regular hydrogel, slurry gel, and fully frozen gel. Slurry gels demonstrated improved mechanical properties over the other two states. A stretchable ionic touch sensor that functions at temperatures well below the freezing point of water was demonstrated.

- A method for the 3D extrusion printing of an ionically conductive PAAm hydrogel and a PDMS dielectric elastomer was developed by targeting several aspects of extrusion printability. By tuning the rheological behavior of the hydrogel precursor and performing oxygen plasma treatments of PDMS surfaces, we demonstrated printing and integration of hydrogels directly with PDMS at sub-millimeter resolution. We demonstrated the printing capability of this platform by fabricating an ionic cable and resistance-based strain sensor.

- A quantitative study of the interfacial adhesion and water contact angle demonstrates that a hydrogel is capable of stabilizing PDMS surface oxidation treatments. Furthermore, we discovered that a macroscopic viscous layer segregates to the interface of a hydrogel-PDMS system if the hydrogel precursor contains a long-chain rheological modifier and the PDMS surface has been treated with oxygen plasma. This viscous layer enhances adhesion by increasing energy dissipation during delamination and results in fully reversible interfacial adhesion.

- Finally, we have successfully demonstrated the viability of the silane coupling agent strategy for hydrogel onto PDMS elastomer extrusion 3D printing. Although some unknown form of condensation inhibition with a rheological modifier was encountered, the combination of a non-charged surfactant and increased coupling agent concentration was sufficient to overcome this barrier to cohesive failure. Evidence suggests the achieved interfacial adhesion was bounded by the material toughness, suggesting that further adhesion enhancement must

investigate mechanical toughening mechanisms for the hydrogel and PDMS materials.

Yet despite the many advancements that have been made, many more challenges and open questions remain. For instance, although viability has been demonstrated for silane-based coupling agents, the curious effects of the rheological modifier have yet to be fully answered and may pose problems in adopting it at a wider or larger scale. In addition the technique itself is prone to time-sensitivity due to thermally driven nature of the condensation process. However, it does solve a potential problem that other 3D printing materials have encountered: anisotropy of printed materials. Although this has yet to be verified as an actual issue in 3D printed soft materials (which in of itself is a study worth undertaking), other materials such as plastics and metals have encountered differences in material properties dependent on printing orientation. Silane coupling agents stand well poised to solve this kind of problem, as its binding properties are completely independent of the network formation process. In addition, none of the studied techniques have made consideration of the recently proposed idea of network topology in adhesion[101]. Intuitively this would open up a significantly wider array of potential adhesive designs for extrusion printing. It does remain to be seen to what extent one would be able to take advantage of this new framework of understanding adhesion in soft materials, particularly when additional constraints must be considered for manufacturing purposes.

Although work has been completed in the field regarding arbitrary sequence printing[107], the technique is not complete. In both the work demonstrated in Chapter 4 and existing literature, no work has quite solved the problem of high resolution transparent elastomer printing. The addition of silane coupling agents in of itself also creates a degree of opacity (in the hydrogel) that worsens with increasing concentrations of coupling agent. These unsolve problems are vital because ultimately these techniques must be scalable, and if printing is limited to certain dimensions due to poor UV transmission then this is a problem that must be addressed. In addition, although extrusion printing is itself a valuable rapid prototyping tool, being able to extend these advances in

manufacturing know-how to other kinds of manufacturing is important due to the inherent limitations of materials extrusion. At the end of the day, materials extrusion is slow if you're making many copies of the same design. This does mean that customization can be a strong selling point for the technique, an advantage that cannot be understated due to current research into personalized medicine [225] and the potential for the printing of organs with patient compatible tissue. However, the moment n must go from 1 to 10000 is the moment that materials extrusion ceases to be competitive.

Nevertheless, materials integration as a problem never quite goes away. Regardless of the manfacturing technique that is eventually selected for hydrogel-based ionotronic devices, dissimilar materials must be made in such a way that strong bonding is achieved. What technique will dominate in a decade? Will this integration be done using chemical, physical, or topological means? All impossible to say at this stage. However, much of the joy in research is turning the crank of problems, both large and small, and seeing what the dice of the universe decides to roll. Since solving one problem leads to many others spawning in its place, there still are (and forever will be) many dice left to roll.

The scientific theorist is not to be envied. For Nature, or more precisely experiment, is an inexorable and not very friendly judge of his work. It never says "Yes" to a theory. In the most favorable cases it says "Maybe," and in the great majority of cases simply "No."

Albert Einstein

A

Experimental Methods

In this appendix, all experimental methods will be detailed for the chapters contained in the main text of this thesis. Each individual section will correspond to the appropriate chapter for which methods are described within. Sections will be listed out in sequential order as it appears in the dissertation as appropriate.

A.1 Chapter 1: Highly stretchable and tough hydrogels below water freezing temperature

A.1.1 Hydrogel synthesis

All chemicals were received and used without further purification. The following substances were purchased from Sigma Aldrich: acrylamide (AAm, A8887), ammonium persulfate (APS, A9164), N,N,N',N'-tetramethylenediamine (TEMED, T7024), N,N'-methylenebis(acrylamide) (MBAA, M7279), calcium sulfate dihydrate ($CaSO_42H_2O$, C3771) and calcium chloride ($CaCl_2$, C1016). Sodium alginate was purchased from FMC Biopolymer (Manugel GMB). Polyacrylamide-alginate double-network hydrogels were prepared following the method described by Sun et al.[8] First, 40.54g of AAm and 6.76g of sodium alginate powder were dissolved in 300mL of distilled water to form an aqueous solution. The solution was stirred overnight for complete mixing. Afterwards, MBAA, TEMED, APS and $CaSO_42H_2O$ in quantities of 0.0006, 0.0025, 0.01 and 0.022 times the weight of AAm were added to the solution in sequence. The prepared pre-gel solution was then degassed, quickly poured into $50x40x1.65mm^3$ acrylic molds, and covered with a glass plate. The samples were kept at room temperature for 24hr to allow complete polymerization. Afterwards, the samples were taken out of the molds and were either directly used for testing (referred as 0 wt% $CaCl_2$ gels) or soaked in 10 wt% or 30 wt% $CaCl_2$ solutions for at least 5 days. To ensure that the concentration of $CaCl_2$ in the external solution remained nearly constant before and after soaking the hydrogel, we prepared the $CaCl_2$ solution with a volume at least 10 times the volume of the hydrogel. The final water contents of the 0 wt%, 10 wt% and 30 wt% $CaCl_2$ gels were 76%, 84% and 78% by weight, respectively. It is worth noting that the precise control of the water content for the different gel compositions is difficult and was not the focus of the present study. Instead, we chose to use a simple and easily reproducible method for preparing the different gel compositions. Extensive

research on the effect of water content has been conducted and discussed in prior work[8,226,227,228]. Eventually, considering the 0 wt% $CaCl_2$ gel as the reference state, the volumetric swelling ratios reached by the 10 wt% and 30 wt% $CaCl_2$ gels were 1.78 and 2.20 respectively.

A.1.2 Mechanical Testing

A minimum of three specimens were used for all test conditions. The nominal stress-stretch curves were tested using the pure shear setup,[8,133] both at ambient and sub-zero temperatures (i.e. 20°C, 0°C, -15°C, -30°C, -50°C and -70°C), see Figure S3 for the full set of data. A thin sheet of hydrogel sample with a rectangular shape (50mm width and 10mm length) was fixed to two rigid acrylic grips, and mounted in an Instron 5966 tensile tester with a 500 N load cell. The temperature of the ambient environment was controlled by an Instron 3119-600 environmental chamber supplied with liquid nitrogen. Tensile tests were performed at a strain rate of 1 min-1, and video-recorded with a digital camera (Canon 7D). The nominal stress was computed by dividing the applied load on the sample by its initial cross-sectional area (the product of width times thickness), while the stretch was calculated by dividing the deformed length by the initial length of the sample. To avoid undercooling of the hydrogel samples, specimens were first held at -90°C for 45 min and then 20 min at the final testing temperature to ensure equilibrium conditions for each experiment (see A.1). To measure the fracture toughness, specimens were cut using a fresh razor blade to create a 20mm notch extending from the edge of the specimen. The stress-stretch curves of identical specimens with and without notch were then measured. The critical stretch for fast fracture of the notched specimens was measured and the associated critical energy release rate was then determined using the method developed by Rivlin and Thomas :[133] $G = HW(\lambda_c)$, (1) where H is the initial length of the sample and W(λ) is the area below the nominal stress stretch curve of the unnotched sample integrated up to the critical stretch λc of the notched sample. Thermal characterization: Samples were characterized using a differential scanning calorimeter (TA Instruments, DSC Q200) with a refrigerated

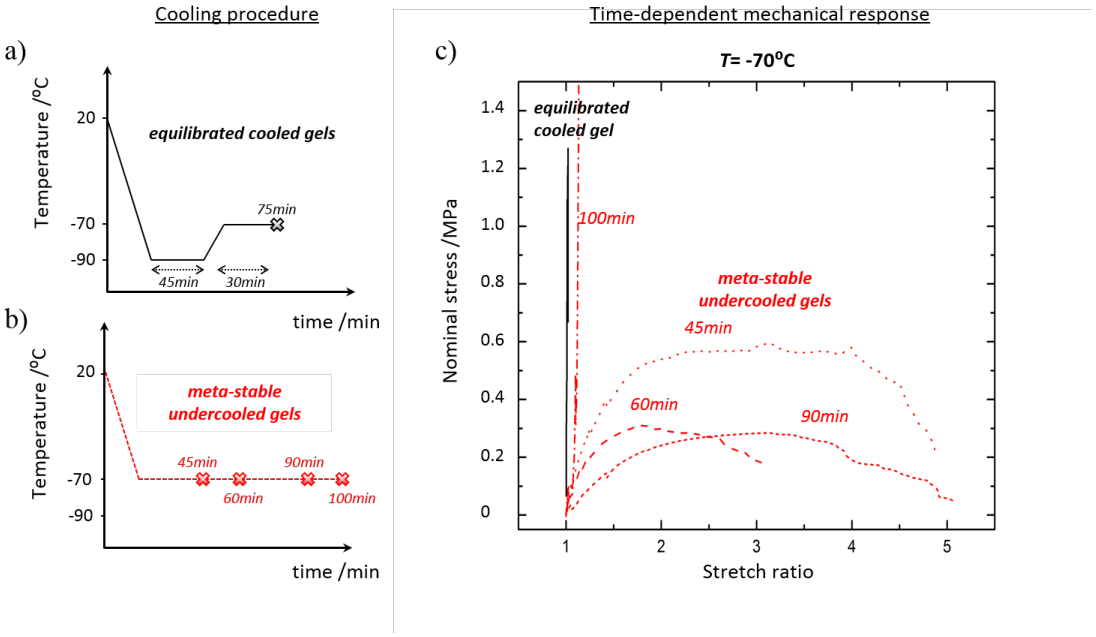

Figure A.1: Time dependent stress-stretch curves of metastable undercooled 30wt% $CaCl_2$ gels at -70°C: (left) two different temperature profiles for the cooling procedures of (a) equilibrated cooled gels versus (b) metastable undercooled gels with different cooling time at -70°C before testing; (c) the corresponding stress-strain curves, showing inconsistent and variable mechanical response for undercooled specimens. Waiting long enough at -70°C will eventually make the gel reach the equilibrated gel response.

cooling system (TA Instruments, RCS90). Samples were contained in hermetically sealed aluminum pans (TA Instruments, Tzero Aluminium Hermetic Pan) for testing, with an empty pan used as inert reference. The DSC was operated under a $40\mu L min^{-1}$ nitrogen flow rate and data were captured at a rate of 1Hz. Samples were first equilibrated at $25C$ and then cooled at a rate of $5C min^{-1}$ to $-90C$. After an isothermal period of at least 90min, samples were heated up at $1C min^{-1}$ to the initial equilibration temperature ($25C$).

A.1.3 Conductivity Measurement

The current passing through a rectangular gel specimen was measured as a function of applied voltage (5 measurements ranging from 0.1 to 1V) with a 2-point probe set up. Sample dimensions were measured to within 0.1 mm. The conductivity of the sample was deduced from the slope of current versus voltage. The measurement was performed for each gel composition at temperatures ranging from room temperature to $-50C$. Ionic touch sensor demonstration: We fabricated a sensor that can detect the pressure of finger touch in a design similar to previous work.[38] The sensor consists of a 20mm x 20mm x 0.5mm acrylic elastomer (VHB 4905, 3M), covered with two 30 wt% $CaCl_2$ hydrogels of 20mm x 20mm x 0.2mm on each side. Copper wires were used to connect the hydrogels to metallic electrodes and the electrodes to a capacitance meter (LCR/ESR meter, Model 885, BK Precision). The capacitance meter was set to a sinusoidal measurement signal with a maximum voltage of 1 V and a frequency of 100 Hz. To demonstrate the sensing ability at low temperature, we attached the sensor to a glass plate, and recorded the change of capacitance as a result of repeated touches at -11^{0}C.

A.2 Chapter 2: Adapting Salt-hydrogels for 3D Printing

A.2.1 Preparation of Polydimethylsiloxane (PDMS)

A UV curable formulation of polydimethylsiloxane elastomer (Shin-Etsu Silicones, KER-4690 A/B) was provided by the manufacturer as a two-part precursor and was used in the recommended 1:1 ratio. After a 2 minute mixing cycle in a planetary centrifugal mixer (Thinky, ThinkyMixer ARE-300) at 2000 RPM, the precursor was used without further preparation and was cured via 365 nm UV light at a dose of $10 mW cm^{-2}$ for a period of 30 minutes, followed by an overnight bake at 65 °C. Prior to further printing, the PDMS was treated with an oxygen plasma (SPI Supplies, Plasma Prep II) at an O2 pressure of 18 psi, vacuum pressure of 275 mTorr, and RF power of 80 W for 60 sec.

A.2.2 Preparation of the hydrogel precursor

The precursor used in the printing process consisted of two components: the rheological modifier and the hydrogel component. The rheological modifier consisted of an un-crosslinked PAAm solution made by UV exposing an acrylamide (AAm, Sigma-Aldrich, A8887) solution containing α-ketoglutaric acid (α-keto, Sigma-Aldrich,) and N,N,N',N'-tetramethylethylenediamine (TEMED, Sigma-Aldrich, T7024) at 25°C with the following ratios (w/w): 92.17% deionized water (resistivity = 18.2 MΩ cm), 7.37% AAm, 0.00044% α-keto, 0.00021% TEMED. The hydrogel component consisted of AAm, α-keto, TEMED, lithium chloride (LiCl, Sigma-Aldrich, 746460), and N,N'-methylenebis(acrylamide) (MBAA, Sigma-Aldrich, 146072). This component was added to the un-crosslinked PAAm solution and mixed using a planetary centrifugal mixer (Thinky, ThinkyMixer ARE-300) at 2000 RPM. Final precursor composition ratios (w/w) were: 63.15% deionized water, 3.86% PAAm, 9.05% AAm, 18.43% LiCl, 0.072% MBAA, 4.95% α-Keto, 0.479% TEMED.

A.2.3 Rheological Characterization

All rheological measurements were made using a TA Instruments Discovery HR-3 Hybrid Rheometer with a cone and plate geometry at a reference temperature of 25°C. Oscillatory rheometry was performed on the PAAm/LiCl portion of the hydrogel precursor using a frequency of 1 Hz and sweeping shear stresses from 1–500 Pa. Viscometry was also performed with shear rates ranging from 0.01–100 s-1.

A.2.4 Device Fabrication

PDMS and hydrogel precursors were directly printed onto a UV-resistant acrylic substrate (6.35mm thickness, McMaster-Carr) rinsed with DI water followed by isopropanol and blown dry with nitrogen. A CNC milling machine (Sherline Products, 5400) was used as a positioning stage, upon which independent linear actuators (Zaber Technologies, T-LA60A) were mounted onto the z-axis of the stage as syringe pumps. Syringes (5 ml, Hapool Medical Technology Co) contained the precursors and were extruded through a 23 gauge blunted syringe tip (0.337mm ID, SAI Infusion Technologies). A displacement rate was prescribed to the actuators and the requisite extrusion force was applied to the syringe end. A steady flow of dry nitrogen piped through a saturated potassium carbonate (Sigma Aldrich) solution was used to purge the printing area of oxygen during the printing process and simultaneously fix the relative humidity. A 6 W UV LED (Instun, SK66) was used to initiate curing of the ink as it is extruded from the syringe at a dose rate of $\approx 3mWcm^{-2}$. Printed samples were then flood exposed to UV using an $8W$, $365nm$ UV Lamp (UVP, UVLS-28 EL) in a nitrogen environment at an effective dose rate of $\approx 6mWcm^{-2}$. Devices began with a printed PDMS layer that was fully cured and baked, as previously described. Prior to additional printing, the PDMS was treated with O_2 plasma and stored in DI water until immediately prior to the printing in order to preserve the hydroxyl groups on the PDMS surface. While this plasma treatment

process is incompatible with hydrogels already present on the PDMS due to vacuum requirements, a UV-Ozone treatment may be substituted to achieve the same effect at a slower rate while maintaining hydrogel integrity[59]. After subsequent hydrogel and PDMS layers were printed, the device was exposed to the flood UV lamp. Since the curing of PDMS has been observed to be inhibited by contact with the hydrogel precursor, the printed device was baked at 65°C for 6 hours to drive the PDMS curing process to completion, followed by a DI water soak of 1 hour to rehydrate the hydrogel from the oven bake.

A.2.5 Sample Characterization

Cross-sectional images and measurements were made using a Coherence Correlation Interferometry (CCI) optical profiler (Taylor Hobson, CCI HD) with 5x and 20x objective lenses. DC electrical measurements were made using multimeters (Fluke, models 8846A and 175). A DC power supply (Dr.Meter, PS-305DM) was used to generate the current used in the four-point probe measurement. For the AC characterization, a waveform generator (Keysight, 33500B) and oscilloscope (Keysight, DSO-1004A) with passive probes (Keysight, N2862B) were used. Uniaxial tensile testing, for both stress-strain and fatigue experiments, was performed on a uniaxial tensile tester (Instron, 3342 Single Column UTS) using a strain rate of 50 mm min-1. For the fatigue experiments, a maximum strain of 20% was used. All PDMS-hydrogel samples were gripped using rubber-coated tensile grips in a region containing only PDMS. Stretch was calculated from the crosshead displacement rate and the initial gauge length of the samples.

A.3 Chapter 3:Adhesion between Hydrophobic Elastomer and Hydrogel through Hydrophilic Modification and Interfacial Segregation

A.3.1 Preparation of PDMS:

Sylgard 184 (Dow Corning) was mixed at the prescribed 10:1 ratio and cast into a 20mm x 200mm x 1.6mm acrylic mold, followed by degassing for 1 hour at 70 kPa vacuum. The degassed PDMS was then sealed by applying pressure with another acrylic plate and cured in an oven at 65°C for 24-hours. The PDMS is either used immediately following removal from the mold or undergoes further surface treatment. Prior to surface treatment the PDMS was rinsed with DI Water and isopropyl alcohol, and then dried with nitrogen. The PDMS is then treated with oxygen plasma (SPI Supplies, Plasma Prep II) at an O2 Pressure of 18 psi, vacuum chamber pressure of 275 mTorr, and RF power of 80 W for 60 seconds. After treatment, the PDMS is immediately placed in DI water for transport and dried with N2 prior to use.

A.3.2 Preparation of hydrogel:

The PDMS segments are placed within a segmented acrylic mold to allow for hydrogel precursor to be cast directly onto the PDMS surface and cured while in direct contact; the mold may then be separated horizontally and removed such that the PDMS-Hydrogel interface is maintained (Figure 3.4 A,B). The hydrogel precursor consisted of acrylamide (AAm, Sigma-Aldrich, A8887), α-ketoglutaric acid (α-keto, Sigma-Aldrich), N,N,N',N'-tetramethylethylenediamine (TEMED, Sigma-Aldrich, T7024), N,N'-methylenebis(acrylamide) (MBAA, Sigma-Aldrich, 146072), and lithium chloride (LiCl, Sigma-Aldrich, 746460) dissolved in either DI water or a polyacrylamide (PAAm) solution. Mixing was performed using a planetary centrifugal mixer (Thinky, ThinkyMixer ARE-300). The PAAm solution was synthesized by UV exposing a solution containing AAm, α-keto, TEMED at

a dose rate of $1.2 mW/cm^2$ at $365 nm$ for 18 hrs at 25 deg C. The PAAm solution precursor used a mass ratio of 94.23% deionized water (resistivity = $18.2 M\Omega cm$), 5.60% AAm, 0.1203% α-keto, and 0.05311% TEMED. The hydrogel precursor final mass ratios were: 63.37% DI water, 3.623% PAAm, 9.88% AAm, 23.036% LiCl, 0.02635% MBAA, 0.0461% α-keto, and 0.0171% TEMED. In the cases where no rheological modifier was introduced, the precursor used the mass ratios: 66.12% DI Water, 9.54% AAm, 24.25% LiCl, 0.02774% MBAA, 0.0485% α-keto, and 0.0180% TEMED. All hydrogel precursors were exposed to a 15 W bench UV Lamp (XX-15, UVP), at a distance of $1 cm$ yielding an average dose rate of $30 mW\, cm^{-2}$ at $365 nm$ for 45 minutes. Bilayer shear debonding test samples were made using the same methods, except with the additional step of adhering the hydrogel to an acrylic sheet using a thin layer of cyanoacrylate adhesive (Krazy Glue).

A.3.3 Contact Angle Measurement:

Measurements were made using a commercial contact angle measurement system (First Ten Angstroms, FTA135) to assist with image capture. Images were then manually processed to obtain the contact angle. Each measurement utilized a single 10 μL drop of DI Water on a previously untested sample surface and was performed after a delay of 20 seconds in order to allow wetting to stabilize. Untreated PDMS was used as a control and a treated PDMS surface was either exposed to atmosphere or made contact with a hydrogel using the segmented mold method described in the "Preparation of hydrogel" section. All samples were stored under a relative humidity of 47%. Due to residue from the hydrogel, PDMS samples kept in contact with a hydrogel were rinsed under DI water for 30 seconds and dried under N2 for 30 seconds prior to contact angle measurements. At least five measurements were made for each condition, and all measurements for the same condition were made within a single five-minute interval.

A.3.4 Mechanical Characterizations:

Peeling tests were performed on a dual column mechanical tester (Instron, 5966), with 10N load cell (Instron, 2530-428) and 90°-peel test fixture (Instron, 2820-035) at a constant displacement rate of 50$mm\ min^{-1}$. The PDMS portion of the sample was peeled off the hydrogel, with the latter physically attached to a glass substrate during curing. Since the PDMS formulation used in this study is relatively stiff with a Young's modulus of 1-3 MPa [229], a backing layer for the PDMS was not necessary to prevent excessive strains under load. All samples were fabricated to be 1.6 mm x 20 mm x 200 mm per material layer and stacked to form a 3.2 mm thick bilayer. A 2mm hole was punched into one end of the PDMS to allow for cotton twine to be fed through and thus extend the distance between sample and load cell to minimize the effect of misalignment. Samples were first aligned and then a small initial crack (2 mm) at the front of sample was made. Peeling was then performed for the remainder of the sample and the interfacial adhesion energy, Γ, was extracted from the steady-state region of the peeling force. Tensile testing of bulk hydrogel samples used the same mechanical testframe with a 500 N load cell (Instron, 2530-500N). Samples for this condition were cast into acrylic molds with a dog-bone geometry (Figure A.2). All samples were tested with a 1500$mm\ min^{-1}$ displacement rate, were deformed to 300% stretch (150mm), and held for 5 min (Figure 3.7). Bilayer shear-debonding tests were completed on a mechanical testframe (Instron, 3342 Single Column UTS) with a 50N load cell (Instron, 2519-50N) at a displacement rate of 10 mm min-1.

A.3.5 Confocal Imaging:

Fluorescence confocal imaging was used to track the distribution of the rheological modifier within the hydrogel-PDMS bilayer. Imaging was performed on a confocal microscope (Leica Microsystem, TCS SP5) with a 10X dry objective and an Argon laser excitation at 488nm. Image acquisitions of 258 μm x 258 μm were made along the z-axis in 1 μm steps. ImageJ software was used in the 3D

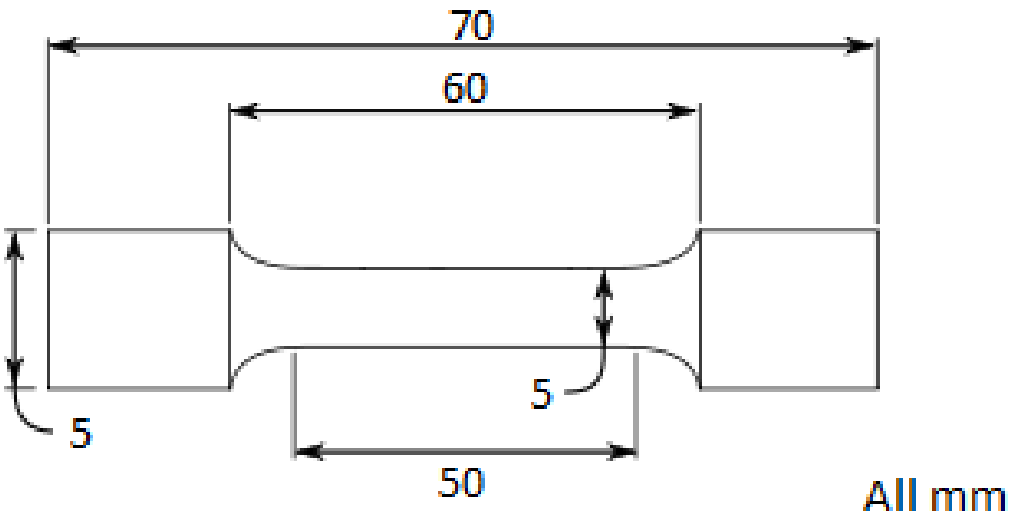

Figure A.2: Dogbone geometry used for stress relaxation hydrogels tests. All units in mm.

reconstruction of the imaging data. The fluorescently-tagged un-crosslinked PAAm solution was prepared by making a separate instance of the PAAm solution precursor that substituted 10 wt% of the AAm with 10 wt% of Fluorescein o-acrylate (FOA, Sigma-Aldrich, 568856) and resulted in FOA copolymerized within the PAAm chains. This tagged-PAAm was mixed with untagged PAAm solution at a ratio of 1:9, and the resulting solution was integrated with the hydrogel precursor as described previously in "Preparation of hydrogel". All other sample preparation steps were otherwise identical.

A.4 Chapter 4: Exploring Hydrogel-Elastomer Adhesion Enhancement Mechanisms

A.4.1 Preparation of Polydimethylsiloxane (PDMS):

Thermal-curing PDMS

The Sylgard 184 (Dow Corning) silicone elastomer kit, consisting of a two-part precursor for base and curing-agent, was used as provided. The base was prepared by first mixing in varying amounts of Brij®L23 (Sigma Aldrich, P1254) and triethoxyvinylsilane (TEOVS, Sigma Aldrich, 175560) via planetary centrifugal mixer (Thinky, ThinkyMixer ARE-300) for 10 minutes at 2000 RPM. The resulting mixture was then allowed to cool for 10 minutes prior to mixing with the curing agent at the prescribed 10:1 ratio for 90 seconds at 2000 RPM. TEOVS content was fixed to 2% w/w relative to the net weight of base and curing agent. Brij®L23 was varied as a weight percentage of the net weight of base and curing agent. Casting was performed using a 20mm x 70mm x 1.6mm acrylic mold, followed by degassing for 30 minutes at 70 kPa vacuum. The degassed PDMS was then sealed by applying pressure with a glass plate and cured at $65^{\circ}C$ for 18 hours.

UV-Curable PDMS

A UV curable formulation of PDMS elastomer (Shin-Etsu Silicones, KER-4690 A/B) was provided by the manufacturer as a two-part precursor and was used in the recommended 1:1 ratio. Part A was first mixed with Brij®L23 and TEOVS for 10 minutes at 2000 RPM, as described for thermal-curing PDMS, then allowed to cool for 10 minutes. The resulting mixture was then mixed with part B for 90 seconds at 2000 RPM and used for extrusion printing immediately. Extrusion printing involved nozzle extrusion and exposure to 365nm UV at a dose rate of 5 $mWcm^{-2}$. Material was flood cured via 365 nm UV light at a dose of 35 $mWcm^{-2}$ for a period of 90 minutes and baked at $65^{\circ}C$ for 18

hours.

A.4.2 Preparation of hydrogel:

The PDMS segments are placed within an acrylic mold to allow for hydrogel precursor to be cast directly onto the PDMS surface and cured while in direct contact (sans-PDMS where specified). Pressure must be applied directly to the PDMS during mold removal to maintain interface integrity for testing. The hydrogel precursor consisted of acrylamide (AAm, Sigma-Aldrich, A8887), 2-Hydroxy-4′-(2-hydroxyethoxy)-2-methylpropiophenone (Irgacure 2959, Sigma-Aldrich, 410896), N,N,N',N'-tetramethylethylenediamine (TEMED, Sigma-Aldrich, T7024), N,N'-methylenebis(acrylamide) (MBAA, Sigma-Aldrich, 146072), 3-(trimethoxysilyl)propylmethacrylate (TMSPMA, Sigma Aldrich, 440159), Acetic Acid (Sigma Aldrich, A6283) and lithium chloride (LiCl, Sigma-Aldrich, 62476) dissolved in either DI water or a polyacrylamide (PAAm) solution. Irgacure 2959 was dissolved in ethanol (459836, Sigma Aldrich) to facilitate dissolution and transfer. TMSPMA concentration is specified in this study as a volume concentration relative to the rheological modifier solution (or DI water) volume. Mixing was performed using planetary centrifugal mixer (Thinky, ThinkyMixer ARE-300). The PAAm solution was synthesized by UV exposing a solution containing AAm and Irgacure 2959 at a dose rate of 35 $mWcm^{-2}$ at 365 nm for 50 minutes. The PAAm solution precursor used a mass ratio of 92.52% deionized water (resistivity = 18.2 MΩ cm), 7.402% AAm, 0.002075% Irgacure 2959, 0.07302% ethanol. The hydrogel precursor final mass ratios with PAAm rheological modifier and [TMSPMA] = 30.4 $\mu L/mL$ were: 62.67% DI water, 4.891% PAAm, 9.172% AAm, 21.30% LiCl, 0.01834% MBAA, 0.002742% Irgacure 2959, 1.9417% TMSPMA, and 0.0037% acetic acid. All hydrogel precursors were exposed to a 15 W bench UV Lamp (XX-15, UVP), at a distance of 1 cm yielding an average dose rate of 30 $mWcm^{-2}$ at 365 nm for 50 minutes.

A.4.3 PDMS-Hydrogel Bilayer preparation:

For cast experiments, hydrogel precursor was placed in contact with pre-cured PDMS segments within an acrylic mold and subsequently sealed within a polypropylene container. The container was then purged with Nitrogen gas bubbled through a saturated salt solution of potassium carbonate, yielding a relative humidity (RH) of 43%; this step displaces oxygen but maintain a stable RH for successful free radical polymerization of the hydrogel. The hydrogel precursor was then cured via UV exposure while in contact with a glass plate, which leads to the adhesion of the glass to the hydrogel without additional modifications. Afterwards, the bilayers were baked in an oven at $65°C$ for 24 hours prior to testing. Printed bilayers underwent similar steps, though casting was replaced by extrusion printing for both PDMS and hydrogel by the customized milling machine described in [64].

A.4.4 Mechanical Characterizations:

Peeling tests were performed on a dual column mechanical tester (Instron, 5966), with 100N load cell (Instron, 2530-100N) and 90-degree peel test fixture (Instron, 2820-035) at a constant displacement rate of 50 $mmmin^{-1}$. The PDMS portion of the sample was peeled off the hydrogel, with the latter attached to a glass substrate during curing due to silane condensation. Since the PDMS formulation used in this study is relatively stiff with a Young's modulus of 1-3 MPa [229], a backing layer for the PDMS was not necessary to prevent excessive strains under load. All cast samples were fabricated to be 1.6 mm x 20 mm x 70 mm per material layer and stacked to form a 3.2 mm thick bilayer. A small mechanical clamp was fixed onto one end of the PDMS that allowed for cotton twine to be fed through and thus extend the distance between sample and load cell to minimize the effect of misalignment. Samples were first aligned and then a small initial crack (5 mm) at the front of sample was made. Peeling was then performed for the remainder of the sample and the interfacial adhesion

energy, Γ, was extracted from the steady-state region of the peeling force.

References

[1] Pierre-Gilles de Gennes. Pierre-Gilles de Gennes – Nobel Lecture, 1991.

[2] R Langer. Drug delivery and targeting. *Nature*, 392(6679 Suppl):5–10, 4 1998.

[3] K Y Lee and D J Mooney. Hydrogels for tissue engineering. *Chemical reviews*, 101(7):1869–79, 7 2001.

[4] Jeanie L. Drury and David J. Mooney. Hydrogels for tissue engineering: scaffold design variables and applications. *Biomaterials*, 24(24):4337–4351, 11 2003.

[5] J.P. Gong, Y. Katsuyama, T. Kurokawa, and Y. Osada. Double-Network Hydrogels with Extremely High Mechanical Strength. *Advanced Materials*, 15(14):1155–1158, 7 2003.

[6] Kevin J. Henderson, Tian C. Zhou, Kathryn J. Otim, and Kenneth R. Shull. Ionically Cross-Linked Triblock Copolymer Hydrogels with High Strength. *Macromolecules*, 43(14):6193–6201, 7 2010.

[7] Jianyu Li, Widusha R. K. Illeperuma, Zhigang Suo, and Joost J. Vlassak. Hybrid Hydrogels with Extremely High Stiffness and Toughness. *ACS Macro Letters*, 3(6):520–523, 6 2014.

[8] Jeong-Yun Sun, Xuanhe Zhao, Widusha R. K. Illeperuma, Ovijit Chaudhuri, Kyu Hwan Oh, David J. Mooney, Joost J. Vlassak, and Zhigang Suo. Highly stretchable and tough hydrogels. *Nature*, 489(7414):133–136, 9 2012.

[9] Yiwan Huang, Daniel R. King, Tao Lin Sun, Takayuki Nonoyama, Takayuki Kurokawa, Tasuku Nakajima, and Jian Ping Gong. Energy-Dissipative Matrices Enable Synergistic Toughening in Fiber Reinforced Soft Composites. *Advanced Functional Materials*, 27(9):1605350, 3 2017.

[10] Ruobing Bai, Jiawei Yang, and Zhigang Suo. Fatigue of hydrogels. *European Journal of Mechanics - A/Solids*, 74:337–370, 3 2019.

[11] Widusha R.K. Illeperuma, Jeong-Yun Sun, Zhigang Suo, and Joost J. Vlassak. Fiber-reinforced tough hydrogels. *Extreme Mechanics Letters*, 1:90–96, 12 2014.

[12] Widusha R K Illeperuma, Philipp Rothemund, Zhigang Suo, and Joost J. Vlassak. Fire-Resistant Hydrogel-Fabric Laminates: A Simple Concept That May Save Lives. *ACS Applied Materials & Interfaces*, 8(3):2071–2077, 1 2016.

[13] Insu Jeon, Jiaxi Cui, Widusha R K Illeperuma, Joanna Aizenberg, and Joost J. Vlassak. Extremely Stretchable and Fast Self-Healing Hydrogels. *Advanced Materials*, pages 4678–4683, 2016.

[14] Danielle Lynne Taylor and Marc in het Panhuis. Self-Healing Hydrogels. *Advanced Materials*, 28(41):9060–9093, 2016.

[15] Kazutoshi Haraguchi, Kazuhisa Uyama, and Hisashi Tanimoto. Self-healing in nanocomposite hydrogels. *Macromolecular Rapid Communications*, 32(16):1253–1258, 2011.

[16] You Seung Rim, Sang-Hoon Bae, Huajun Chen, Nicholas De Marco, and Yang Yang. Recent Progress in Materials and Devices toward Printable and Flexible Sensors. *Advanced Materials*, 28(22):4415–4440, 2 2016.

[17] Nanshu Lu, Chi Lu, Shixuan Yang, and John Rogers. Highly Sensitive Skin-Mountable Strain Gauges Based Entirely on Elastomers. *Advanced Functional Materials*, 22(19):4044–4050, 10 2012.

[18] Ashu K. Bansal, Shuoben Hou, Olena Kulyk, Eric M. Bowman, and Ifor D. W. Samuel. Wearable Organic Optoelectronic Sensors for Medicine. *Advanced Materials*, 27(46):7638–7644, 12 2015.

[19] Andreas Lymberis and André Dittmar. Advanced wearable health systems and applications. *IEEE engineering in medicine and biology magazine : the quarterly magazine of the Engineering in Medicine & Biology Society*, 26(3):29–33, 2007.

[20] Joseph T. Muth, Daniel M. Vogt, Ryan L. Truby, Yiğit Mengüç, David B. Kolesky, Robert J. Wood, and Jennifer A. Lewis. Embedded 3D Printing of Strain Sensors within Highly Stretchable Elastomers. *Advanced Materials*, 26(36):6307–6312, 9 2014.

[21] Andreas Frutiger, Joseph T. Muth, Daniel M. Vogt, Yiğit Mengüç, Alexandre Campo, Alexander D. Valentine, Conor J. Walsh, and Jennifer A. Lewis. Capacitive Soft Strain Sensors via Multicore-Shell Fiber Printing. *Advanced Materials*, 27(15):2440–2446, 4 2015.

[22] Morteza Amjadi, Ki-Uk Kyung, Inkyu Park, and Metin Sitti. Stretchable, Skin-Mountable, and Wearable Strain Sensors and Their Potential Applications: A Review. *Advanced Functional Materials*, 26(11):1678–1698, 3 2016.

[23] Yigit Menguc, Yong-lae Park, Ernesto Martinez-Villalpando, Patrick Aubin, Miriam Zisook, Leia Stirling, Robert J. Wood, and Conor J. Walsh. Soft wearable motion sensing suit for lower limb biomechanics measurements. In *2013 IEEE International Conference on Robotics and Automation*, pages 5309–5316. IEEE, 5 2013.

[24] Michael D. Dickey, Ryan C. Chiechi, Ryan J. Larsen, Emily A. Weiss, David A. Weitz, and George M. Whitesides. Eutectic Gallium-Indium (EGaIn): A Liquid Metal Alloy for the Formation of Stable Structures in Microchannels at Room Temperature. *Advanced Functional Materials*, 18(7):1097–1104, 4 2008.

[25] Arya Tabatabai, Andrew Fassler, Claire Usiak, and Carmel Majidi. Liquid-Phase Gallium–Indium Alloy Electronics with Microcontact Printing. *Langmuir*, 29(20):6194–6200, 5 2013.

[26] Shu Gong, Willem Schwalb, Yongwei Wang, Yi Chen, Yue Tang, Jye Si, Bijan Shirinzadeh, and Wenlong Cheng. A wearable and highly sensitive pressure sensor with ultrathin gold nanowires. *Nature communications*, 5:1–8, 2 2014.

[27] Hiroshi Yabu, Kuniaki Nagamine, Jun Kamei, Yuta Saito, Taiki Okabe, Tatsuaki Shimazaki, and Matsuhiko Nishizawa. Stretchable, transparent and molecular permeable honeycomb electrodes and their hydrogel hybrids prepared by the breath figure method and sputtering of metals. *RSC Adv.*, 5(107):88414–88418, 2015.

[28] Xue Feng, Byung Duk Yang, Yuanming Liu, Yong Wang, Canan Dagdeviren, Zhuangjian Liu, Andrew Carlson, Jiangyu Li, Yonggang Huang, and John A. Rogers. Stretchable Ferroelectric Nanoribbons with Wavy Configurations on Elastomeric Substrates. *ACS Nano*, 5(4):3326–3332, 4 2011.

[29] Z. F. Liu, S. Fang, F. A. Moura, J. N. Ding, N. Jiang, J. Di, M. Zhang, X. Lepro, D. S. Galvao, C. S. Haines, N. Y. Yuan, S. G. Yin, D. W. Lee, R. Wang, H. Y. Wang, W. Lv, C. Dong, R. C. Zhang, M. J. Chen, Q. Yin, Y. T. Chong, R. Zhang, X. Wang, M. D. Lima, R. Ovalle-Robles, D. Qian, H. Lu, and R. H. Baughman. Hierarchically buckled sheath-core fibers for superelastic electronics, sensors, and muscles. *Science*, 349(6246):400–404, 7 2015.

[30] Stéphanie Périchon Lacour, Sigurd Wagner, Zhenyu Huang, and Zhigang Suo. Stretchable gold conductors on elastomeric substrates. *Applied Physics Letters*, 82(15):2404–2406, 4 2003.

[31] Yong Xiang, Teng Li, Zhigang Suo, and Joost J.J. Joost J. Vlassak. High ductility of a metal film adherent on a polymer substrate. *Applied Physics Letters*, 87(16):1–3, 2005.

[32] Ivan R. Minev, Pavel Musienko, Arthur Hirsch, Quentin Barraud, Nikolaus Wenger, Eduardo Martin Moraud, Jérôme Gandar, Marco Capogrosso, Tomislav Milekovic, Léonie Asboth, Rafael Fajardo Torres, Nicolas Vachicouras, Qihan Liu, Natalia Pavlova, Simone Duis, Alexandre Larmagnac, J. Voros, Silvestro Micera, Zhigang Suo, Grégoire Courtine, Stéphanie P. Lacour, Janos Vörös, Silvestro Micera, Zhigang Suo, Grégoire Courtine, and Stéphanie P. Lacour. Electronic dura mater for long-term multimodal neural interfaces. *Science*, 347(6218):159–163, 1 2015.

[33] Zhigang Suo. Mechanics of stretchable electronics and soft machines. *MRS Bulletin*, 37(03):218–225, 3 2012.

[34] Christoph Keplinger, J.-Y. Jeong-Yun Sun, Choon Chiang Foo, Philipp Rothemund, George M. Whitesides, and Zhigang Suo. Stretchable, Transparent, Ionic Conductors. *Science*, 341(6149):984–987, 8 2013.

[35] Can Hui Yang, Baohong Chen, Jing Jing Lu, Jian Hai Yang, Jinxiong Zhou, Yong Mei Chen, and Zhigang Suo. Ionic cable. *Extreme Mechanics Letters*, 3:59–65, 6 2015.

[36] C. Larson, B. Peele, S. Li, S. Robinson, M. Totaro, L. Beccai, B. Mazzolai, and R. Shepherd. Highly stretchable electroluminescent skin for optical signaling and tactile sensing. *Science*, 351(6277):1071–1074, 3 2016.

[37] Can Hui Yang, Baohong Chen, Jinxiong Zhou, Yong Mei Chen, and Zhigang Suo. Electroluminescence of Giant Stretchability. *Advanced Materials*, 28(22):4480–4484, 6 2016.

[38] Jeong-Yun Sun, Christoph Keplinger, George M. Whitesides, and Zhigang Suo. Ionic skin. *Advanced Materials*, 26(45):7608–7614, 12 2014.

[39] Sanlin S. Robinson, Kevin W. O'Brien, Huichan Zhao, Bryan N. Peele, Chris M. Larson, Benjamin C. Mac Murray, Ilse M. Van Meerbeek, Simon N. Dunham, and Robert F. Shepherd. Integrated soft sensors and elastomeric actuators for tactile machines with kinesthetic sense. *Extreme Mechanics Letters*, 5:47–53, 12 2015.

[40] C.-C. Kim, H.-H. Lee, Kyu Hwan Oh, and J.-Y. Sun. Highly stretchable, transparent ionic touch panel. *Science*, 353(6300):682–687, 8 2016.

[41] Michael Wehner, Ryan L. Truby, Daniel J. Fitzgerald, Bobak Mosadegh, George M. Whitesides, Jennifer A. Lewis, and Robert J. Wood. An integrated design and fabrication strategy for entirely soft, autonomous robots. *Nature*, 536(7617):451–455, 8 2016.

[42] Gerald Gerlach, Margarita Guenther, Gunnar Suchaneck, Joerg Sorber, Karl-Friedrich Arndt, and Andreas Richter. Application of sensitive hydrogels in chemical and pH sensors. *Macromolecular Symposia*, 210(1):403–410, 3 2004.

[43] Canhui Yang and Zhigang Suo. Hydrogel ionotronics. *Nature Reviews Materials*, 3(6):125–142, 2018.

[44] Sofia Teixeira de Freitas and Jos Sinke. Test method to assess interface adhesion in composite bonding. *Applied Adhesion Science*, 3(1):1–13, 2015.

[45] P.J. J. Herrera-Franco and L.T. T. Drzal. Comparison of methods for the measurement of fibre / matrix adhesion in composites. *Composites*, 23(1):2–27, 1992.

[46] Sally J. Marshall, Stephen C. Bayne, Robert Baier, Antoni P. Tomsia, and Grayson W. Marshall. A review of adhesion science. *Dental Materials*, 26(2):11–16, 2010.

[47] Noshir S. Pesika, Yu Tian, Boxin Zhao, Kenny Rosenberg, Hongbo Zeng, Patricia McGuiggan, Kellar Autumn, and Jacob N. Israelachvili. Peel-Zone Model of Tape Peeling Based on the Gecko Adhesive System. *The Journal of Adhesion*, 83(4):383–401, 2007.

[48] Bruce P Lee, P B Messersmith, J N Israelachvili, and J H Waite. Mussel-Inspired Adhesives and Coatings. *Annual review of materials research*, 41:99–132, 2011.

[49] W. J. Sames, F. A. List, S. Pannala, R. R. Dehoff, and S. S. Babu. The metallurgy and processing science of metal additive manufacturing. *International Materials Reviews*, 61(5):315–360, 7 2016.

[50] Scott S. Crump. Patent#:US005121329, 1992.

[51] Guy Rundle. *A Revolution in the Making: 3D Printing, Robots and the Future*. Affirm Press, South Melbourne, Victoria Australia, 2014.

[52] Howon Lee and Nicholas X. Fang. Micro 3D Printing Using a Digital Projector and its Application in the Study of Soft Materials Mechanics. *Journal of Visualized Experiments*, (69):1–5, 11 2012.

[53] Jin-Feng Xing, Mei-Ling Zheng, and Xuan-Ming Duan. Two-photon polymerization microfabrication of hydrogels: an advanced 3D printing technology for tissue engineering and drug delivery. *Chemical Society Reviews*, 44(15):5031–5039, 2015.

[54] Dino A. Pardo, Ghassan E. Jabbour, and Nasser Peyghambarian. Application of Screen Printing in the Fabrication of Organic Light-Emitting Devices. *Advanced Materials*, 12(17):1249–1252, 9 2000.

[55] Sean E. Shaheen, Rachel Radspinner, Nasser Peyghambarian, and Ghassan E. Jabbour. Fabrication of bulk heterojunction plastic solar cells by screen printing. *Applied Physics Letters*, 79(18):2996, 10 2001.

[56] Jieke Jiang, Bin Bao, Mingzhu Li, Jiazhen Sun, Cong Zhang, Yang Li, Fengyu Li, Xi Yao, and Yanlin Song. Fabrication of Transparent Multilayer Circuits by Inkjet Printing. *Advanced Materials*, 28(7):1–7, 2 2015.

[57] Mark A Skylar-Scott, Suman Gunasekaran, and Jennifer A. Lewis. Laser-assisted direct ink writing of planar and 3D metal architectures. *Proceedings of the National Academy of Sciences*, 113(22):6137–6142, 5 2016.

[58] Imen Grida and Julian R G Evans. Extrusion freeforming of ceramics through fine nozzles. *Journal of the European Ceramic Society*, 23(5):629–635, 2003.

[59] Jennifer N. Hanson Shepherd, Sara T. Parker, Robert F. Shepherd, Martha U. Gillette, Jennifer A. Lewis, and Ralph G. Nuzzo. 3D Microperiodic Hydrogel Scaffolds for Robust Neuronal Cultures. *Advanced Functional Materials*, 21(1):47–54, 1 2011.

[60] Robert A. Barry, Robert F. Shepherd, Jennifer N. Hanson, Ralph G. Nuzzo, Pierre Wiltzius, and Jennifer A. Lewis. Direct-Write Assembly of 3D Hydrogel Scaffolds for Guided Cell Growth. *Advanced Materials*, 21(23):2407–2410, 6 2009.

[61] Sungmin Hong, Dalton Sycks, Hon Fai Chan, Shaoting Lin, Gabriel P. Lopez, Farshid Guilak, Kam W. Leong, and Xuanhe Zhao. 3D Printing of Highly Stretchable and Tough Hydrogels into Complex, Cellularized Structures. *Advanced Materials*, 27(27):4035–4040, 7 2015.

[62] Shannon E. Bakarich, Marc in Het Panhuis, Stephen Beirne, Gordon G. Wallace, and Geoffrey M. Spinks. Extrusion printing of ionic–covalent entanglement hydrogels with high toughness. *Journal of Materials Chemistry B*, 1(38):4939, 2013.

[63] Shannon E. Bakarich, Paul Balding, Robert Gorkin III, Geoffrey M. Spinks, and Marc in het Panhuis. Printed ionic-covalent entanglement hydrogels from carrageenan and an epoxy amine. *RSC Advances*, 4(72):38088–38092, 8 2014.

[64] Kevin Tian, Jinhye Bae, Shannon E. Bakarich, Canhui Yang, Reece D. Gately, Geoffrey M. Spinks, Marc in het Panhuis, Zhigang Suo, and Joost J. Vlassak. 3D Printing of Transparent and Conductive Heterogeneous Hydrogel-Elastomer Systems. *Advanced Materials*, page 1604827, 2017.

[65] Alexandra L. Rutz, Kelly E. Hyland, Adam E. Jakus, Wesley R. Burghardt, and Ramille N. Shah. A multimaterial bioink method for 3D printing tunable, cell-compatible hydrogels. *Advanced Materials*, 27(9):1607–1614, 2015.

[66] Yifei Jin, Chengcheng Liu, Wenxuan Chai, Ashley Compaan, and Yong Huang. Self-Supporting Nanoclay as Internal Scaffold Material for Direct Printing of Soft Hydrogel Composite Structures in Air. *ACS Applied Materials and Interfaces*, 9(20):17456–17465, 2017.

[67] Kris Pataky, Thomas Braschler, Andrea Negro, Philippe Renaud, Matthias P. Lutolf, and Juergen Brugger. Microdrop Printing of Hydrogel Bioinks into 3D Tissue-Like Geometries. *Advanced Materials*, 24(3):391–396, 1 2012.

[68] David Chimene, Kimberly K. Lennox, Roland R. Kaunas, and Akhilesh K. Gaharwar. Advanced Bioinks for 3D Printing: A Materials Science Perspective. *Annals of Biomedical Engineering*, 44(6):2090–2102, 2016.

[69] D. M. Kirchmajer, R. Gorkin III, and M. in het Panhuis. An overview of the suitability of hydrogel-forming polymers for extrusion-based 3D-printing. *J. Mater. Chem. B*, 3(20):4105–4117, 2015.

[70] Helena N. Chia and Benjamin M. Wu. Recent advances in 3D printing of biomaterials. *Journal of Biological Engineering*, 9(1):1–14, 2015.

[71] Vivian H. M. Mouser, Riccardo Levato, Lawrence J. Bonassar, Darryl D. D'Lima, Daniel A. Grande, Travis J. Klein, Daniel B. F. Saris, Marcy Zenobi-Wong, Debby Gawlitta, and Jos Malda. Three-Dimensional Bioprinting and Its Potential in the Field of Articular Cartilage Regeneration. *CARTILAGE*, 8(4):327–340, 10 2017.

[72] Katherine Bootsma, Martha M. Fitzgerald, Brandon Free, Elizabeth Dimbath, Joe Conjerti, Greg Reese, Dominik Konkolewicz, Jason A. Berberich, and Jessica L. Sparks. 3D printing of an interpenetrating network hydrogel material with tunable viscoelastic properties. *Journal of the Mechanical Behavior of Biomedical Materials*, 70:84–94, 6 2017.

[73] Si Yu Zheng, Yangyang Shen, Fengbo Zhu, Jun Yin, Jin Qian, Jianzhong Fu, Zi Liang Wu, and Qiang Zheng. Programmed Deformations of 3D-Printed Tough Physical Hydrogels with High Response Speed and Large Output Force. *Advanced Functional Materials*, 28(37):1803366, 9 2018.

[74] Sijun Liu, Anil Kumar Bastola, and Lin Li. A 3D Printable and Mechanically Robust Hydrogel Based on Alginate and Graphene Oxide. *ACS Applied Materials and Interfaces*, 9(47):41473–41481, 2017.

[75] Hae-Ryung Lee, Chong-Chan Kim, and Jeong-Yun Sun. Stretchable Ionics - A Promising Candidate for Upcoming Wearable Devices. *Advanced Materials*, 30(42):1704403, 10 2018.

[76] Fengbo Zhu, Libo Cheng, Jun Yin, Zi Liang Wu, Jin Qian, Jianzhong Fu, and Qiang Zheng. 3D Printing of Ultratough Polyion Complex Hydrogels. *ACS Applied Materials & Interfaces*, 8(45):31304–31310, 11 2016.

[77] Fengbo Zhu, Libo Cheng, Zhi Jian Wang, Wei Hong, Zi Liang Wu, Jun Yin, Jin Qian, and Qiang Zheng. 3D-Printed Ultratough Hydrogel Structures with Titin-like Domains. *ACS Applied Materials and Interfaces*, 9(13):11363–11367, 2017.

[78] Zhifang Wang, Geng An, Ye Zhu, Xuemin Liu, Yunhua Chen, Hongkai Wu, Yingjun Wang, Xuetao Shi, and Chuanbin Mao. 3D-printable self-healing and mechanically reinforced hydrogels with host–guest non-covalent interactions integrated into covalently linked networks. *Materials Horizons*, 2019.

[79] Xinyun Zhai, Yufei Ma, Chunyong Hou, Fei Gao, Yinyu Zhang, Changshun Ruan, Haobo Pan, William Weijia Lu, and Wenguang Liu. 3D-Printed High Strength Bioactive Supramolecular Polymer/Clay Nanocomposite Hydrogel Scaffold for Bone Regeneration. *ACS Biomaterials Science & Engineering*, 3(6):1109–1118, 6 2017.

[80] Qian Wu, Junjie Wei, Bing Xu, Xinhua Liu, Hongbo Wang, Wei Wang, Qigang Wang, and Wenguang Liu. A robust, highly stretchable supramolecular polymer conductive hydrogel with self-healability and thermo-processability. *Scientific Reports*, 7(1):41566, 12 2017.

[81] A Sydney Gladman, Elisabetta A Matsumoto, Ralph G Nuzzo, L Mahadevan, and Jennifer A Lewis. Biomimetic 4D printing. *Nature Materials*, 15(4):413–418, 1 2016.

[82] Limei Huang, Ruiqi Jiang, Jingjun Wu, Jizhou Song, Hao Bai, Bogeng Li, Qian Zhao, and Tao Xie. Ultrafast Digital Printing toward 4D Shape Changing Materials. *Advanced Materials*, 29(7):1605390, 2 2017.

[83] Sina Naficy, Reece Gately, Robert Gorkin, Hai Xin, and Geoffrey M. Spinks. 4D Printing of Reversible Shape Morphing Hydrogel Structures. *Macromolecular Materials and Engineering*, 302(1):1–9, 2017.

[84] Shannon E. Bakarich, Robert Gorkin, Marc In Het Panhuis, and Geoffrey M. Spinks. 4D printing with mechanically robust, thermally actuating hydrogels. *Macromolecular Rapid Communications*, 36(12):1211–1217, 6 2015.

[85] Se-Jun Lee, Wei Zhu, Margaret Nowicki, Grace Lee, Dong Nyoung Heo, Junghoon Kim, Yi Y Zuo, and Lijie Grace Zhang. 3D printing nano conductive multi-walled carbon nanotube scaffolds for nerve regeneration. *Journal of Neural Engineering*, 15(1):016018, 2 2018.

[86] Yongzhou Wang, Ying Miao, Jieling Zhang, Jian Ping Wu, Thomas Brett Kirk, Jiake Xu, Dong Ma, and Wei Xue. Three-dimensional printing of shape memory hydrogels with internal structure for drug delivery. *Materials Science and Engineering: C*, 84(October 2017):44–51, 3 2018.

[87] Ming-Jie Yin, Mian Yao, Shaorui Gao, A. Ping Zhang, Hwa-Yaw Tam, and Ping-Kong A. Wai. Rapid 3D Patterning of Poly(acrylic acid) Ionic Hydrogel for Miniature pH Sensors. *Advanced Materials*, 28(7):1394–1399, 2 2016.

[88] Sijun Liu and Lin Li. Ultrastretchable and Self-Healing Double-Network Hydrogel for 3D Printing and Strain Sensor. *ACS Applied Materials & Interfaces*, 9(31):26429–26437, 8 2017.

[89] Rüdiger Landers and Rolf Mülhaupt. Desktop manufacturing of complex objects, prototypes and biomedical scaffolds by means of computer-assisted design combined with computer-guided 3D plotting of polymers and reactive oligomers. *Macromolecular Materials and Engineering*, 282(Llm):17–21, 2000.

[90] Maria Lukic, Jane Clarke, Christopher Tuck, William Whittow, and Garry Wells. Printability of elastomer latex for additive manufacturing or 3D printing. *Journal of Applied Polymer Science*, 133(4):1–7, 2016.

[91] Kun Che Hung, Ching Shiow Tseng, and Shan Hui Hsu. Synthesis and 3D Printing of biodegradable polyurethane elastomer by a water-based process for cartilage tissue engineering applications. *Advanced Healthcare Materials*, 3(10):1578–1587, 2014.

[92] Peter E. Petrochenko, Jan Torgersen, Peter Gruber, Lucas A. Hicks, Jiwen Zheng, Girish Kumar, Roger J. Narayan, Peter L. Goering, Robert Liska, Jürgen Stampfl, and Aleksandr Ovsianikov. Laser 3D Printing with Sub-Microscale Resolution of Porous Elastomeric Scaffolds for Supporting Human Bone Stem Cells. *Advanced Healthcare Materials*, 4(5):739–747, 4 2015.

[93] Gordon Paul, Russel Torah, Steve Beeby, and John Tudor. The development of screen printed conductive networks on textiles for biopotential monitoring applications. *Sensors and Actuators, A: Physical*, 206:35–41, 2014.

[94] Yong Lae Park, Carmel Majidi, Rebecca Kramer, Phillipe Brard, and Robert J. Wood. Hyperelastic pressure sensing with a liquid-embedded elastomer. *Journal of Micromechanics and Microengineering*, 20(12), 2010.

[95] Jonathan Rossiter, Peter Walters, and Boyko Stoimenov. Printing 3D dielectric elastomer actuators for soft robotics. *Proceedings of SPIE*, 7287:1–10, 2009.

[96] Bryan N. Peele, Thomas J. Wallin, Huichan Zhao, and Robert F. Shepherd. 3D printing antagonistic systems of artificial muscle using projection stereolithography. *Bioinspiration & Biomimetics*, 10(5):055003, 9 2015.

[97] A. K. Bastola, V. T. Hoang, and L. Li. A novel hybrid magnetorheological elastomer developed by 3D printing. *Materials and Design*, 114:391–397, 2017.

[98] Xiao Kuang, Kaijuan Chen, Conner K. Dunn, Jiangtao Wu, Vincent C.F. Li, and H. Jerry Qi. 3D Printing of Highly Stretchable, Shape-Memory, and Self-Healing Elastomer toward Novel 4D Printing. *ACS Applied Materials and Interfaces*, 10(8):7381–7388, 2018.

[99] Dinesh K. Patel, Amir Hosein Sakhaei, Michael Layani, Biao Zhang, Qi Ge, and Shlomo Magdassi. Highly Stretchable and UV Curable Elastomers for Digital Light Processing Based 3D Printing. *Advanced Materials*, 29(15):1606000, 4 2017.

[100] Sangchul Roh, Dishit P. Parekh, Bhuvnesh Bharti, Simeon D. Stoyanov, and Orlin D. Velev. 3D Printing by Multiphase Silicone/Water Capillary Inks. *Advanced Materials*, 29(30):1–7, 2017.

[101] Jiawei Yang, Ruobing Bai, and Zhigang Suo. Topological Adhesion of Wet Materials. *Advanced Materials*, 30(25):1–7, 2018.

[102] Kevin Tian, Jinhye Bae, Zhigang Suo, and Joost J Vlassak. Adhesion between Hydrophobic Elastomer and Hydrogel through Hydrophilic Modification and Interfacial Segregation. *ACS Applied Materials & Interfaces*, 10(49):43252–43261, 12 2018.

[103] Mohammad Ali Darabi, Ali Khosrozadeh, Rene Mbeleck, Yuqing Liu, Qiang Chang, Junzi Jiang, Jun Cai, Quan Wang, Gaoxing Luo, and Malcolm Xing. Skin-Inspired Multifunctional Autonomic-Intrinsic Conductive Self-Healing Hydrogels with Pressure Sensitivity, Stretchability, and 3D Printability. *Advanced Materials*, 29(31):1–8, 2017.

[104] Shaoting Lin, Hyunwoo Yuk, Teng Zhang, German Alberto Parada, Hyunwoo Koo, Cunjiang Yu, and Xuanhe Zhao. Stretchable Hydrogel Electronics and Devices. *Advanced Materials*, pages 1–9, 2015.

[105] German A. Parada, Hyunwoo Yuk, Xinyue Liu, Alex J. Hsieh, and Xuanhe Zhao. Impermeable Robust Hydrogels via Hybrid Lamination. *Advanced Healthcare Materials*, 6(19):1–8, 2017.

[106] Hyunwoo Yuk, Teng Zhang, Shaoting Lin, German Alberto Parada, and Xuanhe Zhao. Tough bonding of hydrogels to diverse non-porous surfaces. *Nature Materials*, 15(November):1–25, 2 2015.

[107] Hang Yang, Chenghai Li, Meng Yang, Yudong Pan, Qianfeng Yin, Jingda Tang, Hang Jerry Qi, and Zhigang Suo. Printing Hydrogels and Elastomers in Arbitrary Sequence with Strong Adhesion. *Advanced Functional Materials*, 1901721:1901721, 3 2019.

[108] Qihan Liu, Guodong Nian, Canhui Yang, Shaoxing Qu, and Zhigang Suo. Bonding dissimilar polymer networks in various manufacturing processes. *Nature Communications*, 9(1):1–11, 2018.

[109] Paul Le Floch, Xi Yao, Qihan Liu, Zhengjing Wang, Guodong Nian, Yu Sun, Li Jia, and Zhigang Suo. Wearable and Washable Conductors for Active Textiles. *ACS Applied Materials & Interfaces*, 9(July):acsami.7b07361, 8 2017.

[110] Xavier P. Morelle, Widusha R. Illeperuma, Kevin Tian, Ruobing Bai, Zhigang Suo, and Joost J. Vlassak. Highly Stretchable and Tough Hydrogels below Water Freezing Temperature. *Advanced Materials*, 1801541:1801541, 2018.

[111] Hainan Gao, Ziguang Zhao, Yudong Cai, Jiajia Zhou, Wenda Hua, Lie Chen, Li Wang, Jianqi Zhang, Dong Han, Mingjie Liu, and Lei Jiang. Adaptive and freeze-tolerant heteronetwork organohydrogels with enhanced mechanical stability over a wide temperature range. *Nature Communications*, 8(May):15911, 6 2017.

[112] G. Wieslander, D. Norbäck, and T. Lindgren. Experimental exposure to propylene glycol mist in aviation emergency training: Acute ocular and respiratory effects. *Occupational and Environmental Medicine*, 58(10):649–655, 2001.

[113] David A. Pillard. Comparative toxicity of formulated glycol deicers and pure ethylene and propylene glycol to Ceriodaphnia dubia and Pimephales promelas. *Environmental Toxicology and Chemistry*, 14(2):311–315, 1995.

[114] Jeff R. Fowles, Marcy I. Banton, and Lynn H. Pottenger. A toxicological review of the propylene glycols. *Critical Reviews in Toxicology*, 43(4):363–390, 4 2013.

[115] A. Mohiley, J. Franzaring, O. C. Calvo, and A. Fangmeier. Potential toxic effects of aircraft de-icers and wastewater samples containing these compounds. *Environmental Science and Pollution Research*, 22(17):13094–13101, 9 2015.

[116] Widusha Illeperuma, Zhigang Suo, and Joost J. Vlassak. Hydrogels with improved mechanical properties below water freezing temperature, 3 2017.

[117] Manuel R. Conde. Properties of aqueous solutions of lithium and calcium chlorides: Formulations for use in air conditioning equipment design. *International Journal of Thermal Sciences*, 43(4):367–382, 2004.

[118] Worth H. Rodebush. THE FREEZING POINTS OF CONCENTRATED SOLUTIONS AND THE FREE ENERGY OF SOLUTION OF SALTS. *Journal of the American Chemical Society*, 40(8):1204–1213, 8 1918.

[119] Stephen A. Ketcham, L. David Minsk, Robert R. Blackburn, and Edward J. Fleege. MANUAL OF PRACTICE FOR AN EFFECTIVE ANTI-ICING PROGRAM: A Guide For Highway Winter Maintenance Personnel. Technical report, Federal Highway Administration, Hanover, New Hampshire, 1996.

[120] Occidental Chemical Corporation (OxyChem). Calcium Chloride A Guide to Physical Properties.

[121] Wisconsin Transportation Information Center. Techniques for Winter Road Maintenance, 2005.

[122] W. Block. To Freeze or Not to Freeze? Invertebrate Survival of Sub-Zero Temperatures. *Functional Ecology*, 5(2):284–290, 1991.

[123] John G. Duman, Ding Wen Wu, Lei Xu, Donald Tursman, and T. Mark Olsen. Adaptations of Insects to Subzero Temperatures. *The Quarterly Review of Biology*, 66(4):387–410, 1991.

[124] I. K. Voets. From ice-binding proteins to bio-inspired antifreeze materials. *Soft Matter*, 13(28):4808–4823, 2017.

[125] Yuanyuan Bai, Baohong Chen, Feng Xiang, Jinxiong Zhou, Hong Wang, and Zhigang Suo. Transparent hydrogel with enhanced water retention capacity by introducing highly hydratable salt. *Applied Physics Letters*, 105(15):151903, 10 2014.

[126] A.J. Kinloch, S.J. Shaw, D.A. Tod, and D.L. Hunston. Deformation and fracture behaviour of a rubber-toughened epoxy: 1. Microstructure and fracture studies. *Polymer*, 24(10):1341–1354, 10 1983.

[127] R. A. Pearson and A. F. Yee. Toughening mechanisms in elastomer-modified epoxies - Part 2 Microscopy studies. *Journal of Materials Science*, 21(7):2475–2488, 1986.

[128] Han E.H. Meijer and Leon E. Govaert. Mechanical performance of polymer systems: The relation between structure and properties. *Progress in Polymer Science (Oxford)*, 30(8-9):915–938, 2005.

[129] A. J. Kinloch, R. D. Mohammed, A. C. Taylor, C. Eger, S. Sprenger, and D. Egan. The effect of silica nano particles and rubber particles on the toughness of multiphase thermosetting epoxy polymers. *Journal of Materials Science*, 40(18):5083–5086, 2005.

[130] Alfred J. Crosby, Kenneth R. Shull, Hamed Lakrout, and Costantino Creton. Deformation and failure modes of adhesively bonded elastic layers. *Journal of Applied Physics*, 88(5):2956–2966, 2000.

[131] Hamed Lakrout, Philippe Sergot, and Costantino Creton. Direct observation of cavitation and fibrillation in a probe tack experiment on model acrylic pressure-sensitive-adhesives. *Journal of Adhesion*, 69(3-4):307–359, 3 1999.

[132] K.R. Brown and C. Creton. Nucleation and growth of cavities in soft viscoelastic layers under tensile stress. *The European Physical Journal E*, 9(1):35–40, 9 2002.

[133] R. S. Rivlin and A. G. Thomas. Rupture of Rubber. I. Characteristic Energy for Tearing. In *Collected Papers of R.S. Rivlin*, volume 10, pages 291–318. Springer New York, New York, NY, 1953.

[134] Baohong Chen, Jing Jing Lu, Can Hui Yang, Jian Hai Yang, Jinxiong Zhou, Yong Mei Chen, and Zhigang Suo. Highly Stretchable and Transparent Ionogels as Nonvolatile Conductors for Dielectric Elastomer Transducers. *ACS Applied Materials & Interfaces*, 6(10):7840–7845, 5 2014.

[135] Mingyu Li, Jianyu Li, Hui Na, and Joost J. Vlassak. Mechanical behavior of poly(methyl methacrylate)-based ionogels. *Soft Matter*, 10(40):7993–8000, 8 2014.

[136] Przemysław Kubisa. Ionic liquids as solvents for polymerization processes—Progress and challenges. *Progress in Polymer Science*, 34(12):1333–1347, 12 2009.

[137] Margaret Robson Wright. *An Introduction to Aqueous Electrolyte Solutions*. John Wiley & Sons, Ltd, West Sussex, 2007.

[138] W. M. Haynes and David R. Lide, editors. *CRC Handbook of Chemistry and Physics, 92nd Edition*. CRC Press, Boca Raton, FL, USA, 92 edition, 2011.

[139] Lewis Greenspan. Humidity fixed points of binary saturated aqueous solutions. *Journal of Research of the National Bureau of Standards Section A: Physics and Chemistry*, 81A(1):89, 1 1977.

[140] Dayong Chen, Jinhwan Yoon, Dinesh Chandra, Alfred J. Crosby, and Ryan C. Hayward. Stimuli-responsive buckling mechanics of polymer films. *Journal of Polymer Science Part B: Polymer Physics*, 52(22):1441–1461, 11 2014.

[141] David B. Braun and Meyer R. Rosen. Commercially Available Rheology Modifiers. In *Rheology Modifiers Handbook*, chapter 2, pages 71–191. William Andrew Publishing, Norwich, NY, 1999.

[142] Tim Femmer, Alexander J. C. Kuehne, and Matthias Wessling. Print your own membrane: direct rapid prototyping of polydimethylsiloxane. *Lab on a Chip*, 14(15):2610, 2014.

[143] James O. Hardin, Thomas J. Ober, Alexander D. Valentine, and Jennifer A. Lewis. Microfluidic Printheads for Multimaterial 3D Printing of Viscoelastic Inks. *Advanced Materials*, 27(21):3279–3284, 6 2015.

[144] David B. Kolesky, Ryan L. Truby, A. Sydney Gladman, Travis A. Busbee, Kimberly A. Homan, and Jennifer A. Lewis. 3D Bioprinting of Vascularized, Heterogeneous Cell-Laden Tissue Constructs. *Advanced Materials*, 26(19):3124–3130, 5 2014.

[145] Simonetta Grilli, Sara Coppola, Veronica Vespini, Francesco Merola, Andrea Finizio, and Pietro Ferraro. 3D lithography by rapid curing of the liquid instabilities at nanoscale. *Proceedings of the National Academy of Sciences*, 108(37):15106–15111, 9 2011.

[146] Thomas J. Hinton, Andrew Hudson, Kira Pusch, Andrew Lee, and Adam W. Feinberg. 3D Printing PDMS Elastomer in a Hydrophilic Support Bath via Freeform Reversible Embedding. *ACS Biomaterials Science and Engineering*, 2(10):1781–1786, 10 2016.

[147] Bin Duan, Laura A. Hockaday, Kevin H. Kang, and Jonathan T. Butcher. 3D Bioprinting of heterogeneous aortic valve conduits with alginate/gelatin hydrogels. *Journal of Biomedical Materials Research Part A*, 101A(5):1255–1264, 5 2013.

[148] Peter H. von Hippel and Kwok-Ying Wong. The Effect of Ions on the Kinetics of Formation and the Stability of the Collagen-Fold. *Biochemistry*, 1(4):664–674, 7 1962.

[149] A.-M. Hermansson, E. Eriksson, and E. Jordansson. Effects of potassium, sodium and calcium on the microstructure and rheological behaviour of kappa-carrageenan gels. *Carbohydrate Polymers*, 16(3):297–320, 1 1991.

[150] Ivan Donati and Sergio Paoletti. Material Properties of Alginates. In Bernd H. A. Rehm, editor, *Alginates: Biology and Applications*, pages 1–53. Springer Berlin Heidelberg, Berlin, 2009.

[151] A. Mourchid, E. Lécolier, H. Van Damme, and P. Levitz. On Viscoelastic, Birefringent, and Swelling Properties of Laponite Clay Suspensions: Revisited Phase Diagram. *Langmuir*, 14(17):4718–4723, 8 1998.

[152] Quoc-Hung Nguyen and Ngoc-Diep Nguye. Incompressible Non-Newtonian Fluid Flows. In Yong Gan, editor, *Continuum Mechanics - Progress in Fundamentals and Engineering Applications*. InTech, 3 2012.

[153] Gareth H. McKinley and Michael Renardy. Wolfgang von Ohnesorge. *Physics of Fluids*, 23(12):127101, 2011.

[154] Say Hwa Tan, Nam Trung Nguyen, Yong Chin Chua, and Tae Goo Kang. Oxygen plasma treatment for reducing hydrophobicity of a sealed polydimethylsiloxane microchannel. *Biomicrofluidics*, 4(3):1–8, 2010.

[155] I-Jane Chen and Ernö Lindner. The Stability of Radio-Frequency Plasma-Treated Polydimethylsiloxane Surfaces. *Langmuir*, 23(6):3118–3122, 3 2007.

[156] X. Ren, M. Bachman, C. Sims, G. P. Li, and N. Allbritton. Electroosmotic properties of microfluidic channels composed of poly(dimethylsiloxane). *Journal of Chromatography B: Biomedical Sciences and Applications*, 762(2):117–125, 2001.

[157] Madalyn D. Kern, Joan Ortega Alcaide, and Mark E. Rentschler. Soft material adhesion characterization for in vivo locomotion of robotic capsule endoscopes: Experimental and modeling results. *Journal of the Mechanical Behavior of Biomedical Materials*, 39:257–269, 2014.

[158] Hyunwoo Yuk, Teng Zhang, German Alberto Parada, Xinyue Liu, and Xuanhe Zhao. Skin-inspired hydrogel-elastomer hybrids with robust interfaces and functional microstructures. *Nature Communications*, 7:12028, 6 2016.

[159] Jinwen Zhou, Amanda Vera Ellis, and Nicolas Hans Voelcker. Recent developments in PDMS surface modification for microfluidic devices. *Electrophoresis*, 31(1):2–16, 1 2010.

[160] David T. Eddington, John P. Puccinelli, and David J. Beebe. Thermal aging and reduced hydrophobic recovery of polydimethylsiloxane. *Sensors and Actuators B: Chemical*, 114(1):170–172, 2006.

[161] Jongsoo Kim, Manoj K. Chaudhury, Michael J. Owen, and Tor Orbeck. The Mechanisms of Hydrophobic Recovery of Polydimethylsiloxane Elastomers Exposed to Partial Electrical Discharges. *Journal of Colloid and Interface Science*, 244(1):200–207, 12 2001.

[162] Dhananjay Bodas and Chantal Khan-Malek. Hydrophilization and hydrophobic recovery of PDMS by oxygen plasma and chemical treatment-An SEM investigation. *Sensors and Actuators, B: Chemical*, 123(1):368–373, 2007.

[163] Jonathan A. Ja Vickers, Meghan M. Mm Caulum, and Charles S. Cs Henry. Generation of hydrophilic poly(dimethylsiloxane) for high-performance microchip electrophoresis. *Analytical Chemistry*, 78(21):7446–7452, 2006.

[164] Dirk Hegemann, Herwig Brunner, and Christian Oehr. Plasma treatment of polymers for surface and adhesion improvement. *Nuclear Instruments and Methods in Physics Research Section B: Beam Interactions with Materials and Atoms*, 208(1-4):281–286, 8 2003.

[165] S. Bhattacharya, A. Datta, J.M. Berg, and S. Gangopadhyay. Studies on surface wettability of poly(dimethyl) siloxane (PDMS) and glass under oxygen-plasma treatment and correlation with bond strength. *Journal of Microelectromechanical Systems*, 14(3):590–597, 6 2005.

[166] T. Suni, K. Henttinen, I. Suni, and J. Mäkinen. Effects of Plasma Activation on Hydrophilic Bonding of Si and SiO[sub 2]. *Journal of The Electrochemical Society*, 149(6):G348, 2002.

[167] Vikash Sharma, Marshal Dhayal, Govind, S. M. Shivaprasad, and S. C. Jain. Surface characterization of plasma-treated and PEG-grafted PDMS for micro fluidic applications. *Vacuum*, 81(9):1094–1100, 2007.

[168] Dhananjay Bodas and Chantal Khan-Malek. Formation of more stable hydrophilic surfaces of PDMS by plasma and chemical treatments. *Microelectronic Engineering*, 83(4-9 SPEC. ISS.):1277–1279, 2006.

[169] András Tóth, Imre Bertóti, Marianne Blazsó, György Bánhegyi, Alajos Bognar, and Pál Szaplonczay. Oxidative damage and recovery of silicone rubber surfaces. I. X-ray photoelectron spectroscopic study. *Journal of Applied Polymer Science*, 52(9):1293–1307, 5 1994.

[170] Alvaro Mata, Aaron J. Fleischman, and Shuvo Roy. Characterization of polydimethylsiloxane (PDMS) properties for biomedical micro/nanosystems. *Biomedical microdevices*, 7(4):281–293, 2005.

[171] Yevgeny Berdichevsky, Julia Khandurina, András Guttman, and Y.-H. Lo. UV/ozone modification of poly(dimethylsiloxane) microfluidic channels. *Sensors and Actuators B: Chemical*, 97(2-3):402–408, 2 2004.

[172] C. Borcia, I.L. Punga, and G. Borcia. Surface properties and hydrophobic recovery of polymers treated by atmospheric-pressure plasma. *Applied Surface Science*, 317:103–110, 10 2014.

[173] Tatsunosuke Murakami, Shin-ichi Kuroda, and Zenjiro Osawa. Dynamics of Polymeric Solid Surfaces Treated with Oxygen Plasma: Effect of Aging Media after Plasma Treatment. *Journal of Colloid and Interface Science*, 202(1):37–44, 6 1998.

[174] Firas Awaja, Michael Gilbert, Georgina Kelly, Bronwyn Fox, and Paul J. Pigram. Adhesion of polymers. *Progress in Polymer Science*, 34(9):948–968, 9 2009.

[175] Pressure Sensitive Tape Council. International Standard for Peel Adhesion of Pressure Sensitive Tape. In *Test Methods for Pressure Sensitive Adhesive Tapes*, chapter PSTC-101, pages 1–10. Oakbrook Terrace, IL, USA, 15th editi edition, 2012.

[176] R.S. Court, M.P.F. Sutcliffe, and S.M. Tavakoli. Ageing of adhesively bonded joints-fracture and failure analysis using video imaging techniques. *International Journal of Adhesion and Adhesives*, 21(6):455–463, 1 2001.

[177] H. Ollendorf and D. Schneider. A comparative study of adhesion test methods for hard coatings. *Surface and Coatings Technology*, 113(1-2):86–102, 1999.

[178] R. H. Dauskardt, M. Lane, Q. Ma, and N. Krishna. Adhesion and debonding of multi-layer thin film structures. *Engineering Fracture Mechanics*, 61(1):141–162, 1998.

[179] Youbo Lin, Ting Y. Tsui, and Joost J. Vlassak. Water diffusion and fracture in organosilicate glass film stacks. *Acta Materialia*, 55(7):2455–2464, 2007.

[180] Jingda Tang, Jianyu Li, Joost J. Vlassak, and Zhigang Suo. Adhesion between highly stretchable materials. *Soft Matter*, 12(4):1093–1099, 2015.

[181] Melvina Leolukman and Seong H. Kim. Effect of rubbing-induced polymer chain alignment on adhesion and friction of glassy polystyrene surfaces. *Langmuir*, 21(2):682–685, 2005.

[182] H. K. Yuen, E. P. Tam, and J. W. Bulock. On the Glass Transition of Polyacrylamide. In J.F. Johnson and P.S. Gill, editors, *Analytical Calorimetry*, pages 13–24. Springer, Boston, MA, 1984.

[183] A. Terreros. Gomez, B J Rubio Retama, B. Lopez. Ruiz, P. A. Galera. Gomez, C Rueda Rodriguez, C. Arias. Garcia, and E. Lopez. Cabarcos. Encapsulation of alkaline phosphatase in polyacrylamide microparticles using the concentrated emulsion polymerisation method. In *Trends in Colloid and Interface Science XVI*, pages 169–173. Springer Berlin Heidelberg, Berlin, Heidelberg, 6 2004.

[184] M. E. S. Ribeiro E Silva, J. Caetano Machado, V. Mano, and G. Goulart Silva. Positron annihilation and differential scanning calorimetry studies of polyacrylamide and poly(dimethylacrylamide)/poly(ethylene glycol) blends. *Journal of Polymer Science Part B: Polymer Physics*, 41(13):1493–1500, 7 2003.

[185] K. Butler, P. R. Thomas, and G. J. Tyler. Stereospecific polymerization of some polar vinyl monomers. *Journal of Polymer Science*, 48(150):357–366, 12 1960.

[186] Jak Li, Jinli Qiao, and Keryn Lian. Investigation of polyacrylamide based hydroxide ion-conducting electrolyte and its application in all-solid electrochemical capacitors. *Sustainable Energy & Fuels*, 1(7):1580–1587, 2017.

[187] Costantino Creton and Matteo Ciccotti. F racture and adhesion of soft materials : a review. *Reports on Progress in Physics*, 00:46601, 2015.

[188] Jennifer L. Fritz and Michael J. Owen. Hydrophobic recovery of plasma-treated polydimethylsiloxane. *The Journal of Adhesion*, 54(1-4):33–45, 1995.

[189] D Maugis and M Barquins. Fracture mechanics and the adherence of viscoelastic bodies. *Journal of Physics D: Applied Physics*, 11(14):1989–2023, 10 1978.

[190] P. G. Saffman and G. Taylor. The Penetration of a Fluid into a Porous Medium or Hele-Shaw Cell Containing a More Viscous Liquid. *Proceedings of the Royal Society A: Mathematical, Physical and Engineering Sciences*, 245(1242):312–329, 6 1958.

[191] Animangsu Ghatak, Manoj K. Chaudhury, Vijay Shenoy, and Ashutosh Sharma. Meniscus Instability in a Thin Elastic Film. *Physical Review Letters*, 85(20):4329–4332, 11 2000.

[192] M. Adda-Bedia and L. Mahadevan. Crack-front instability in a confined elastic film. *Proceedings of the Royal Society A: Mathematical, Physical and Engineering Sciences*, 462(2075):3233–3251, 2006.

[193] Richard Villey, Costantino Creton, Pierre-Philippe Cortet, Marie-Julie Dalbe, Thomas Jet, Baudouin Saintyves, Stéphane Santucci, Loïc Vanel, David J Yarusso, and Matteo Ciccotti. Rate-dependent elastic hysteresis during the peeling of pressure sensitive adhesives. *Soft matter*, 11(17):3480–91, 2015.

[194] Jafar Alvankarian and Burhanuddin Yeop Majlis. Exploiting the oxygen inhibitory effect on UV curing in microfabrication: A modified lithography technique. *PLoS ONE*, 10(3):1–12, 2015.

[195] J. R. Torres, G. D. Jay, K.-S. Kim, and G. D. Bothun. Adhesion in hydrogel contacts. *Proceedings of the Royal Society of London A: Mathematical, Physical and Engineering Sciences*, 472(2189):20150892, 5 2016.

[196] W. Brown and R. M. Johnsen. Diffusion in polyacrylamide gels. *Polymer*, 22(2):185–189, 1981.

[197] Armand Adjari, Françoise Brochard-Wyart, Pierre Gilles de Gennes, Ludwik Leibler, Jean Louis Viovy, and Michael Rubinstein. Slippage of an entangled polymer melt on a grafted surface. *Physica A: Statistical Mechanics and its Applications*, 204(1-4):17–39, 1994.

[198] Bin Zhang. Separation strain rate dependence on the failure of polymer adhesion with mobile promoters. *International Journal of Solids and Structures*, 50(25-26):4349–4354, 2013.

[199] A. N. Gent and R. P. Petrich. Adhesion of Viscoelastic Materials to Rigid Substrates. *Proceedings of the Royal Society A: Mathematical, Physical and Engineering Sciences*, 310(1502):433–448, 5 1969.

[200] E. H. Andrews and A. J. Kinloch. Mechanics of Adhesive Failure. I. *Proceedings of the Royal Society A: Mathematical, Physical and Engineering Sciences*, 332(1590):401–414, 3 1973.

[201] J. A. Greenwood and K. L. Johnson. The mechanics of adhesion of viscoelastic solids. *Philosophical Magazine A*, 43(3):697–711, 3 1981.

[202] Dae-Hyeong D.-H. Kim, Nanshu Lu, Rui Ma, Y.-S. Yun-Soung Kim, R.-H. Rak-Hwan Kim, Shuodao Wang, Jian Wu, Sang Min Won, Hu Tao, Ahmad Islam, Ki Jun Yu, Tae-il T.-i. Kim, Raeed Chowdhury, Ming Ying, Lizhi Xu, Ming Li, Hyun-Joong H.-J. Chung, Hohyun Keum, Martin McCormick, Ping Liu, Y.-W. Yong-Wei Zhang, Fiorenzo G. Omenetto, Yonggang Huang, Todd Coleman, and John A. Rogers. Epidermal Electronics. *Science*, 333(6044):838–843, 8 2011.

[203] Jingjing Guo, Xinyue Liu, Nan Jiang, Ali K. Yetisen, Hyunwoo Yuk, Changxi Yang, Ali Khademhosseini, Xuanhe Zhao, and Seok-Hyun Yun. Highly Stretchable, Strain Sensing Hydrogel Optical Fibers. *Advanced Materials*, 28(46):10244–10249, 12 2016.

[204] Baohong Chen, Yuanyuan Bai, Feng Xiang, Jeong Yun Sun, Yong Mei Chen, Hong Wang, Jinxiong Zhou, and Zhigang Suo. Stretchable and transparent hydrogels as soft conductors for dielectric elastomer actuators. *Journal of Polymer Science, Part B: Polymer Physics*, 52(16):1055–1060, 2014.

[205] Prakash Manandhar, Paul D. Calvert, and John R. Buck. Elastomeric Ionic Hydrogel Sensor for Large Strains. *IEEE Sensors Journal*, 12(6):2052–2061, 6 2012.

[206] Daehoon Han, Zhaocheng Lu, Shawn A. Chester, and Howon Lee. Micro 3D Printing of a Temperature-Responsive Hydrogel Using Projection Micro-Stereolithography. *Scientific Reports*, 8(1):1–10, 2018.

[207] Lanlan Li, Lijia Pan, Zhong Ma, Ke Yan, Wen Cheng, Yi Shi, and Guihua Yu. All Inkjet-Printed Amperometric Multiplexed Biosensors Based on Nanostructured Conductive Hydrogel Electrodes. *Nano Letters*, 18(6):3322–3327, 6 2018.

[208] Andrea Negro, Thibaud Cherbuin, and Matthias P. Lutolf. 3D Inkjet Printing of Complex, Cell-Laden Hydrogel Structures. *Scientific Reports*, 8(1):17099, 12 2018.

[209] Shannon E. Bakarich, Robert Gorkin, Marcinhet Panhuis, Geoffrey M. Spinks, Marc in het Panhuis, and Geoffrey M. Spinks. Three-dimensional printing fiber reinforced hydrogel composites. *ACS Applied Materials and Interfaces*, 6(18):15998–16006, 9 2014.

[210] Rüdiger Landers, Ute Hübner, Rainer Schmelzeisen, and Rolf Mülhaupt. Rapid prototyping of scaffolds derived from thermoreversible hydrogels and tailored for applications in tissue engineering. *Biomaterials*, 23(23):4437–4447, 2002.

[211] J. A. A. A. Lewis. Direct Ink Writing of 3D Functional Materials. *Advanced Functional Materials*, 16(17):2193–2204, 11 2006.

[212] Qian Du, Quan Tang, Kaixiang Yang, Haiyang Yang, Chao Xu, and Xingyuan Zhang. One-Step Preparation of Tough and Self-Healing Polyion Complex Hydrogels with Tunable Swelling Behaviors. *Macromolecular Rapid Communications*, 1800691:1–6, 2018.

[213] Feng Luo, Tao Lin Sun, Tasuku Nakajima, Takayuki Kurokawa, Yu Zhao, Koshiro Sato, Abu Bin Ihsan, Xufeng Li, Honglei Guo, and Jian Ping Gong. Oppositely Charged Polyelectrolytes Form Tough, Self-Healing, and Rebuildable Hydrogels. *Advanced Materials*, 27(17):2722–2727, 5 2015.

[214] Peng Dou, Zhi Liu, Zhenzhen Cao, Jiao Zheng, Chao Wang, and Xinhua Xu. Rapid synthesis of hierarchical nanostructured Polyaniline hydrogel for high power density energy storage application and three-dimensional multilayers printing. *Journal of Materials Science*, 51(9):4274–4282, 2016.

[215] Feng Luo, Tao Lin Sun, Tasuku Nakajima, Daniel R. King, Takayuki Kurokawa, Yu Zhao, Abu Bin Ihsan, Xufeng Li, Honglei Guo, and Jian Ping Gong. Strong and Tough Polyion-Complex Hydrogels from Oppositely Charged Polyelectrolytes: A Comparative Study with Polyampholyte Hydrogels. *Macromolecules*, 49(7):2750–2760, 4 2016.

[216] Ryan L. Truby and Jennifer A. Lewis. Printing soft matter in three dimensions. *Nature*, 540(7633):371–378, 12 2016.

[217] Aaron P. Gerratt, Hadrien O. Michaud, and Stéphanie P. Lacour. Elastomeric electronic skin for prosthetic tactile sensation. *Advanced Functional Materials*, 25(15):2287–2295, 2015.

[218] Edwin P. Plueddemann. Silane adhesion promoters in coatings. *Progress in Organic Coatings*, 11(3):297–308, 1 1983.

[219] G.L. Witucki. BACK TO BASICS A Silane Primer: Chemistry and Applications of AIkoxy Silanes. *Journal of Coatings Technology*, 65(822):57–60, 1992.

[220] S. Savard, L.-P. Blanchard, J. Léonard, and R. E. Prud'homme. Hydrolysis and condensation of silanes in aqueous solutions. *Polymer Composites*, 5(4):242–249, 10 1984.

[221] Zhigang Wu and Klas Hjort. Surface modification of PDMS by gradient-induced migration of embedded Pluronic. *Lab on a Chip*, 9(11):1500, 2009.

[222] Hui Tak Kim, Jeong Koo Kim, and Ok Chan Jeong. Hydrophilicity of Surfactant-Added Poly(dimethylsiloxane) and Its Applications. *Japanese Journal of Applied Physics*, 50(6):06GL04, 6 2011.

[223] Hojjat Madadi and Jasmina Casals-Terré. Long-term behavior of nonionic surfactant-added PDMS for self-driven microchips. *Microsystem Technologies*, 19(1):143–150, 2013.

[224] G J Lake and A G Thomas. The strength of highly elastic materials. *Proceedings of the Royal Society of London. Series A. Mathematical and Physical Sciences*, 300(1460):108–119, 8 1967.

[225] Elizabeth O Lillie, Bradley Patay, Joel Diamant, Brian Issell, Eric J Topol, and Nicholas J Schork. The n-of-1 clinical trial: the ultimate strategy for individualizing medicine? *Personalized medicine*, 8(2):161–173, 2011.

[226] Enrui Zhang, Ruobing Bai, Xavier P. Morelle, and Zhigang Suo. Fatigue fracture of nearly elastic hydrogels. *Soft Matter*, 14(18):3563–3571, 2018.

[227] Jianyu Li, Yuhang Hu, Joost J. Vlassak, and Zhigang Suo. Experimental determination of equations of state for ideal elastomeric gels. *Soft Matter*, 8(31):8121, 2012.

[228] Wei Hong, Zishun Liu, and Zhigang Suo. Inhomogeneous swelling of a gel in equilibrium with a solvent and mechanical load. *International Journal of Solids and Structures*, 46(17):3282–3289, 8 2009.

[229] I D Johnston, D K McCluskey, C K L Tan, and M C Tracey. Mechanical characterization of bulk Sylgard 184 for microfluidics and microengineering. *Journal of Micromechanics and Microengineering*, 24:035017, 2014.

This thesis was typeset using LaTeX, originally developed by Leslie Lamport and based on Donald Knuth's TeX. The body text is set in 11 point Egenolff-Berner Garamond, a revival of Claude Garamont's humanist typeface. A template that can be used to format a PhD thesis with this look and feel has been released under the permissive MIT (XII) license, and can be found online at github.com/suchow/Dissertate or from its author, Jordan Suchow, at suchow@post.harvard.edu.